Microfluidics based on silicon/polymer and all-polymer technologies as an alternative to silicon/glass:

A case study for TopSpot printheads

Dissertation
zur Erlangung des Doktorgrades der Technischen Fakultät der Albert-Ludwigs-Universität Freiburg im Breisgau

vorgelegt von
Dipl.-Ing. Kiril Kalkandjiev

Freiburg im Breisgau, 2015

Dekan
Prof. Dr. Georg Lausen

Referenten
Prof. Dr. Roland Zengerle
Prof. Dr. rer. nat. Heinz Kück

Tag der Prüfung
09.03.2015

Kiril Kalkandjiev
Lehrstuhl für Anwendungsentwicklung (Prof. Dr. Roland Zengerle)
Institut für Mikrosystemtechnik (IMTEK)
Technische Fakultät
Albert-Ludwigs-Universität Freiburg

CONTENTS

ABSTRACT

The sample volumes handled in microfluidic devices are typically in the range of micro- to millilitres. This leads to spatially extended structures, which often cannot be manufactured in a cost-effective way by using established silicon/glass technologies. Therefore, microfluidic devices for cost-sensitive diagnostic applications are already realised solely on the basis of polymer materials. So far, there is no established alternative to silicon/glass technologies for the production of large-scale fluidic components with high aspect ratio microstructures and with high demands in terms of mechanical stability.

An interesting example of combining such requirements is given by TopSpot printheads for printing of microarrays. The storage of up to 96 different biological samples in reservoirs with a capacity of typically 1 µl to 6 µl requires spatially extended microfluidic structures. At the same time, the 500 µm pitched microarray grid and the requirement to connect each nozzle to the corresponding reservoir by an individual supply channel demand for high integration density. Therefore, the fluidic channels have typical widths of 70 µm to 80 µm, depths of 80 µm to 300 µm – i.e. an aspect ratio of up to 4.3 – and the distance between two neighbouring channels in the nozzle array is only 55 µm to 180 µm. Currently, the fabrication process for TopSpot printheads is based on 100mm wafers and utilises deep reactive ion etching (DRIE) of silicon and anodic bonding of the silicon to semi-finished glass wafers with fluidic inlets and outlets. These established technologies enable outstanding printing performance and long lifetime of the printheads but are related to high manufacturing costs, long lead times and are only little responsive in terms of application specific designs.

The scientific challenge of this work is therefore to explore alternative material combinations and processes for realisation of the TopSpot printheads. A starting point is the analysis of the current fabrication process with respect to a set of criteria. The focus of the thesis is the reduction of the manufacturing costs and production lead time without any compromise in terms of performance and lifetime compared to the established silicon/glass printheads.

A common way to reduce manufacturing costs is the reduction of the device dimensions and the transition to a larger wafer size. The underlying principle is that most fabrication processes take a fixed amount of time and do not depend on the size of the wafer or the number of devices on it. It was found that for production volumes of 10 to 100 printheads, the reduction of the printhead size from 655 mm^2 to 310 mm^2 and the transition to 150mm wafers leads to a cost reduction of 20 to 50 % (depending on the production volume and considering a higher cost fraction due to size dependent processes and material purchasing). The expected lead time

is not affected by the scaling and remains 42 days, with 7 days due to rework-related activities and a relatively high uncertainty of 24 days.

The present work describes improvements that go beyond optimisation by scaling the established technology. Two alternative fabrication approaches were investigated and are described in more detail below. Both approaches were quantitatively evaluated with the analytic hierarchy process (AHP), a multi-criteria decision-making method. The AHP was used to measure the significance of the criteria performance, lead time, lifetime and costs and to identify the most appropriate technology with respect to these criteria.

The first approach involves hybrid printheads where the semi-finished glass wafers are replaced by polymer layers. The hybrid printheads consist of a silicon layer with microfluidic structures, a layer of dry film resist allowing for selective microchannel sealing and a conventionally machined polymer layer with fluidic reservoirs as an interface to laboratory equipment such as pipettes and dispensing robots. The functionality of the hybrid printheads was determined experimentally and found to be well comparable to the silicon/glass printheads. For production volumes of 10 to 100 printheads, the cost reduction was calculated to be close to 60 % without changing the printhead or wafer size. The major contributors to this improvement are the lower material costs (up to 43 % reduction) and shorter process times (up to 52 % reduction) as well as the increase of the manufacturing yield from 60 % to 70 %. With the hybrid printheads, the expected lead time can be reduced from 42 to 28 days and the lead time for rework from 7 to 4 days. The uncertainty in lead time prediction is only 6 days, thus by a factor of 4 smaller compared to the silicon/glass printheads.

The second approach enables the production of all-polymer printheads by means of repeated lamination-exposure-development cycles of a dry film resist on a semi-finished polymer substrate with fluidic access holes. In this way, all microfluidic components are patterned directly on the printhead interface, thus eliminating the need of assembling discrete components such as channels, nozzles and reservoirs. Major advantages of the all-polymer printheads are the non-use of glass and respectively the short-term availability of all semi-finished components (as long as silicon-based processes are considered available) as well as their lower manufacturing costs and short lead times. This second technological approach allows for a cost reduction close to 80 % and lead time reduction from 42 to 8 days. The manufacturing feasibility and functionality of the all-polymer printheads were demonstrated by experimental results, however, the printing performance was insufficient to compete with the silicon/glass and the hybrid printheads. Major drawbacks are inferior printing accuracy, short lifetime and higher risk of cross-talk and carryover contamination.

ZUSAMMENFASSUNG

In mikrofluidischen Bauelementen werden in der Regel Flüssigkeitsvolumina im Bereich von Mikro- bis Millilitern gehandhabt. Dies führt zu räumlich ausgedehnten Strukturen, welche in der etablierten Silizium/Glas Technologie, dem technologischen Standard der Mikrosystemtechnik, häufig nicht mehr kosteneffizient gefertigt werden können. Mikrofluidische Bauelemente für kostensensitive diagnostische Anwendungen werden daher heute schon ausschließlich auf Basis von Polymermaterialien realisiert. Für großflächige fluidische Bauelemente, welche gleichzeitig Mikrostrukturen mit hohen Aspektverhältnissen beinhalten und darüber hinaus hohe Anforderungen an die mechanische Stabilität besitzen, haben sich bislang noch keine kostengünstigen Alternativen zur Silizium/Glass Technologie etabliert.

Ein interessantes Beispiel für die Kombination derartiger Anforderungen sind TopSpot Druckköpfe zum Drucken von Mikroarrays. Die Notwendigkeit der Vorlagerung von bis zu 96 unterschiedlichen biologischen Substanzen in Reservoirs mit einem Fassungsvermögen von typischerweise 1 µl bis 6 µl erfordert flächig ausgedehnte mikrofluidische Strukturen. Das in der Anwendung geforderte Druckraster von nur 500 µm gepaart mit der Anforderung, die Düsen mit individuellen Fluidleitungen aus den Reservoirs zu versorgen, erfordert gleichzeitig eine hohe Integrationsdichte. Die fluidischen Kanäle haben daher typische Breiten von 70 µm bis 80 µm, Tiefen von 80 µm bis 300 µm – also ein Aspektverhältnis von bis zu 4,3 – und sind im Düsenbereich in einem Abstand von lediglich 55 µm bis 180 µm zueinander angeordnet. Derzeit werden TopSpot Druckköpfe auf Basis von 100mm Wafern mittels reaktiven Ionentiefenätzens und anodischen Bondens mit zwei strukturierten Glaswafern produziert. Diese etablierten Fertigungstechnologien ermöglichen eine herausragende Funktionalität und lange Lebensdauer der Druckköpfe, nachteilig sind jedoch die damit verbundenen hohen Herstellkosten und die lange Durchlaufzeit (der Zeitbedarf für den Durchlauf einer Produktionscharge) sowie der hohe Aufwand bei der Herstellung anwendungsspezifischer Designvarianten.

Die wissenschaftliche Herausforderung der vorliegenden Arbeit ist daher die Erforschung alternativer Materialkombinationen und mikrotechnischer Prozesse für die Realisierung der TopSpot Druckköpfe. Der Ausgangspunkt für die durchgeführten Untersuchungen ist die Analyse der aktuellen Prozesskette hinsichtlich funktionaler und wirtschaftlicher Kriterien. Im Fokus der Arbeit steht die Reduzierung der Herstellkosten und Durchlaufzeit ohne Einbußen hinsichtlich der Funktionalität und ohne Beeinträchtigung der Lebensdauer im Vergleich zum Silizium/Glas Standard.

Ein etablierter Ansatz Herstellungskosten zu senken, ist die Reduzierung der Chipabmessungen sowie die Skalierung der bestehenden Technologie auf ein größeres Waferformat. Das zugrunde liegende Prinzip basiert auf der Tatsache, dass die meisten Prozesse der Mikrosystemtechnik unabhängig von der Wafergröße und der Anzahl von Chips auf dem Wafer sind. Bei einem Produktionsvolumen von 10 bis 100 Druckköpfen würde eine Reduzierung der Druckkopfgröße von aktuell 655 mm^2 auf 310 mm^2 sowie der Übergang zu 150mm Wafern zu einer Kostenreduktion von 20 % bis 50 % führen (abhängig vom Produktionsvolumen und unter Berücksichtigung höherer Kostenanteile für größenabhängige Prozesse und Materialbeschaffung). Die erwartete Durchlaufzeit ist von der Skalierung nicht beeinflusst und beträgt 42 Tage, mit 7 Tagen Nacharbeit und einer relativ hohen Unschärfe von 24 Tagen.

Gegenstand der vorliegenden Arbeit sind nun Verbesserungen, welche über das Optimierungspotential der beschriebenen Skalierung der bestehenden Technologie hinausgehen. Hierzu wurden zwei alternative Ansätze untersucht, die nachfolgend beschrieben werden. Beide Alternativen wurden quantitativ mit Hilfe des Analytischen Hierarchieprozesses (AHP), einem Verfahren zur Lösung multikriterieller Entscheidungsprobleme, bewertet. Mit dem AHP wurden Prioritäten bezüglich der Bewertungskriterien Herstellkosten *(costs)*, Funktionalität *(performance)*, Durchlaufzeit *(lead time)* und Lebensdauer *(lifetime)* bestimmt, und die am besten geeignete Technologie in Bezug auf diese Anforderungen ermittelt.

Als erste Alternative wurde ein Hybridansatz untersucht, bei welchem die beiden Glaswafer durch Kunststofflagen ersetzt sind. Die daraus resultierenden Hybriddruckköpfe bestehen aus einer Siliziumlage mit mikrofluidischen Strukturen, einer Lage Trockenresist zum selektiven Verschließen dieser Strukturen und einer konventionell strukturierten Kunststofflage für Fluidreservoire als Schnittstelle zu Laborgeräten wie Handpipetten und Dosierrobotern. Experimentelle Untersuchungen haben gezeigt, dass die Funktionalität der Hybriddruckköpfe vergleichbar ist mit der Funktionalität der Silizium/Glas Druckköpfe. Die Kostenreduzierung für das infrage kommende Produktionsvolumen von 10 bis 100 Druckköpfen beträgt knapp 60 % bei gleichbleibender Druckkopf- und Wafergröße. Die wichtigsten Faktoren für diese Kostenersparnis sind die Reduzierung der Materialkosten (bis zu 43 %) und der Prozesszeiten (bis zu 52 %) sowie die Steigerung der Fertigungsausbeute von 60 % auf 70 %. Mit der Hybridtechnologie kann die Durchlaufzeit von 42 auf 28 Tage und die Nacharbeit von 7 auf 4 Tage reduziert werden. Die Unsicherheit bei der Prognose der Durchlaufzeit beträgt 6 Tage und ist somit um den Faktor 4 geringer im Vergleich zur Silizium/Glas Technologie.

Als zweite Alternative wurden Druckköpfe vollständig aus Kunststoff gefertigt. Sie wurden durch wiederholte Laminierung, Belichtung und Entwicklung des Tro-

ckenresist TMMF auf einem Kunststoffsubstrat mit fluidischen Zugangsbohrungen hergestellt. Dadurch werden alle mikrofluidischen Komponenten direkt auf der Druckkopfschnittstelle strukturiert, und der Herstellungsprozess bedarf keiner Montage diskreter Komponenten wie Kanäle, Düsen oder Reservoire. Die wesentlichen Vorteile dieser vollständig aus Kunststoff gefertigten Druckköpfe sind der Verzicht auf mikrostrukturierte Glaswafer und somit die kurzfristige Verfügbarkeit aller Ausgangsmaterialien (sofern die Prozesse der Silizium-Mikromechanik als vorhanden vorausgesetzt werden können), niedrige Herstellungskosten und die sehr kurze Durchlaufzeit. Diese zweite technologische Alternative führt zu einer Kostenreduzierung von knapp 80 % und Verkürzung der Durchlaufzeit von 42 auf 8 Tage. Die Herstellbarkeit und Funktionalität der Kunststoffdruckköpfe wurden experimentell bestätigt. Dennoch ist die Funktionalität dieser Druckköpfe den Silicium/Glas und den Hybriddruckköpfen unterlegen. Wesentliche Nachteile sind die verringerte Druckpräzision, kürzere Lebensdauer und das höhere Risiko der Querkontamination und Verschleppung.

PUBLICATIONS

Based on the findings within this thesis, the following peer reviewed articles have been published and were authored or co-authored by Kiril Kalkandjiev.

Peer-reviewed international journals

[1] C. P. Steinert, K. Kalkandjiev, R. Zengerle, P. Koltay; "TopSpot® Vario: a novel microarrayer system for highly flexible and highly parallel picoliter dispensing"; Biomedical Microdevices, Vol. 11, 4, pp. 755-761 (2009)

[2] K. Kalkandjiev, L. Riegger, D. Kosse, M. Welsche, L. Gutzweiler, R. Zengerle, P. Koltay; "Microfluidics in silicon/polymer technology as a cost efficient alternative to silicon/glass"; Journal of Micromechanics and Microengineering (JMM) 21 (2011) 025008 (8pp)

[3] N. Wangler, L. Gutzweiler, K. Kalkandjiev, C. Müller, F. Mayenfels, H. Reinecke, R. Zengerle, N. Paust; "High-resolution permanent photoresist laminate TMMF for sealed microfluidic structures in biological applications"; Journal of Micromechanics and Microengineering (JMM) 21 (2011) 095009 (9pp)

[4] J. Schoendube, A.M. Yusof, K. Kalkandjiev, R. Zengerle, P. Koltay; "Wafer level fabrication of single cell dispenser chips with integrated electrodes for particle detection"; Journal of Micromechanics and Microengineering (JMM) 25 (2015) 025008 (10pp)

Peer-reviewed conferences

[5] K. Kalkandjiev, R. Zengerle, P. Koltay; "Fertigung von Hybriddruckköpfen aus Silizium und Kunststoff / Fabrication of hybrid printheads using silicon and plastic"; Proc. Mikrosystemtechnik-Kongress; Berlin, Germany; 12 14 October 2009, pp. 641-644

[6] K. Kalkandjiev, R. Zengerle, P. Koltay; "Hybrid Fabrication of Microfluidic Chips Based on COC, Silicon and TMMF Dry Resist"; Proc. IEEE Conference on Micro Electro Mechanical Systems (IEEE MEMS); Hong Kong, China; 24-28 January 2010, pp. 400-403

[7] K. Kalkandjiev, L. Gutzweiler, M. Welsche, R. Zengerle, P. Koltay; "A Novel Approach for the Fabrication of All-Polymer Microfluidic devices"; Proc.

IEEE Conference on Micro Electro Mechanical Systems (IEEE MEMS); Hong Kong, China; 24-28 January 2010, pp. 1079-1082

[8] K. Kalkandjiev, L. Gutzweiler, R. Zengerle, P. Koltay; "Kostengünstige Fertigung großflächiger Druckköpfe durch Lamination von Trockenlacken auf vorstrukturierte Polymersubstraten"; Proc. Mikrosystemtechnik-Kongress; Darmstadt, Germany; 10 12 October 2011, paper 10.2

Other peer reviewed publications that have been authored or co-authored by Kiril Kalkandjiev

[9] S. Schädel, J. Neukammer, J. Theisen, K. Brattke, H. Yildirim, K. Kalkandjiev, T. Guschauski, A. Kummrow, Ch. Sprenger, M. Malcher, M. Schmidt; "Development of Microfluidic Structures for High Throughput Flow Cytometric Characterization of Blood Cells"; Proc. 23rd Congress of the International Society for Advancement of Cytometry (ISAC); Quebec City, Canada; 20-24 May 2006, paper 263

[10] A. Yusof* , K. Kalkandjiev*, J. Schöndube, R. Zengerle, P. Koltay; "Wafer Level Fabrication of an Integrated Microdispenser with Electrical Impedance Detection for Single-cell Printing"; Proc. Smart Systems Integration; Zurich, Switzerland; 21-22 March 2012; (*Equally contributed to this work)

[11] K. Kalkandjiev, A. Yusof, J. Schöndube, R. Zengerle, P. Koltay; „Wafer Level fabrication of microfluidic sensors for impedance spectroscopy with integrated opposing electrodes"; Proc. Eurosensors; Athens, Greece; 4-7 September, ID 1202

[12] J. Schöndube, A. Yusof, Daniel Wright, K. Kalkandjiev, R. Zengerle, P. Koltay; "Picoliter Droplet Dispenser with Integrated Impedance Detector for Single-cell Printing"; Proc. International Conference of New Actuators and Drive Systems (Actuator); Bremen, Germany; 18 20 June 2012, pp. 418-421

Non peer reviewed presentations

[13] J. Specht, D. Stüwe, A. Spribille, K. Zengerle, F. Clement, D. Biro, K. Kalkandjiev, U. Abidin, G. Birkle, R. Zengerle, P. Koltay; „Entwicklung adaptiver Produktionsverfahren für hocheffiziente Solarzellen"; Symposium der Baden-Württemberg Stiftung; Stuttgart, Germany; June 2010

[14] K. Kalkandjiev, R. Zengerle, P. Koltay; „Dry film resists in microfluidics and BioMEMS"; MicroMountains Innovationsforum für Mikrotechnik; Villingen-Schwenningen, Germany; 21 January 2009

GLOSSARY

Terms and definitions

Term	Definition
All-polymer printheads	Printheads manufactured entirely from polymers (as opposite to silicon/glass and silicon/polymer printheads)
Analytical hierarchy process	A multi-criteria decision-making method
BMR	Developer for Ordyl dry film resist
Consistency index	A parameter that enables to measure the consistency of a comparison matrix.
Consistency ratio	A measure for the consistency of a comparison matrix
Die yield	The percentage of acceptable devices on one wafer
Dry film resist	Photoresist with a very high viscosity
First pass yield	The percentage of good parts coming out of a process without rework
Hybrid printheads	Printheads manufactured in silicon/polymer technology
Lead time	Period of time between the start and the completion of a production cycle
Lead time uncertainty	The period of time between the pessimistic and optimistic lead time
Manufacturing flexibility	The ability to respond to changing designs and fluctuating demands at short lead times and low costs
Optimistic lead time	Lead time based on the assumption that no rework is needed
Pessimistic lead time	Lead time based on the assumption that each process needs to be reworked once (or rework is not possible)
Priority	A measure for the importance of criteria and for the degree of fulfilment of the criteria by a given alternative
Process worksheet	A documentation of a given production batch containing the involved processes, machine and operator times. Depending on the level of detail, process worksheets might additionally contain setup times, yield, recipe names, rework related information etc.
Process yield	The percentage of good parts coming out of a process after rework
Pyrex	Borosilicate glass by Corning
Random index	A statistic that enables to measure the consistency of a comparison matrix.

Realistic lead time	Lead time considering rework probability and rework duration
Rework	Repetition of a process or a series of processes in case of non-compliance to specifications
Rework duration	Period of time between the start and the completion of a rework
Rework probability	Estimation of the probability that a process will cause a rework
Silicon on insulator	A silicon substrate with an insulating layer serving as an etch stop in the formation of silicon microstructures
Total yield	The percentage of good parts at the end of a process chain
USP Class VI	A series of standardised tests to evaluate the biological reactivity of polymer materials in vivo
Wafer yield	The percentage of wafers that are not completely bad
Weighted rework duration	Rework duration considering the rework probability

Abbreviations

Abbreviation	**Explanation**
AHP	Analytical hierarchy process
CAGR	Compound annual growth rate
CI	Consistency index
CNC	Computer numerical control
COC	Cyclic olefin copolymer
CR	Consistency ratio
CTE	Coefficient of thermal expansion
CV	Coefficient of variation
DFR	Dry film resist
DNA	Deoxyribonucleic acid
dpi	Dots per inch
DRIE	Deep reactive ion etching
ELISA	Enzyme-linked immunosorbent assay
FDA	Food and Drug Administration
FPY	First pass yield
IPA	Isopropanol

LT	Lead time
M.U.	Monetary unit
MEMS	Microelectromechanical systems
n/a	not applicable
PC	Polycarbonate
PCR	Polymerase chain reaction
PDMS	Poly(dimethylsiloxane)
PEB	Post exposure bake
PGMEA	Propylene glycol monomethyl ether acetate
PMMA	Poly(methyl methacrylate)
px	Pixel
RD	Rework duration
RI	Random index
RIE	Reactive ion etching
RP	Rework probability
SOI	Silicon on insulator
STS	Surface Technology Systems Plc.
UV	Ultraviolet

Latin variables and symbols

Symbol	**Explanation**	**Unit**
a	Priority of a technology with respect to a given criterion	-
A	Alternative	-
C	Costs	M.U.
C	Criterion	-
h	Height	m
n	Number of printheads per wafer	-
N	Process complexity factor	-
p	Priority of a technology with respect to the goal	-
P	Capillary pressure	$N\ m^{-2}$

S	Wafer lot size	-
w	Priority of a criterion (local or global)	-
w	Width	m
$\vec{\boldsymbol{w}}$	Principal eigenvector of a matrix	-
$\vec{\boldsymbol{w}}_{PR}$	Priority vector	-
Y	Yield	%

Greek variables and symbols

Symbol	**Explanation**	**Unit**
λ	Eigenvalue of a matrix	-
θ	Contact angle	°
γ	Surface tension	N m^{-1}

1 INTRODUCTION

1.1 Microarrays

According to a widely used definition, a microarray is a spatially ordered, miniaturised arrangement of a multitude of immobilised reagents [1]. Microarrays enable parallel detection of thousands of addressable elements in a single experiment [2]. The basic concept was introduced in the late 1980s by Ekins *et al*., who established that the sensitivity of immunoassays can be improved by using microspots on a solid support and that multianalyte assays can be carried out using an array of such spots [3,4]. This has fuelled the scaling down of molecular procedures and since the late 1990s microarrays have been recognised as a powerful technique for large-scale, high-throughput analysis. Over the years, the scientific attention on microarray technology has rapidly increased with a peak in 2008/2009 (Figure 1-1).The research in the field has led to the optimisation of the technology and the development of commercially available microarray platforms. Today, after more than two decades of research and development, microarrays are being used in a wide range of applications across the life sciences. Based upon the nature of the immobilised reagents, microarrays can be classified into the following three main categories: DNA microarrays, protein microarrays and cell microarrays.

1.1.1 DNA Microarrays

The development of microarrays started in 1991 with the introduction of the light-directed, spatially addressable parallel chemical synthesis by Fodor *et al*. [5]. Although the technology was first demonstrated for the synthesis of peptides, further development of the light-directed synthesis in the field of peptide arrays was held back due to the relatively low efficiency [6]. In 1994, the light-directed synthesis

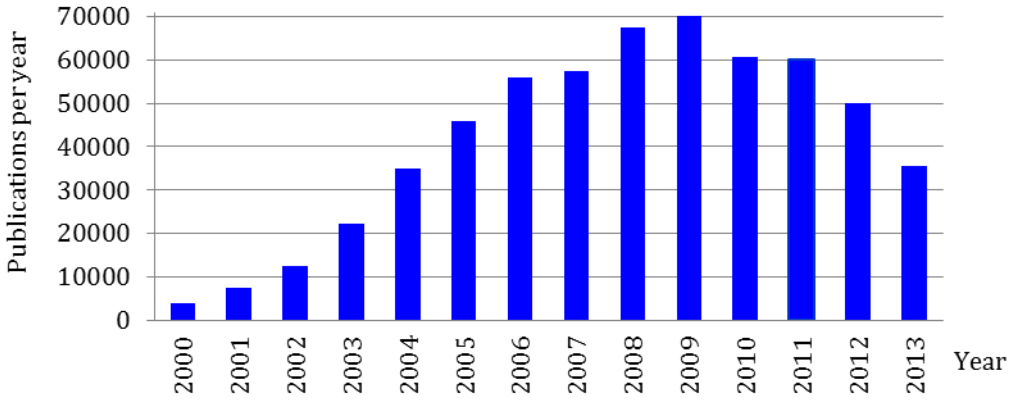

Figure 1-1: Number of publications per year according to Google Scholar using "microarray" as a search string.

was extended, allowing the fabrication of oligonucleotide arrays for DNA sequence analysis [7]. This technological development, the publication of the first microarray study and the development of the microarray printer [8] made a significant contribution to DNA microarrays becoming a widely used screening tool. Before microarrays became available, DNA experiments involved single genes or, at most, a handful of genes and analysis was performed in a low-throughput fashion, one gene at a time. DNA microarrays have produced a shift of interest from the study of single genes to a more ambitious endeavour: the study of the entire set of genes that define an organism – the genome. The suffix *-ome* refers to a *totality of some sort* and DNA microarrays are therefore considered as a tool for genome (all genes) and transcriptome (all active genes) research. As of today, there are 1841 complete genome sequences in the public domain and roughly 9000 on-going genome projects [9]. The most remarkable effort to sequence a genome was the human genome: a project that was published in 2001 [10] and finally corrected in 2004 [11].

1.1.2 Protein microarrays

The success of these genome sequencing projects, among others, led to the realisation that the genome cannot provide enough information to understand complex cellular events. Although the genetic information provides the sequence of each protein, it is static and contains only little data about the structure, modifications, interactions, activities, and, ultimately, the function of proteins [12]. Gene sequence data alone does not provide insight into dynamic cellular events and is of relatively little clinical use unless it is directly linked to disease relevance. Proteins, on the other hand, are highly dynamic molecules that change their conformation. They are involved in almost every biological process that takes place in living organisms and are ultimately responsible for all of an organism's properties [13]. This observation, in turn, yielded a stronger focus on proteins and further boosted the shift of interest from the genome to the proteome [14,15].

A major issue arising in this context is to use the genetic information not just to decode the amino acid sequence of the encoded proteins but also to explore their function. In response to the availability of complete genome sequences, the field of proteomics has emerged with the goal to provide a comprehensive, quantitative description of protein expression and its changes under the influence of biological perturbations such as disease or drug treatment [16,17]. Since traditional proteomic techniques such as electrophoresis, liquid chromatography and mass spectrometry provide effective quantitative data for only small numbers of samples, protein microarrays have been developed for high-throughput screening of protein-protein interactions [18-21]. Among many challenges, when building a viable protein microarray, a manufacturer needs to ensure that immobilised proteins retain their biological activities. While DNA is highly resistant to a range of conditions such as humidity, temperature and pressure, proteins are much less robust

and may lose biological activity outside their native environment. Hence, it is unclear whether they remain functional when immobilised on the chip. Even though stringent environmental control may help to prevent denaturation, full functionality of proteins is often provided only in living cells and this observation has led to the development of cell microarrays.

1.1.3 Cell microarrays

Cell microarrays can be obtained by depositing DNA microspots on a solid support which is then placed in a culture dish with cells in a medium [22]. Under very special and artificial conditions, cells that adhere to the spots take up the underlying genomic material and become transfected. The result is a living cell microarray in which each feature is a cluster of cells overexpressing the particular gene as a recombinant protein. Transfected cell microarrays, however, measure the average response of large cell populations, assuming that this is representative of a typical cell within the population. In many cases, this is an oversimplification because single-cell responses play an important role in understanding of the properties of cell populations. Therefore, recent research efforts are increasingly focused on producing microarrays of living single cells [23,24] and profiling cell responses at the single-cell level [25-27].

1.2 Clinical and market relevance of microarrays

The result of a microarray experiment depends on numerous factors such as chip design, sample preparation, image acquisition and data normalisation. It is a well-known fact that comparison of microarray experiments might reveal poor correlation between different platforms and laboratories [28-31]. At the same time, clinical decisions require data that is absolutely unambiguous and independent of the used microarray platform, so that standardisation has become a key issue in the microarray industry [32]. Although the commercial relevance of microarrays has been shown by numerous market studies, the number of companies marketing microarrays is still small. In the past, some vendors became insolvent (Febit), while others have exited the market as they found it unattractive for growth (Nanogen, Life Technologies, GE). Besides, small vendors seem to witness less growth, as researchers increasingly prefer to use products from leading vendors. This makes the microarray market very unattractive for new participants. Nevertheless, many existing vendors are optimistic [33]. DNA microarrays represent the largest segment of the microarray market. In 2010, the global DNA microarray market was valued at $760 million and is expected to reach $1.4 billion by 2015 with a compound annual growth rate (CAGR) of 13.4%. The market is dominated by Affymetrix with 48 % market share, which is mainly attributed to the high density of their microarrays, large number of patents, first-to-market presence as well as many research and commercial partnerships. The second largest share is taken by Illu-

mina (23 %), followed by Agilent Technologies (12 %), Roche NimbleGen (9 %) and Sequenom (7 %). Currently, about 80 % of the DNA microarray research takes place in academic institutions, either on an individual basis or in collaboration with the industry. It is expected that academic research will retain this prominent position but at a slower pace, so its market share will drop to 70 % by 2015. At the expense of academics, the commercial segment is becoming more important and is gaining a greater share of the global market for DNA microarrays [34].

The first microarray-based clinical test, the AmpliChip by Roche and Affymetrix [35], was approved by the U.S. Food and Drug Administration (FDA) in 2005 (Figure 1-2). The DNA-based AmpliChip diagnostic test identifies specific genotypes that regulate how the patient metabolises certain medicines and allows doctors to personalise drug choice and dosing accordingly. Even though approved by the FDA, some insurance companies do not cover the check-up on the ground that the clinical utility and benefit to net health outcomes have not been established [36]. The costs of AmpliChip range between $600 and $1300.

In 2004, Genomic Health launched Oncotype DX, a DNA microarray-based diagnostic test that quantifies the likelihood of breast cancer recurrence by analysing a panel of 21 genes [37]. By distinguishing lower and higher risk tumours, Oncotype DX allows patients with breast cancer to avoid unnecessary chemotherapy, which, apart from side effects, can cost tens of thousands of dollars per patient per year. Oncotype DX has not been cleared by the FDA and its current list price is $3650.

In February 2007, another DNA microarray-based breast cancer recurrence assay, the MammaPrint developed by Agendia, was cleared by the FDA [38]. The MammaPrint test identifies which early-stage breast cancer patients are at risk of

Figure 1-2: AmpliChip by Roche and Affymetrix, the first microarray for clinical applications, enables the detection of genetic variations that can influence drug efficacy and adverse drug reactions [35].

distant recurrence following surgery by stratifying patients into low and high risk groups. Thus, MammaPrint allows doctors to select the appropriate postoperative medical treatment, e.g. hormonal therapy alone if the patient is Low Risk or more aggressive therapy including chemotherapy if she is High Risk. The costs of the test are $4200 in the U.S. and €2675 in Europe.

The success of DNA microarrays was responsible for much of the enthusiasm within the protein microarray area. In theory, protein microarrays offer numerous advantages over DNA microarrays. Almost all products of modern pharmaceutical biotechnology are protein based [39]. Therefore, one would expect protein microarrays to play a prominent role in diagnostics and proteomic studies. In practice, studies based on protein microarrays are only rarely used whereas less meaningful genome analyses based on DNA microarrays are widely accepted. This is mainly due to the low availability, high price and poor quality of protein microarrays.

In fact, protein microarray technology turned out more difficult than originally expected and the initial enthusiasm has been cooled by several technical hurdles. One major issue is that it is fundamentally far harder to work with proteins than with DNA. While DNA is a molecule with a defined hydrophilic backbone and structure, proteins are comprised of 20 amino acids capable of forming different complex structures. Proteins may be hydrophobic, hydrophilic, acidic or basic. Additionally, there are many more proteins than genes; latest estimates predict that the human genome has around 30 000 genes, but there may be as many as 1 million protein-based structures in the human proteome [40]. Purification, maintenance and attachment of proteins to a solid surface are more complicated than the corresponding techniques used for DNA microarrays [15,41]. While large custom-made DNA sequences can be provided at moderate costs and within short timelines [42], protein production is both expensive and time-consuming. In contrast to DNA which can be stored for years without any significant degradation [43], proteins denature and lose their function after only a few months in storage.

In the early 2000s, these issues caused several companies to delay preannounced protein microarray products, others even dropped plans to commercialise protein microarrays. However, by now several protein microarray products have entered the diagnostics market. The first commercially available protein microarray, ExpressArray p53, is a tool for cancer research and was launched in 2002 by Sense Proteomic. In 2004, Invitrogen launched their ProtoArray Human Protein Microarray: a high-density protein microarray, containing more than 1 800 unique human proteins. The latest version, ProtoArray 5.0, contains 9400 proteins and has a list price of €1360 [44]. In order to maintain their native structure, all proteins immobilised on the ProtoArray are purified under non-denaturing conditions in a controlled environment. ProtoArray microarrays can be used for a broad

range of applications, including identifying protein biomarkers and drug target pathways, profiling antibody specificity and mapping protein-protein interactions. The ProtoArray Kit has a list price of €2955 and allows identifying binding partners of proteins of interest in as little as one day. At present, there are lots of commercial suppliers of protein microarrays, e.g. PEPperPRINT, LC Sciences, JPT Peptide Technologies, Protagen, imaGenes, but there is no dominant format. A comprehensive list of commercially available protein microarrays and their applications has recently been provided in [45].

Another recent study reported that the protein microarray market is growing and the CAGR is expected to reach 19.9 % before 2015 [46]. Nevertheless, before protein microarrays can finally make the leap to the lucrative and highly competitive diagnostics market, there is a need for more solid proof of their ability to provide therapeutically relevant results and realistic opportunities for cost reduction. Despite many advances in recent years, the protein microarray vision of using just one drop of blood to screen patients for relevant pathologic information in the doctor's office before a personalised drug is prescribed is still far away [45,47].

Regarding cell microarrays, major issues for their successful commercialisation are intrinsic to the process of cell transfection, the collection of high-content images of each cell population and automated data analysis [48,49]. Cell microarrays have the potential to find broad use in the pharmaceutical industry, enabling cell-based sensors with high throughput and manifold capabilities [50]. In 2009, Silicon Biosystems has launched DEPArray – a cell microarray designed to identify, manipulate and sort specific single cells within a heterogeneous population. DEPArray features up to 76 800 dielectrophoretic cages, whose size can be set to accommodate one single cell each. During manipulation, cells maintain viability, the cell DNA remains completely intact and the proliferation capability unmodified. Possible applications of DEPArray include prenatal and cancer diagnosis, cell therapy and single cell resolution biology.

1.3 Methods for microarray fabrication

The production of the microarray, i.e. the application and binding of the reagents to a solid support, is an important step before performing a microarray assay. Since reagents are often very expensive, one of the most important requirements on microarray production methods is to work reliably and to waste only tiny quantities of reagents. At the most basic level, methods for producing microarrays can be classified into two main groups: printing techniques, where pre-synthesised probes are immobilised on a support by some type of robotic printer, and in situ-synthesis, where the probe sequences are generated on the chip. A few other less frequently used methods have also been reported. Which fabrication method fits

best depends on the nature of the study with attention being paid to budget constraints, throughput needs, type of reagents and surface on which the reagents will be immobilised [51]. The salient features of several platforms are outlined in [52]. Some of the most widely used methods for fabrication of microarrays are outlined in the sections below, a full description of these and other methods can be found in the literature [53-56].

1.3.1 Printing techniques

Printing techniques were the first ones used to demonstrate the usefulness of the microarray technology [8]. Printed microarrays can be easily tailored to specific research requirements since there are many suppliers for compatible hardware such as printing robotics, scanners and washing and hybridisation stations. Usually, experiments with printed microarrays use a solid support with the size of a standard microscope slide and can be performed with the same instruments regardless of the type of the immobilised reagents. The performance of a printed microarray, characterised by the array geometry, spot density, spot performance, background and specificity, is strongly influenced by a large number of factors such as robotics, environment conditions, probe concentration, printing buffer, immobilisation chemistry, hybridisation conditions etc. [57]. Printing techniques can be further divided into contact and non-contact.

Contact techniques

Contact printing devices include quills and tweezers, capillary tubes, solid pins, split pins, micro spotting pins and pins-and-rings (Figure 1-3(a)) [51]. The printing tools are dipped into the reagent solution and deliver the reagents by direct contact to the microarray surface (Figure 1-3(b)). The delivery volume and the spot size are defined by the surface interactions of the printing tool, fluid and slide [58]. The typical volume is in the picoliter to nanoliter range, which is quite below the range of typical liquid handling systems such as micropumps, pipettes or autosamplers. The most widely used contact printing devices are provided by TeleChem International, a subsidiary of Arrayit Corporation. Other suppliers of contact printing tools are Labnext (ceramic pins), Parallel Synthesis Technology (silicon pins) and Point Technologies (tungsten pins). TeleChem's Micro Spotting pins are made of stainless steel using micro-machining with a manufacturing tolerance of 2.5 µm. The pins can hold between 0.2 µl and 1.25 µl of reagent solution (Figure 1-3(c)) and the delivery volume is about 600 pl per spot. In order to increase the speed of microarray manufacturing, pins can be mounted together into a printhead. Figure 1-3(d) shows a printhead by Arrayit with 48 pins mounted into it. Currently, Arrayit provides printheads with up to 192 pins.

One issue common to all contact printing technologies is the risk to damage the microarray surface through mechanical contact during printing. Besides, it has

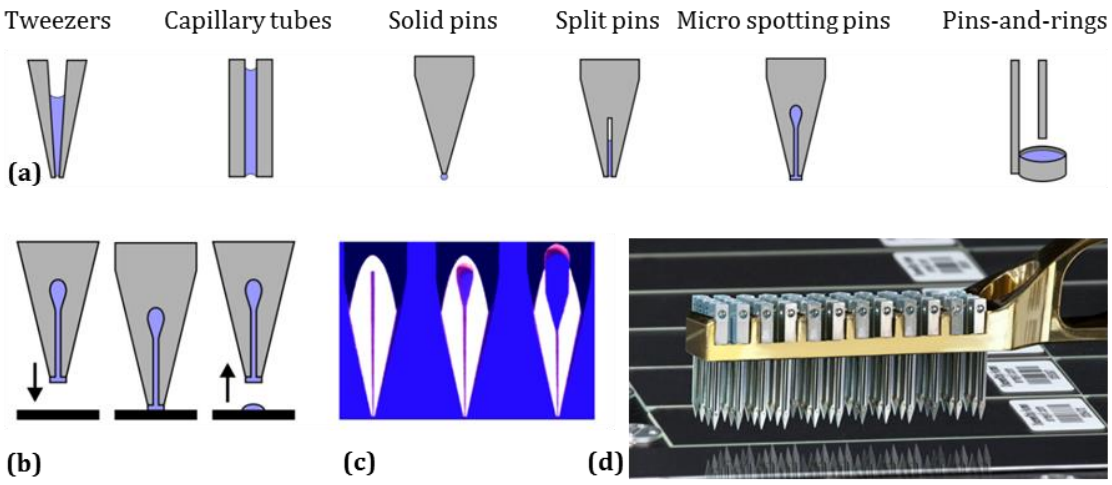

Figure 1-3: Contact printing of microarrays. **(a)** Different pin types [59]. **(b)** Working principle based on surface tension and adhesion (adapted from [60]). **(c)** A variety of pins allows users to define the delivery volume and the number of spots per loading [60]. **(d)** 48-pin printhead by Arrayit [61].

been reported that contact printing provides a high spot to spot and chip to chip variability [62], which makes sharing and comparison of experimental data difficult. The major requirements for successfully setting up and running a microarray contact printing facility can be found in [63,64].

Non-contact techniques

When using non-contact printing, a liquid droplet is formed and detached from a nozzle prior to being deposited on the microarray substrate. The reagents are loaded into reservoirs and transported to the printing tips using capillary forces or other pumping mechanisms. Generally, non-contact methods are best when the number of reagents to spot is low and the number of times to spot these reagents is high. Non-contact methods also become advantageous when the microarray surface is fragile [51]. Since a key element of any non-contact printing device is its actuator, it is common to classify non-contact printing according to the actuation method, with piezoelectric and thermal technologies being the most prominent ones. Arrayjet, BioFluidix, GeSim, microdrop Technologies, PerkinElmer and Scienion are among the companies providing piezoelectric driven devices for the fabrication of microarrays (Figure 1-4).

The printing technology used by Arrayjet comes from Xaar, a market leader in industrial ink jet solutions. The technology is based on a piezoelectric printhead which was adapted to meet the requirements of microarray fabrication. The printhead has 126 nozzles in a linear arrangement and is able to aspirate up to 32 samples simultaneously from 96 or 384 microtiter plates. It provides a significantly higher throughput compared to competitive products by PerkinElmer (parallel

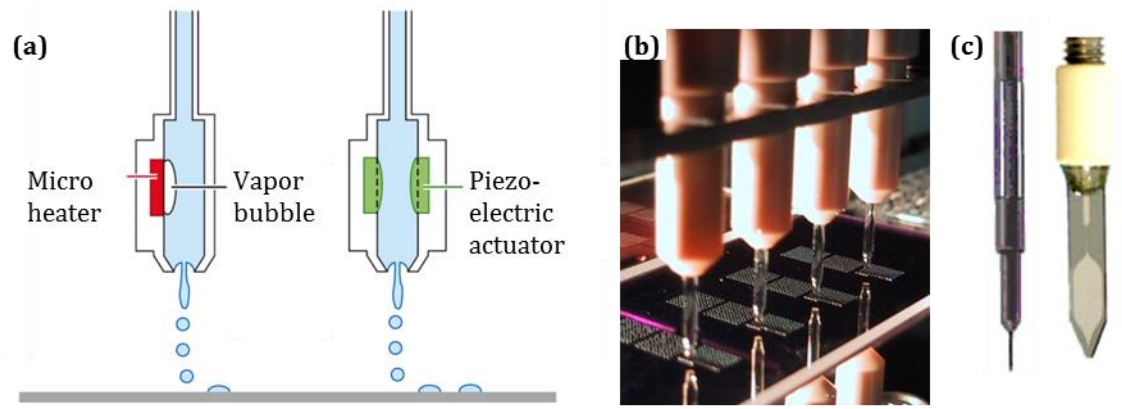

Figure 1-4: Non-contact printing. **(a)** Working principle based on a thermal and piezoelectric actuation (adapted from [65]). **(b)** Four tip printhead by PerkinElmer [66]. **(c)** Non-contact dispensing tips by microdrop Technologies (left) and GeSim (right) [59].

dispensing of up to four reagents), GeSim (up to 16) and BioFluidix (up to 96). Besides, the Arrayjet technology features high robustness as it was originally developed for industrial applications. The core of the printing technologies used by microdrop Technologies, PerkinElmer and Scienion is a glass capillary which is surrounded by a piezoelectric actuator. The free end of the capillary forms a dispensing nozzle. When actuated, the actuator compresses the capillary and generates a pressure wave into the liquid that causes a single droplet to be ejected from the nozzle. The droplet volume is in the picoliter range, depending mainly on the nozzle diameter and fluid properties. Besides filling the glass capillary from a supply reservoir through tubing, dispensers provided by microdrop Technologies and Scienion enable sample aspiration from a microtiter well plate through the nozzle tip in the capillary. This feature minimises the dead volume, which is essential when dealing with expensive reagents. GeSim, on the other hand, relies on a MEMS based silicon/glass dispenser with a piezoelectric actuator placed on top of it. When triggered, the actuator causes a displacement of a silicon diaphragm which leads to a compression of the liquid and ejection of a droplet from the nozzle.

Just as piezoelectric devices, thermal printing devices (bubble-jets) were originally developed for dispensing of ink [67]. The first reports of using bubble-jet technology for the fabrication of microarrays were published in the late 1990s and early 2000s [68-71]. In all studies, the authors used commercially available thermal inkjet printheads, which were adapted to print biomolecules. Many reports have indicated that there was no significant functional damage to the deposited biological samples caused by high temperatures applied in thermal inkjet technology (200 °C - 300 °C) [72]. However, heating of the reagents to such high temperatures, even for the short period of typically 2 µs, raises concerns about their possible

thermal degradation. For example, Setti *et al*. reported the activity loss of enzymes after they were printed with a modified Olivetti thermal printhead [73] and Xu *et al*. observed cell lysis of approx. 8 % after cells were printed with a modified Hewlett Packard thermal printhead [74]. Nevertheless, the degree of degradation depends significantly on the thermal sensitivity of the reagents and has to be considered individually for each application. For this technology to go mainstream, there are also technical hurdles to overcome, e.g. efficiently picking up the biological reagents from a micro plate and avoiding carryover contamination when changing the reagents in the reservoirs [51]. So far, there is no product enabling fabrication of microarrays using bubble jet technology.

1.3.2 In situ synthesis

In situ (on chip) synthesised oligonucleotide microarrays are manufactured by using a method developed by Fodor *et al*. [5]. The method combines solid-phase chemistry, photosensitive protecting groups and photolithography in order to achieve light-directed, spatially addressable parallel chemical synthesis of chemical products. Affymetrix, the industry leader in the field, has pioneered the field of in situ microarrays by introducing the GeneChip. The fabrication of the GeneChip involves semiconductor-based photochemical DNA synthesis on a five-inch square quartz substrate (Figure 1-5). GeneChips consist of up to 25 base-pair long probes (25-mer). For each layer and each base, another photolithographic mask is re-

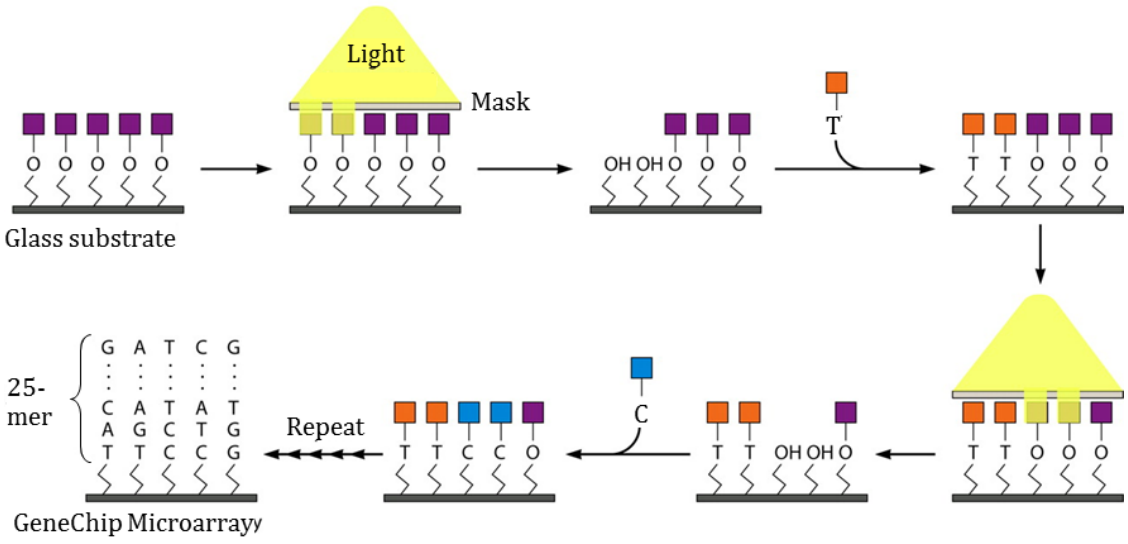

Figure 1-5: GeneChips - Schematic representation of the DNA synthesis cycle (adapted from [53]). Synthetic linkers containing photochemically removable protecting groups are attached to a quartz substrate. Subsequently, photolithography is applied to produce localised deprotection. Chemical building blocks are incubated with the substrate, and chemical coupling occurs in those regions that have been illuminated. The synthesis proceeds by repeating the steps of deprotection and coupling until the reagent sequences, usually 25-mers, are completed.

quired, i.e. a set of up to 100 masks is necessary for one GeneChip layout. Changing the layout requires a new mask set which makes the Affymetrix technology reasonable for fabricating large numbers of microarrays of the same design. Once the DNA synthesis is complete, the substrate is diced into individual arrays which are packaged into cartridges. A typical array has a size of 1.28 cm^2 and contains about 1.4 million features at a pitch of eleven microns. A reduction of the pitch down to five microns, as available since 2005, yields more than 6.5 million features on the same format [75].

In 1999, a more flexible, maskless method for producing DNA microarrays by means of light-directed chemistry was described by Singh-Gasson and Green *et al*. [76]. Soon afterwards, the method was commercialised by Xeotron (acquired by Invitrogen in 2004), Febit (insolvent since 2004) and Roche NimbleGene. At the heart of the maskless method is a digital micromirror array that replaces the physical chrome masks with "virtual masks" by switching individually addressable mirrors "on" and "off" according to a digital mask file. The mirror input signal is coordinated with the synthesis chemistry in a way that enables the synthesis of DNA fragments on solid glass supports. The method was most successfully implemented by Roche NimbleGene with up to 4.2 million 85-mer DNA fragments synthesised in a single microarray [77]. The maskless approach provides a more cost-efficient method to create high-density custom microarrays as compared to the Affymetrix approach.

Agilent Technologies, a spin-off of Hewlett-Packard, manufactures in situ synthesised DNA microarrays based on the SurePrint technology. The technology can be traced back to a method for in situ oligonucleotide synthesis based on a modified ink-jet printing [78]. The method was further developed and characterised by Hughes *et al*. [79]. Instead of printing pre-synthesised oligonucleotides, the in situ SurePrint technology prints 60-mer length oligonucleotide probes, base-by-base, from digital sequence files onto surface-modified glass slides (Figure 1-6). SurePrint employs a five-"ink" technology – four bases plus catalyst. The order of the

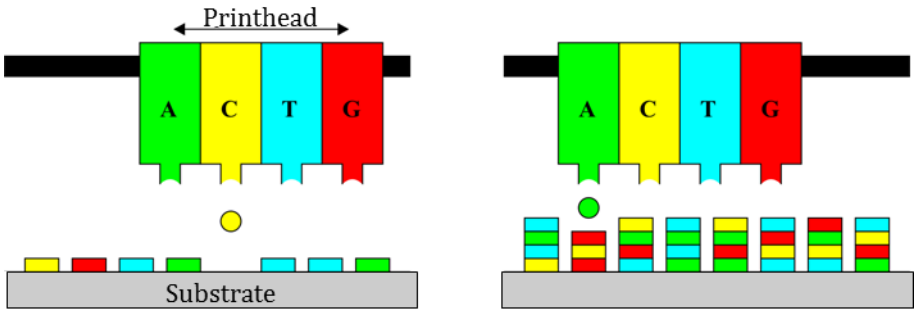

Figure 1-6: In-situ DNA microarray fabrication with the Agilents SurePrint technology.

printed bases determines the probe sequence. Caused by the natural limitation of liquid handling, microarrays fabricated by the SurePrint technology contain 1 million features at most, which is significantly lower compared to light-directed synthesis. In addition to buying catalogue microarrays, researchers can use the eArray web-based application provided by Agilent in order to design and order their own microarray layouts.

1.4 Fabrication of microarrays using the TopSpot technology

Due to the complex nature of chemical synthesis and the expense involved in production, in situ synthesis is only suitable for custom microarrays to a limited extent. The non-contact TopSpot technology is an alternative to piezo tip and pin printers which currently dominate the market for custom microarrays. The TopSpot technology is based on reusable piezo-actuated printheads which enable non-contact microarray fabrication at a pitch of typically 500 µm. The technology was developed by HSG-IMIT and IMTEK and is currently commercialised by BioFluidix. The printheads can be operated in two different ways, i.e. the pneumatically actuated standard technology and the Vario technology which is based on direct liquid displacement (Figure 1-7).

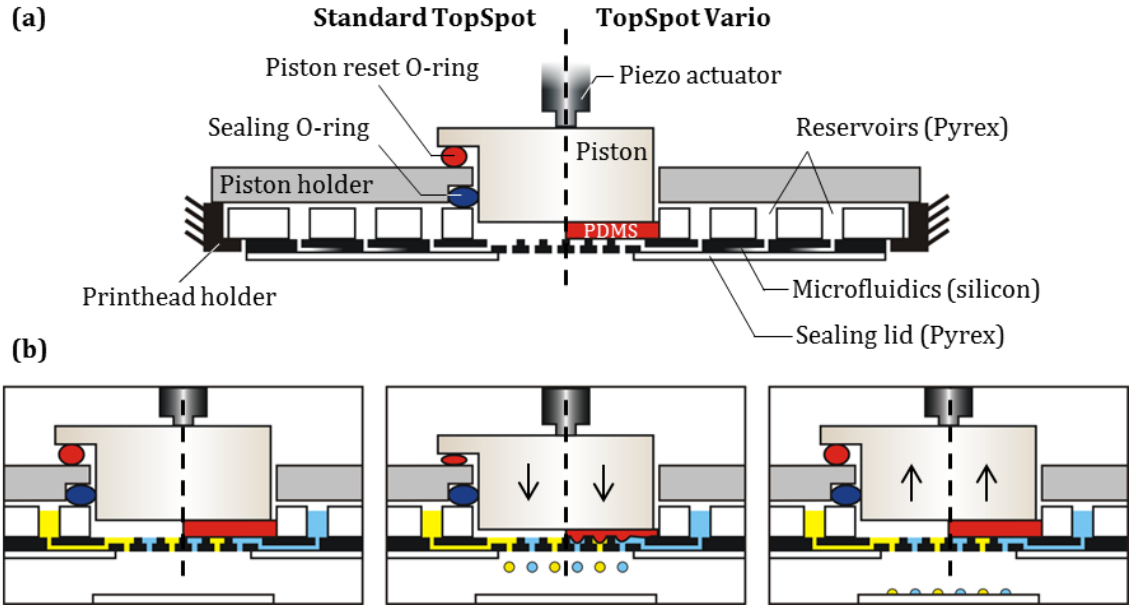

Figure 1-7: TopSpot technology. **(a)** Schematic cross-sectional view of a standard TopSpot printhead (left) and TopSpot Vario printhead (right). **(b)** Working principle of the pneumatically actuated standard printhead (left sequence) and the Vario printhead (right sequence).

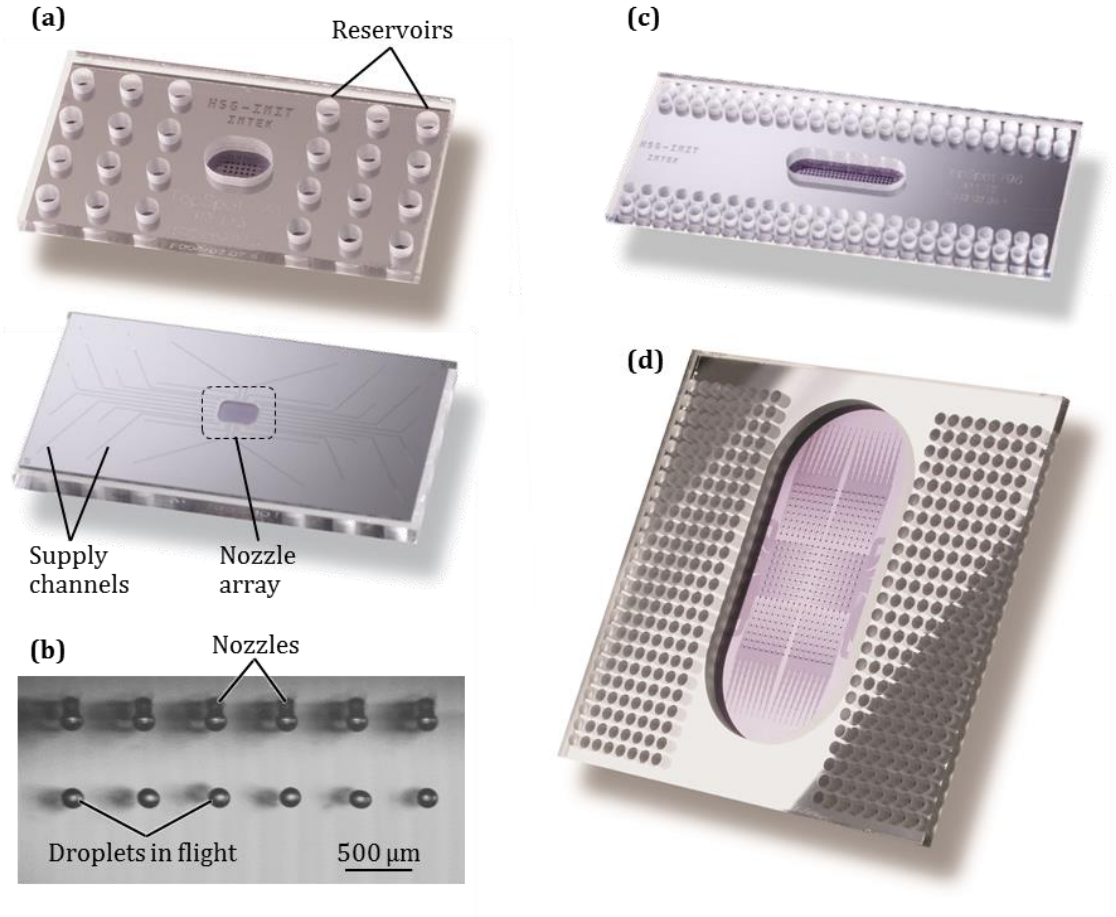

Figure 1-8: Overview of different printhead formats. **(a)** Top and bottom side of a 24-channel printhead. **(b)** Stroboscopic image droplets in flight. **(c)** Top side of a 96-channel printhead. **(d)** Top side of a 384-channel printhead.

1.4.1 Standard TopSpot technology

In the standard TopSpot technology, a piezo-stack actuator is used to drive a piston in the sealed gas cavity above the nozzles of a silicon/glass printhead. The downward stroke of the piston generates a pressure increase by compression of the gas volume in the cavity. The pressure simultaneously affects all nozzles and causes the parallel ejection of a single droplet out of each nozzle (Figure 1-7(b), left sequence). The volume of the ejected droplets is in the range of 1 nl, which allows for over 5000 dispensing cycles without reloading the printhead. The printheads contain up to 384 reservoirs, each one being connected to a dispensing nozzle by a microfluidic channel. The nozzles are arranged in a grid of 6×4, 24×4 or 24×16 for the 24-, 96- and 384-nozzle printheads, respectively (Figure 1-8). A one-to-one format conversion from the microtiter plate format of the reservoirs to the microarray format of the nozzles is provided according to a patented method for format conversion [80].

To improve the printing reproducibility, the nozzles are coated with a hydrophobic silane. For a 24-nozzle printhead, the inter nozzle reproducibility indicated by the volume variation of the dispensed droplets (CV) is less than 3 % [81]. A stroboscopic image of a parallel droplet ejection out of a 24-nozzle printhead is shown in Figure 1-8(b). The microchannels of the printheads are rendered hydrophilic by oxygen plasma treatment to support the sample transport from the reservoirs to the nozzles by capillary forces. Gutmann *et al*. have demonstrated the suitability of the standard TopSpot technology for manufacturing DNA microarrays [82], protein microarrays [83] and living cell microarrays [84].

1.4.2 TopSpot Vario

The actuation principle of the TopSpot Vario technology is based on direct liquid displacement by using an incompressible elastomer instead of a compressible gas cavity between the piston and the nozzles. The downward stroke of the piston drives the elastomer into the displacement chambers, thus causing the parallel ejection of single droplets out of each nozzle (Figure 1-7(b), right sequence). The TopSpot Vario technology is characterised by a linear relationship between piston stroke and droplet volume. By tuning the stroke between 2.5 µm and 13.5 µm, the droplet volume can be tuned between 250 pl and 1500 pl [85]. Priming of the TopSpot Vario microchannels is realised by implementing a principle for bubble-free priming of blind microchannels [86]. Currently, TopSpot Vario printheads are available as a laboratory prototype.

1.5 Aim and structure of the thesis

In a general sense, the objective of the thesis is to provide greater manufacturing flexibility and to reduce the costs of silicon/glass microfluidic devices manufactured by means of standard MEMS based technologies. In this context, the term “manufacturing flexibility” refers to the ability for fast verification of new designs and the ability to handle low production volumes and fluctuating demands at short lead times.

The more specific aim of the thesis is to *identify the most appropriate technology for production of TopSpot printheads with respect to a set of requirements for production volumes between 10 and 100*. The focus is on the development and characterisation of flexible fabrication technologies and low cost printhead designs.

Currently, TopSpot printheads are manufactured using established MEMS technologies: Silicon micromachining is applied to realise the microfluidic structures, the interface layers are manufactured in glass and the individual components are joined by silicon/glass anodic bonding. The advantages of this configuration are obvious: Fast and precise fabrication of deep trenches in silicon wafers, optical transparency of the glass covers and high mechanical stability of the printheads.

Another important aspect is the possibility to combine the individual components by anodic bonding: a strong chemical bonding process without additional intermediate layers. Anodic bonding eliminates the common risk of clogging or deformation of the microchannels when the components are combined using adhesive techniques. As the printheads were gradually optimised to meet the stringent requirements for microarray fabrication, manufacturing flexibility and costs have not been considered at the same level of detail as functional requirements such as printing performance and parallelisation.

A major drawback of the silicon/glass printheads is that they are less responsive to the fast changing and increasingly diverse customer needs. Important contributors to this situation are the semi-finished glass components because they have long delivery times or need to be ordered in advance and lay in stock. Obviously, the use of such special semi-finished components is contradictory when it comes to manufacturing flexibility and low costs. Against this background, one specific objective of the thesis is the development and characterisation of *silicon/polymer printheads* which provide higher flexibility at lower costs by using polymer materials instead of glass. As a consequence of the new material combination, special emphasis is placed on the technological challenge to combine silicon and polymers in one device, making the microfluidics in silicon and the reservoirs and sealing lid in polymers. Another objective of the thesis is to identify possible technologies for the production of *all-polymer printheads* and verify their general applicability for the production of microarrays.

The classification of costs and basic knowledge about cost drivers in microfluidic manufacturing are presented in *Chapter 2*. This chapter also describes the main differences between microfluidic and semiconductor devices and motivates the examination of cost reduction approaches different from those in the semiconductor industry. Besides, Chapter 2 explains the theoretical background related to cost calculation and techniques for cost reduction.

Chapter 3 covers the basics of the analytical hierarchy process (AHP), a multi-criteria decision-making method. In the thesis, the AHP is used to measure the importance of individual printhead requirements and find the most appropriate technology for production of TopSpot printheads with respect to those requirements.

The initial situation including description of the fabrication process as well as cost, yield and lead time analysis is presented in *Chapter 4*. Special emphasis in this chapter is placed on the relationship between manufacturing costs and production volume.

Chapter 5 exploits the potential for cost reduction by scaling, i.e. reducing the printhead size and/or using larger wafers. It gives an introduction in dry film resists together with a systematic overview of research publications related to dry film resists for microfluidic and MEMS applications. The main differences between dry film resists and liquid resists are discussed. Finally, the chapter presents two alternative printhead designs that make use of dry film resist: the silicon/polymer and the all-polymer printhead. In both designs, one or more printhead components are provided by dry film resists.

Chapter 6 deals with the experimental aspects of dry film resist technology. The main focus is on processing and characterisation of three resist types regarding essential properties such as wetting behaviour, optical transparency and biocompatibility.

Chapter 7 and *Chapter 8* present the fabrication and experimental characterisation of the silicon/polymer and the all-polymer printheads, respectively. The main focus is placed on printhead performance, manufacturing costs, lead time, yield and lifetime. Additionally, in Chapter 7, the flexibility of the silicon/polymer technology is demonstrated by scaling up the fabrication process to a larger wafer format and implementing printheads with microchannels of extremely high density.

In *Chapter 9*, the different printhead concepts are evaluated using the AHP. The evaluation considers two customer profiles with different requirements on the printheads. The main conclusions of the thesis are given in *Chapter 10*.

2 COST STRUCTURE OF MICROFLUIDIC MANUFACTURING

2.1 Classification of costs

In a commercial company, costs are generally defined as the monetary value of resources required for manufacturing and delivering products. Resources in this context might include machines, employees, materials, time, intellectual properties etc. The basic costs that originate with the product itself are the manufacturing costs, i.e. costs that can be assigned directly to the manufacturing process. In addition, there are overhead costs that cannot be directly assigned to a product, e.g. electricity and administration. Overhead costs combined with the manufacturing costs form the total costs of a product. The total costs, in turn, contribute to the lifecycle costs which are costs that accrue to the product user. These include installation, training, maintenance etc. (Figure 2-1) [87].

There is a number of ways to classify costs. One common classification method is according to the cost type, e.g. material costs, personnel costs, or machine costs. Another classification is based on whether costs can be directly assigned to a specific product or activity and breaks costs down into direct and overhead costs. Costs can be further classified based on their dependence on the production quantities: Variable costs accrue only when production takes place and are proportional to the production quantity. Typical variable costs are material costs or machine and operator cost that accrue during the production of a product. Fixed costs on the other side are typically nonrecurring and independent of the production quantity, e.g. costs for lithography masks, tooling or CNC programming. As shown in Figure 2-2, these are not "other" costs but just different ways of looking at costs.

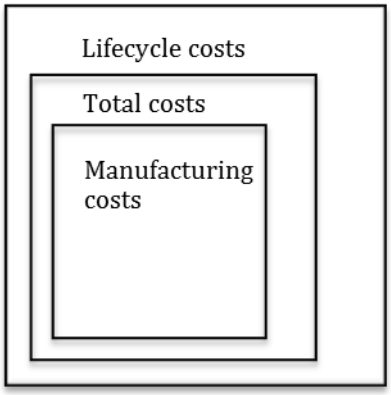

Figure 2-1: Classification of costs. Manufacturing costs and overhead form the total costs of a product. The total costs, in turn, contribute to the lifecycle costs, which are costs that accrue to the product user [87].

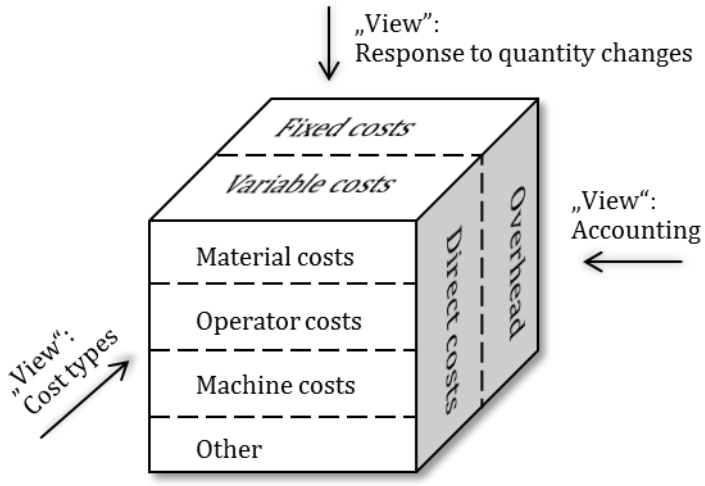

Figure 2-2: Different "views" on the cost of a product [87].

The development of cost-effective products is a team task with responsibilities shared between different company departments. In the R&D department, information coming from different areas is used to develop marketable products. One of the most important aspects in product development is the requirement to consider company-specific technological limits and to bridge the gap between the requirements of the customer and what is technically and economically feasible. When the design is complete, the product costs are largely fixed. Therefore, manufacturing costs have to be considered from the very beginning of product development [87].

2.2 Comparison to semiconductors

One industry that is frequently used to draw parallels to microfluidics is the semiconductor industry. Both industries are based on microscale structures and consider miniaturisation as the main factor for technological advances and low costs. Many of the early works in microfluidics utilised fabrication methods directly borrowed from the semiconductor industry. Moore's Law [88] and the huge economic impact of semiconductor devices have raised hopes of similar development in analytical sciences using microfluidics as the driving innovation [89]. Indeed, microfluidics has become a huge field of research with more than 13 000 publications in 2013 [90]. On the other hand, this research is mainly limited to proof-of-concept demonstrations and only a few of the developed prototypes have been transformed into commercial devices [91]. While the purely technological ability to manufacture microfluidics has ceased to be a challenge since about a decade, the high manufacturing costs are still one of the most important hurdles for the commercial success of microfluidic devices [91,92]. If Moore's Law would hold true for microfluidics, the costs of microfluidic devices would have to drop by a factor of two every two years. Since this is not the case, the cost analogy between microflu-

idic and semiconductor devices is misleading. This section provides an overview of the main cost drivers in microfluidics and shows the key differences when compared to semiconductors.

2.2.1 Materials

For semiconductor devices, silicon is by far the dominant material and consequently, silicon wafers are thoroughly characterised by having a standard size and well known properties such as purity, doping level, thickness variation, warp, bowl etc. In contrast, the field of microfluidics relies on a loose collection of materials, e.g. silicon, glass, ceramics and, increasingly often, polymers. The reason for this material diversity is the diversity of microfluidic applications. Although appreciated in academia, this variety slows down standardisation and the associated increase of market share and cost reduction. Material selection in microfluidics is not as straightforward when compared to semiconductors. It is a very important process that largely determines the performance of a device in terms of functionality and economic feasibility. A common approach for material selection is to define the requirements and to narrow down the choices by the method of elimination.

2.2.2 Manufacturing yield

The manufacturing yield is the ratio of devices within the specifications to the overall number of possible devices at the beginning of the manufacturing process. It is an important factor to determine costs: Doubling the yield leads to reduction of the manufacturing costs by 50 %. The total manufacturing yield is the product of the process yields of all individual processes required to produce the device:

$$Y_{\mathrm{tot}} = \prod_{\mathrm{i}=1}^{\mathrm{m}} Y_{\mathrm{i}} \tag{2.1}$$

where Y_{tot} and Y_{i} denote the total and the process yield, respectively. Figure 2-3 shows the total yield as a function of the process yield for different number of processes. In the semiconductor industry, the total yield is routinely above 90 % whereas yields in microfluidic production are often considerably lower [93]. In fact, Equation 2.1 and Figure 2-3 give an oversimplified view of a complex issue and are not useful in answering the critical question: How many devices meet the specification?

In semiconductor manufacturing, the percentage of acceptable devices is typically represented by the die yield. The term *die* refers to the area of a wafer which represents one functional unit. Assuming that defects are randomly distributed over the wafer and that the yield is inversely proportional to the complexity of the fabrication process, the die yield is given by the following empirical model:

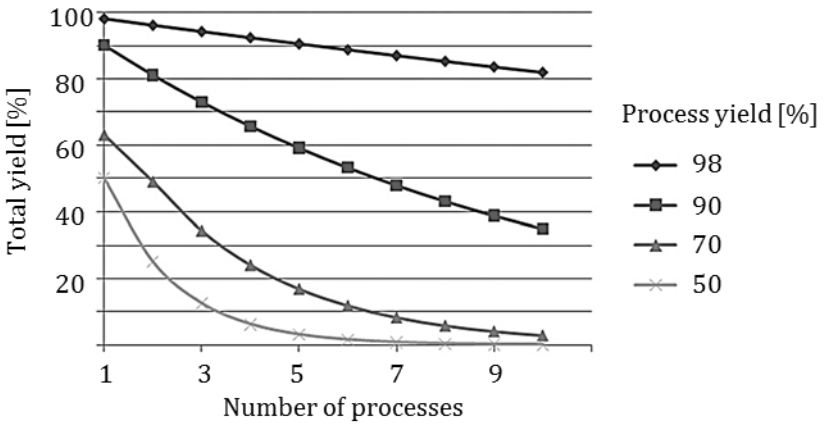

Figure 2-3: Simplified representation of the total yield as a function of the process yields and the number of processes [91].

$$Die\ yield = Wafer\ yield \times \frac{1}{(1 + Defects\ per\ unit\ area\ \times Die\ area)^N} \qquad (2.2)$$

where N is a parameter called *process-complexity factor* and *wafer yield* accounts for wafers that are not completely bad (typically close to 100 %). In the semiconductor industry in 2010, the defects per square centimetre were typically 0.016 to 0.057 and N ranged from 11.5 to 15.5 [94]. Substituting these values in Equation 2.2, the die yield and correspondingly the manufacturing costs for any die size can be reliably estimated early in the design phase and before starting production. In contrast, the final device yield and costs in microfluidics often cannot be predicted before going into serial production.

2.2.3 Learning curve and manufacturing volume

It is well known that manufacturing costs decrease over time even without improvements in the basic technology. The underlying principle is the learning curve which depends on the manufacturing volume and which is best measured by change in yield. The manufacturing volume affects costs in several ways: Larger volumes not only decrease the time needed to get down the learning curve but also decrease costs by increasing purchasing and manufacturing efficiency. Besides, larger volumes decrease the amount of fixed costs that must be amortised by each device, thus allowing manufacturing cost and selling price to be closer to each other [94].

Cost reduction by large quantities is known as *economies of scale*. In semiconductor terminology, a small production quantity means a lot size of less than 1 million parts. The production capacities of typical semiconductor fabrication plants are in

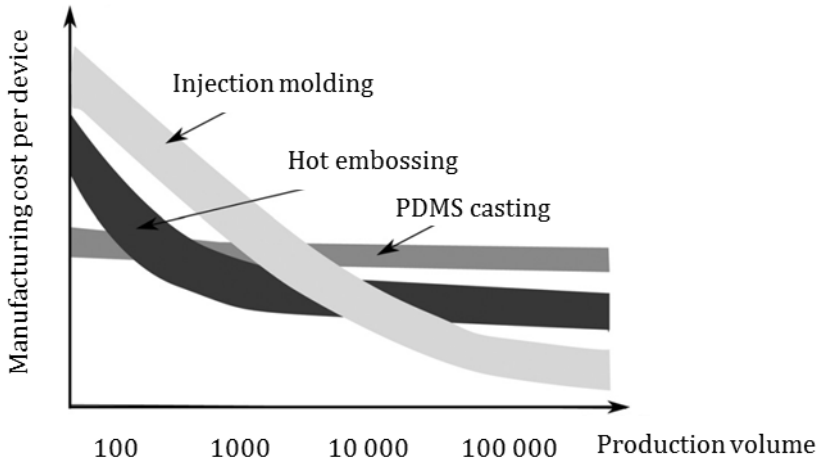

Figure 2-4: A qualitative representation of the economies of scale for replication techniques commonly used in microfluidic manufacturing [97].

the range of 35 000 to 80 000 wafer starts per month and the learning curves lead to a cost reduction of about 10 % for each doubling of the lot size [94].

In contrast, microfluidic devices are often ordered in lots of 50-100 pieces [95], and sometimes the number of pieces to be created of one specific design is even as low as one [96]. This poses a serious challenge to engineers and is one important factor for the comparatively high costs of microfluidic devices. The economies of scale of commonly used replication techniques for microfluidic devices are shown in Figure 2-4. For small production volumes, e.g. for custom designs and prototyping, PDMS casting and hot embossing are more cost-effective than injection moulding, and vice versa.

2.2.4 Feature size, die size, wafer size

Since 1965, the semiconductor industry follows Moore's Law towards smaller circuit elements and today feature sizes have decreased down to 22 nm [98]. According to the roadmap of ASML, the world's leading manufacturer of lithography systems, a resolution of 10 nm will be commercially available in the 2016 time frame [99] and the transition to the next generation 450mm wafer size is scheduled for 2018 [100].

Different wafer sizes are shown in Figure 2-5. The number of dies per wafer can be estimated by [101]:

$$Dies\ per\ wafer = \frac{\pi \cdot (\frac{Wafer\ diameter}{2} - 0.58 \cdot \sqrt{Die\ size})^2}{Die\ size} \tag{2.3}$$

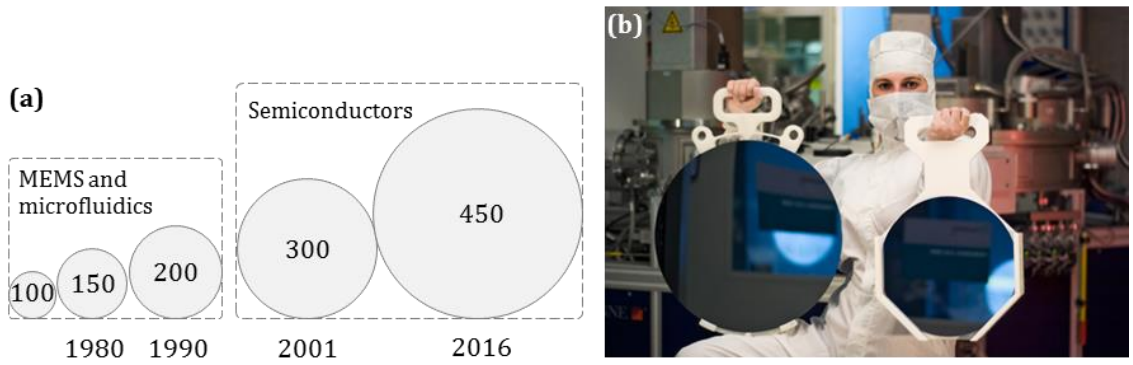

Figure 2-5: Comparison between different wafer sizes. **(a)** Wafers sizes used in the different industries and the corresponding year of introduction. **(b)** Semiconductor state-of-the-art 300 mm wafer and next generation 450mm wafer (image taken from [102]).

Figure 2-6: An example demonstrating the relationship between yield and die size.

Currently, the processing of a 300mm semiconductor wafer in a leading edge technology costs between $5000 and $6000 [94]. Using Equation 2.3 and assuming a die size of 239 mm^2, as used in Intel's Core i7-980, the number of dies per wafer can be calculated to be 261. Assuming a die yield of 90 % and using Equation 2.4, the manufacturing costs per die for Intel's Core i7-980 are calculated to be in the range of $21 to $26. Many microprocessors are even smaller, e.g. 32-bit processors are sometimes as small as 0.10 cm^2, and processors used for embedded control, e.g. in printers, microwaves etc., are often smaller than 0.04 cm^2 [94].

In contrast, the overall size of common microfluidic devices is significantly larger. It has been reported that typical sizes are in the range of 25 mm by 75 mm [103], which corresponds well to the size of the TopSpot printheads considered in this work. Substituting the above dimensions in Equation 2.3 and in consideration of the fact that silicon/glass microfluidic devices are processed on 200mm or smaller wafers, the number of devices per wafer is calculated to be less than 10. The fluidic

features are in the range of some tens of microns to a few millimetres, which is by orders of magnitude larger than the features in semiconductor devices. The further miniaturisation in microfluidics is limited by several factors, most notably by the need for large interfaces to laboratory equipment and by the requirements for minimum flow rates and channel dimensions [104]. For this reason, cost reduction by producing more features per area is not that powerful.

An important cost factor which is affected by the large size of microfluidic devices is the yield. The relationship between yield and size is exemplarily demonstrated in Figure 2-6, showing a yield improvement from 0 % to 77 % by reducing the size and placing more devices on a wafer. From the considerations above, it can be stated that miniaturisation in microfluidics provides fewer opportunities for cost reduction when compared to microelectronic devices.

2.2.5 Standardisation in product generation and manufacturing

Standardisation is generally accepted as a cost-reduction driver. The semiconductor industry is based on standard circuits which can be incorporated into different devices using accurate models and established design rules. Basically, semiconductor manufacturing follows standard processes which are common to all devices: oxidation, lithography, etching, doping, chemical vapour deposition and metallisation.

In contrast, the field of microfluidics is heterogenic and incorporates different platforms, e.g. capillary driven test strips, pressure driven devices, electrokinetic devices, centrifugal analysers, droplet based platforms and dispensing systems [105]. This diversity prevented the introduction of standards in the process of product generation and manufacturing. The development of microfluidic devices often starts from scratch and goes through several iterations making it slow and expensive. In order to speed up the research and reduce prototyping costs, researchers spend a lot of effort on developing simple and low cost fabrication processes. A very important aspect in this context is to consider the production-oriented use of the process at an early stage of the development. If this requirement is not properly considered, the step towards commercialisation might eliminate much of the development effort and require additional work to make the device function properly [106].

In a recent publication devoted to standardisation issues in microfluidics, it was suggested to adopt existing standards instead of trying to implement new approaches on a technological basis and not driven by market needs [89]. Due to the variety of microfluidic devices, standardisation is challenging but in fact there are standards that can be used. Recently, microfluidic engineers have demonstrated that widely used instruments like laboratory centrifuges, DVD drives and real-time PCR cyclers can be used to run microfluidic devices. The devices were either solid

plastic that can be produced by injection moulding, or foil cartridges manufactured using a thermoforming technology derived from the pharmaceutical blister packaging [107]. Besides the CD format, the micro titerplate [108] and the microscope slide [109] are other standard formats which provide enough space for common microfluidic applications and which can be well handled with existing laboratory equipment.

2.2.6 Back-end costs

In semiconductor manufacturing, back-end processing refers to operations that take place after the integrated circuits are created on the wafer. These operations are dicing, electrical wiring, packaging and final testing and they are typically executed according to a fixed sequence [110]. Likewise, back-end processing in microfluidics comes after micromachining. A major difference is that each microfluidic device requires an individual back-end procedure. Which steps are necessary and the order in which they have to be performed depends on the device and the application. Back-end processing in microfluidics accounts for a very significant part of the manufacturing costs and may cause up to 80 % of the total manufacturing costs [111].

Examples for back-end processes with a divergent contribution to costs in semiconductors and microfluidics are assembly, packaging and dicing. The assembly and packaging of microfluidic inkjet printheads can amount to several times the chip costs [93]. For thermal printheads, dicing is used to separate the dies and to expose the dispensing nozzles. Since a chip on the nozzle edge may deflect ejected droplets from their intended trajectory, dicing has to provide a smooth surface without chipped edges. To meet this requirement, the ink-jet industry uses high performance dicing saws with dynamic balancing, precision temperature control of the water jet cooling and adapted dicing blades [112]. Examples for other back-end processes of particular importance to microfluidics but of no relevance to semiconductors are wafer bonding, drilling of fluidic access holes, surface modification and the encapsulation of reagents.

2.2.7 Cost models

In the semiconductor industry, methods for calculation of the manufacturing costs are widely used and can reliably predict the costs per area depending on the used technology and the manufacturing volume. In microfluidics there are no cost models due to the fact that there are no standard processes. The costs in microfluidics are highly dependent on the individual product and the costs per area might range from comparable to those of semiconductors on the low side to orders of magnitude more expensive on the high side. Given the wide range and diversity of processes involved in the fabrication of microfluidic devices, it is practically impossible to provide a general model that allows accurate cost estimation. Rough cost

estimates can be obtained by using available MEMS cost models [113,114]. With those models, however, even though the process chain is known, it is very difficult to provide an estimation with reasonable accuracy until the device is in volume production [93].

2.3 Calculation

Like any other performance parameter, the costs of a microfluidic device can be measured with some degree of accuracy. Generally, when different approaches have to be compared, engineers disregard overhead and concentrate on the direct manufacturing costs. Each company has its own accounting method which suits best to its products and the used manufacturing processes. The costs of a silicon/glass microfluidic device can be calculated by the following equations:

$$Costs\ per\ device = \frac{Costs\ per\ wafer}{Devices\ per\ wafer \times Device\ yield} \tag{2.4}$$

$$Costs\ per\ wafer = \frac{Total\ manufacturing\ costs}{Wafer\ batch\ size} \tag{2.5}$$

$$Total\ manufacturing\ costs = Material\ costs + Machine\ costs + Operator\ costs \tag{2.6}$$

2.4 Techniques for cost reduction

Cost reduction can be achieved by different techniques, each of them associated with a different amount of effort. An important question that has to be answered at the beginning of a cost reduction project is how much effort is justified. The obvious answer is that the effort must not become more expensive than the achievable total reduction over the lifetime of the product. Identifying the appropriate effort is essential and depends on the cost per device, the production quantity and the achievable cost reduction. Usually, higher effort is reasonable for expensive products in single-unit production and for low cost products in large quantities. In all cases, any changes applied once a device has entered production, e.g. if it turns out that manufacturing costs are higher than expected, are costly and time consuming [91]. In cost reduction projects, consideration has to be given to the company size and its core competence. Large companies have advantages due to their financial power but organisational hierarchies and departmental thinking might be a hurdle. Small to medium companies have the advantage of more informality because employees are active in multiple functions, but they often do not manage cost projects systematically [115].

One of the greatest opportunities to reduce manufacturing costs is through proper setting of product requirements and specifications. Manufacturing tolerances are an important factor, with tighter tolerances leading to higher costs. Since extremely tight tolerances add cost but do not explicitly add value to the device, tolerances appropriately meeting the requirements have to be specified. In many cases, product developers tend to consider only processes and materials which they are familiar with. As a consequence, new and cost-effective alternatives, e.g. new developments in the suppliers market, are often neglected.

Empirical studies indicate that about 10 % reduction of the manufacturing costs can be achieved by slimming down the product, i.e. better control in manufacturing, standardisation of parts etc. Another 20 % to 30 % might result from an adaptive design project. In an adaptive design, the working principle remains the same but sizes, materials or manufacturing processes are adapted to new requirements and constraints. A reduction of more than 40 % often requires the development of new concepts. Such concepts are developed within original design projects in which problems are solved using new approaches or new combinations of known solution principles [87]. Two commonly used methods for cost reduction are value analysis and target cost oriented development.

2.4.1 Value analysis

Value analysis was developed in the 1940s by L. D. Miles in order to identify unnecessary product costs, i.e. costs that do not provide functionality. Miles predicted that 15 % to 25 % and very often even more of the manufacturing costs of a product are unnecessary because they can be saved without any compromise in functionality. Even though value analysis has additional advantages which do not show up as cost reduction, its main objective is to provide equivalent performance for lower cost [116]. By a widely accepted definition, the value of a product is the ratio of function to costs and it can be increased by either improving the function or reducing the costs:

$$Value = \frac{Function}{Costs} \tag{2.7}$$

Over the years, the application areas of value analysis were extended to include original design, i.e. development of new products, and immaterial objects [117]. However, in about 60 % of the cases, value analysis is still used for its originally intended purpose: to eliminate unnecessary costs of existing products [87]. A study based on 800 value analyses showed that in 80 % of the cases the repayment period was less than one year [118]. By now, the potential of value analysis has been confirmed by numerous studies. Recent data released by the Association of German Engineers (VDI) and based on several thousand value analysis projects

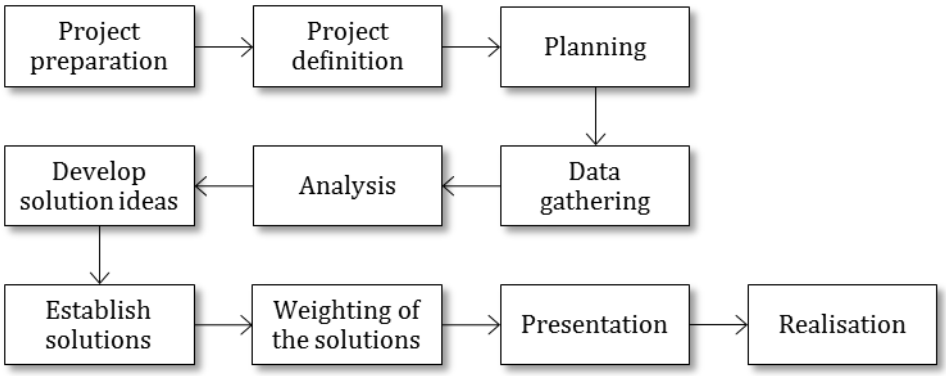

Figure 2-7: Value analysis workflow according to DIN EN 12973 [120].

shows a reduction of the manufacturing costs between 5 % and 60 % with an average of 20 % to 25 % [119]. These values are not static because cost improvements are affected by a number of conditions that change with time and there is no stable optimum. Eliminating unnecessary costs is a form of continued technical progress and value analysis should be repeatedly updated in order to reflect technological and other changes.

Originally, value analysis was performed following a six-step procedure: the value analysis job plan. Today, a value analysis is conducted on the basis of ten steps according to EN 12973 [120]. An overview of these steps is shown in Figure 2-7.

2.4.2 Target cost oriented development

Target cost oriented development originates from the cost management process in Japanese companies. In the traditional product development, the primary focus is on performance with manufacturing costs being the basis for determining the selling price. In target costing, product development is based on what the customer is willing to pay and not on what the manufacturing costs are. Therefore, the first step is to establish a competitive selling price and, based on this, the target manufacturing costs are calculated by [121]:

$$Target\ cost = Selling\ price - Profit \tag{2.8}$$

Target cost oriented development provides the financial framework at the very beginning of the development process and has proven to be successful in different industries. Similar to the evolution of value analysis, target costing has grown from a simple cost reduction procedure to a strategic profit planning model. In fact, some authors even consider value analysis as an integral part of target costing which can be used as a tool to achieve the defined cost target [121].

2.4.3 General rules

Ehrlenspiel *et al.* used input from both value analysis and target costing and defined a guideline with simple and generally applicable rules for the reduction of manufacturing costs [87]. The guideline follows a natural way of thinking and, in a more general sense, provides an adaptive procedure for the solution of different problems. The guideline of Ehrlenspiel *et al.* does not provide a standard recipe but rather an assistance in developing own solutions according to company and product characteristics. According to this guideline, the reduction of manufacturing costs can be broken down into three main steps: (1) task clarification, (2) solution search and (3) solution selection.

The first step includes analysis of the current manufacturing costs, cost targets and functional requirements. In the second step, alternative materials, processes and assembly sequences are considered. Problems are split into sub-problems to simplify the search for possible solutions. In the last step, the solutions are analysed and evaluated with respect to the requirements. Here, engineers face the challenge of deciding how important one requirement is with respect to the others and which solution is the best. The decision process is based on simulations and/or experiments and is often supported by multi-criteria decision methods. Such methods are taken into consideration in order to analyse and understand complex relationships. The analytic hierarchy process (AHP), one of the most widely used methods for multi-criteria analysis, is used in this thesis and described in the next chapter.

3 DECISION MAKING WITH THE ANALYTICAL HIERARCHY PROCESS

The analytic hierarchy process (AHP) is a multi-criteria decision-making method used to facilitate decisions that involve multiple criteria. The method was originally devised by Saaty in the 1970s [122] and has been extensively analysed and refined since then. Nowadays, the AHP is practised by scientists and engineers in different application areas, e.g. manufacturing, social, management, political etc. [123]. The fundamental input to the AHP are answers to a series of pairwise comparison questions which are used to establish priorities for the decision criteria and to rank alternatives with respect to these criteria. In the comparison process, the decision makers can use existing data but they also can judge based on their personal impression. The comparison scale consists of verbal judgments which can be transformed into numerical values according to the nine point importance scale in Table 3-1. Thus, attributes measured on different scales, e.g. performance and costs, can be compared to one another in a rational and consistent way. This flexibility is one important property of the AHP. Once a set of criteria and alternatives has been identified, the AHP can be performed by the flowchart presented in Figure 3-1. The main steps of the AHP are described in the next sections.

Table 3-1: The fundamental scale of the AHP. The scale enables to transform verbal judgments into numerical values in order to establish priorities for the decision criteria and rank different alternatives with respect to those criteria [122].

Importance scale	Definition	Explanation
1	Equal importance	Two activities contribute equally to the objective.
3	Moderate importance	Experience and judgment slightly favour one activity over another.
5	Strong importance	Experience and judgment strongly favour one activity over another.
7	Very strong importance	An activity is strongly favoured and its dominance is demonstrated in practice.
9	Extreme importance	The evidence favouring one activity over another is of the highest possible order of affirmation.
2, 4, 6, 8	Intermediate values between two adjacent judgments	
Reciprocals	If activity *i* has one of the above numbers assigned to it when compared with activity *j*, then *j* has the reciprocal value when compared with *i*.	

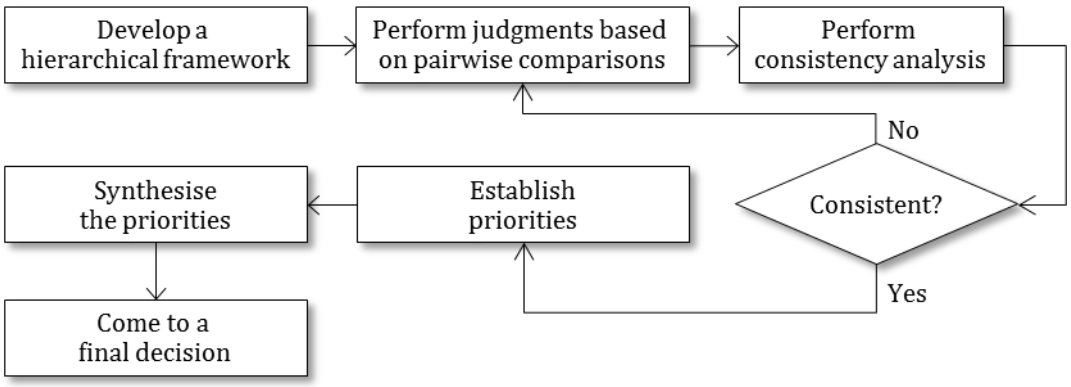

Figure 3-1: The workflow of the AHP.

3.1 The hierarchical framework

In the AHP, the first step is to provide an overall view of the decision problem by decomposing it into a multi-level hierarchic structure. In its simplest form, the hierarchy comprises three levels: The overall goal is in the top level, in the second level are the criteria which contribute to the goal, and the lowest level represents the alternatives which have to be evaluated in terms of the criteria. Figure 3-2 shows a three-level hierarchy with four criteria and three alternatives. In AHP terminology, each box is called a *node*. A node that is connected to one or more nodes in a level below is called a *parent* and the nodes in the level below are its *children*. The number of nodes in one hierarchical level should be no more than seven. The background for this conclusion is the experimental finding that there is a limit of human capacity to process information on simultaneously interacting elements with reliable accuracy, and that this limit is seven [124]. Therefore, criteria are often arranged in a cluster. In this way, it is possible to focus more narrowly on one specific part of the problem while keeping the complexity at a manageable level.

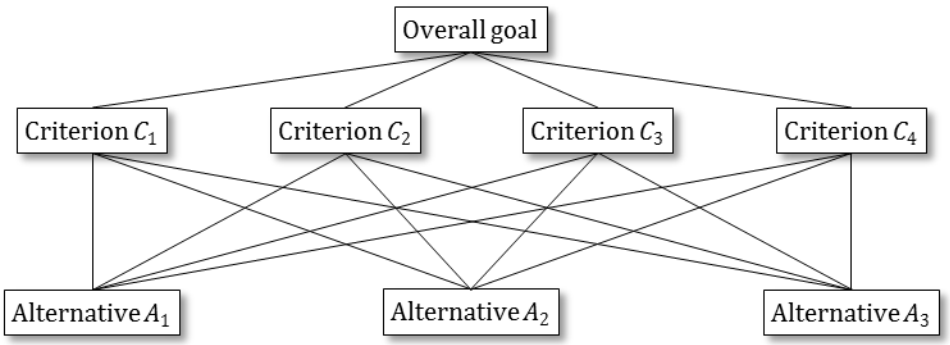

Figure 3-2: A hierarchical framework with four criteria and three possible alternatives.

3.2 The pairwise comparison process

After the hierarchical framework has been set, the comparison process is accomplished by comparing the nodes having a common parent in the hierarchical framework. The comparison process starts at the top of the hierarchy by asking a question like: "How important is criterion C_1 relative to criterion C_2 with respect to the overall goal?". The judgments are performed by using the fundamental scale in Table 3-1 and arranged in a quadratic matrix as shown in Table 3-2. The diagonal elements, i.e. when one node is compared to itself, are always 1, and the elements below the diagonal are the reciprocal mirror image of the elements above it. Mathematically, such comparison matrix is characterised by:

$$\boldsymbol{A} = (a_{ij}) \tag{3.1}$$

$$a_{ii} = 1 \tag{3.2}$$

$$a_{ij} = 1/a_{ji}. \tag{3.3}$$

Once the pairwise comparison for one level is completed, a series of further comparisons are performed for the nodes in the lower levels. The comparisons at the lowest level give the relative performance of the alternatives with respect to their parent criterion. Here, the questions to be answered are of the kind: "How is alternative A_1 performing compared to alternative A_2 with respect to criterion C_1?".

Generally, if a decision problem has m alternatives and n criteria, then n comparison matrices of order $m \times m$ and one additional matrix of order $n \times n$ have to be built. In case of the hierarchy in Figure 3-2, there will be a total of five comparison matrices: four 3×3 matrices for comparing the three alternatives with respect to each of the four criteria and one 4×4 matrix for comparing the criteria with respect to the goal.

Table 3-2: An example of a pairwise comparison matrix for evaluating the relative importance of the four criteria C_1 to C_4 with respect to the overall goal.

	C_1	C_2	C_3	C_4
Criterion C_1	**1**	7	5	9
Criterion C_2	1/7	**1**	1/3	3
Criterion C_3	1/5	3	**1**	3
Criterion C_4	1/9	1/3	1/3	**1**

3.3 Consistency analysis

A comparison matrix $\boldsymbol{A}$ is completely consistent if the following condition is satisfied:

$$a_{ik} \cdot a_{kj} = a_{ij} \tag{3.4}$$

However, perfect consistency rarely occurs in practice and inconsistent judgments occur due to different reasons, especially when dealing with a high number of comparisons. For example, the judgments $a_{ik} = 3 \; and \; a_{kj} = 5$ cause inconsistency simply because $a_{ij} = 15$ is outside the upper limit of the scale (which is 9). Besides, it might be difficult to achieve consistency because, given three alternatives A_1, A_2 and A_3 the decision maker might prefer A_1 over A_2, A_2 over A_3 but A_3 over A_1. Obviously, it is unrealistic to expect judgments which are absolutely consistent and insisting on an absolute consistency in the AHP is not advisable [125]. Instead, the AHP provides a measure of inconsistency and as long as the inconsistency does not exceed a certain threshold, it is considered as a natural phenomenon and not as a consequence of judgment errors.

A comparison matrix has satisfactory consistency when the consistency ratio $CR < 0.1$. If $CR > 0.1$, judgment iterations have to be performed again. The CR is defined as the ratio of the consistency index CI to the so called random index RI:

$$CR = \frac{CI}{RI} \tag{3.5}$$

The RI can be taken from Table 3-3 and the consistency index can be calculated to:

$$CI = \frac{\lambda_{\max} - n}{n - 1} \tag{3.6}$$

where $\lambda_{\max}$ is the maximum eigenvalue and n is the dimension of the comparison matrix. Using Equations 3.5 and 3.6, the consistency ratio of the sample matrix from Table 3-2 was is calculated to be $CR = 0.064$, and consequently the consistency condition is met.

Table 3-3: Random index (RI) for different matrix dimensions n obtained by Saaty [122]. The RI is the arithmetic mean of consistency indexes obtained from randomly generated matrices. The value depends on the simulation method and the number of matrices involved in the process.

n	3	4	5	6	7	8	9	10
RI	0.58	0.9	1.12	1.24	1.32	1.41	1.45	1.49

3.4 Prioritisation

Prioritisation assigns priorities to the nodes in the hierarchy so that the judgments from the comparison matrices are satisfied. The priorities are represented by the priority vector $\vec{\boldsymbol{w}}_{\mathbf{PR}}$ which is typically the normalised principal eigenvector of the matrix [122]. Mathematically speaking, the principal eigenvector $\vec{\boldsymbol{w}}$ of a matrix is the eigenvector corresponding to the eigenvalue of largest magnitude and can be obtained by:

$$\boldsymbol{A} \cdot \vec{\boldsymbol{w}} = \lambda_{\max} \cdot \vec{\boldsymbol{w}} \tag{3.7}$$

where $\boldsymbol{A}$ is the comparison matrix and $\lambda_{\max}$ is its maximal eigenvalue. For the sample matrix in Table 3-2, the principal eigenvector was calculated to:

$$\vec{\boldsymbol{w}} = (0.950 \quad 0.143 \quad 0.267 \quad 0.076) \tag{3.8}$$

The priority vector $\vec{\boldsymbol{w}}_{\mathbf{PR}}$ is obtained by normalisation of the eigenvector, i.e. dividing each component by the sum of all components so that the sum of all priorities equals one. The priority vector corresponding to the eigenvector above was calculated to:

$$\vec{\boldsymbol{w}}_{\mathbf{PR}} = (0.662 \quad 0.099 \quad 0.186 \quad 0.053) \tag{3.9}$$

The higher the priority of a criterion, the more important it is for achieving the goal, and the higher the priority of an alternative, the better it satisfies the criterion, i.e. the most important criterion is C_1, followed by C_3, C_2 and C_4. When the hierarchy has more than one criteria level, the priorities obtained in this way are called *local priorities* because they only represent the priority of each criterion with respect to the parent at the next higher level. In this case, the importance of a given criterion in the overall context is represented by its *global priority* which is obtained by multiplying the local priority by the global priority of its parent. At the level immediately below the goal, there is no difference between local and global priorities because the priority of the goal is by definition equal to 1.

3.5 Synthesis

In this step, the priority of each alternative with respect to the overall goal is obtained. Considering a decision-making problem with m alternatives and n criteria, the prioritisation results are collected in a decision matrix of the dimension $m \times n$ (Table 3-4). In contrast to the pairwise comparison matrix, the decision matrix is not necessarily quadratic. After the decision matrix is completed, the global priority p_{Ai} for a given alternative A_i is calculated by:

Table 3-4: A decision matrix with m alternatives and n criteria. a_{ij} is the priority of the alternative A_i with respect to the criterion C_j, and w_j is the priority of C_j. In contrast to the comparison matrix, the decision matrix is not necessarily quadratic.

Criteria C_j	C_1	C_2	…	C_n
Priority of C_j	w_1	w_2	…	w_n
Alternative A_1	a_{11}	a_{12}	…	a_{1n}
Alternative A_2	a_{21}	a_{22}	…	a_{2n}
…	…	…	…	…
Alternative A_m	a_{m1}	a_{m2}	…	a_{mn}

$$p_{Ai} = \sum_{j=1}^{n} w_j \cdot a_{Ai(j)} \tag{3.10}$$

where a_{ij} is the priority of the alternative A_i with respect to the criterion C_j and w_j is the priority of C_j. Synthesis can be performed in either the *distributive mode* or *ideal mode*. The choice of the synthesis mode depends on the purpose of the decision making process. As shown in Table 3-5, the distributive and the ideal mode lead to different priorities and might even lead to a different ranking of the alternatives. The main characteristics of the two modes are outlined in the sections below, a detailed description and a guideline for selection can be found in [126].

3.5.1 Distributive mode

The distributive mode is appropriate when all alternatives are relevant and the purpose of the decision making process is to prioritise the alternatives against each other. In the distributive mode, the rank order of the alternatives may change when alternatives are added or deleted. This phenomenon is called *rank reversal* and it occurs because the priority of each alternative is based on normalised priorities that sum up to 1:

$$\sum_{i=1}^{m} a_i = 1 \tag{3.11}$$

Rank reversal means, for example, that even though alternative A_1 might be preferred to A_2 before A_3 has been introduced, A_2 might become preferred to A_1 with the introduction of A_3.

3.5.2 Ideal mode

In contrast to the distributive mode, the ideal mode preserves the rank of the alternatives when new alternatives are added. The ideal mode is used when the concern of the decision making process is to identify the one best alternative and the

others do not matter. In the ideal mode, the priority of each alternative with respect to a given criterion is divided by the largest priority. In this way, the priority of the most preferred alternative becomes *ideal*: it receives the value of 1 and respectively the entire priority of the criterion (Table 3-5). The ideal mode avoids the effect of alternatives with equal or similar priorities on the decision outcome: for example when A_1 and A_2 are both low-cost and have both reasonable performance, and A_3 is expensive but has an outstanding performance. In the distributive mode, A_1 and A_2 would cut into each other's priority because the priority with respect to cost would be distributed among all alternatives. In contrast, the ideal mode gives the entire priority of cost to the device with lowest cost (A_1 or A_2), thereby making it a stronger competitor to A_3.

At the end of this chapter it should be mentioned that the AHP is a complex mathematical science and the analysis performed in the thesis represents a small part of the topic. For further reading, [127] and the references therein are recommended.

Table 3-5: Synthesis with the distributive and the ideal mode. In this example, both modes assign different priorities but lead to the same ranking of the alternatives. The numerical values for this example were adapted from [128].

Distributive mode

	C_1 0.662	C_2 0.292	C_3 0.055	C_4 0.064	Priority	**Rank**
Alternative A_1	0.754	0.233	0.754	0.333	0.630	1st
Alternative A_2	0.181	0.055	0.065	0.333	0.161	3rd
Alternative A_3	0.065	0.713	0.181	0.333	0.282	2nd

Ideal mode

	C_1 0.662	C_2 0.292	C_3 0.055	C_4 0.064	Priority	**Rank**
Alternative A_1	1.000	0.327	1.000	1.000	0.876	1st
Alternative A_2	0.240	0.007	0.086	1.000	0.250	3rd
Alternative A_3	0.086	1.000	0.240	1.000	0.426	2nd

4 ANALYSIS OF THE CURRENT FABRICATION PROCESS

In this chapter, the current printhead fabrication process is analysed with a focus on costs, lead time, yield and lifetime. The analysis is used to identify the optimisation potential and is based on process worksheets from the serial printhead production. Primarily, these worksheets provide information about the involved processes and the corresponding machine and operator times but they also help to determine yield limiting factors and estimate the rework durations and lead time. The chapter is structured as follows: First, the current silicon/glass fabrication process is described and the manufacturing yield and lead time are estimated. The machine and operator times from the worksheets are used to perform cost analysis: the individual cost drivers are identified and the relationship between manufacturing costs and production volume is shown. Finally, the printhead lifetime is discussed.

4.1 Fabrication

The current printheads, revision R24, are fabricated in silicon/glass technology using 100mm wafers. The footprint of one silicon die is approx. 19 mm × 35 mm and the maximum number of printheads that can be placed one wafer is six, which corresponds well to Equation 2.3. As shown in Figure 4-1, the production can be represented by twelve process blocks. Each process block consists of one or more process steps which are shown in Table A 1 in the Appendix. The fabrication process is illustrated in Figure 4-2.

On the top side, two masking materials are required in order to achieve two different depth levels: one level for the microfluidic structures and another level for trenches for dicing release. The masking materials are photoresist and oxide for the first and second etching step, respectively. This combination enables selective removal of the photoresist mask before performing the second etching step. The oxide mask is patterned by lithography and reactive ion etching (RIE), and the resist mask by lithography. The wafer is etched by deep reactive ion etching (DRIE).

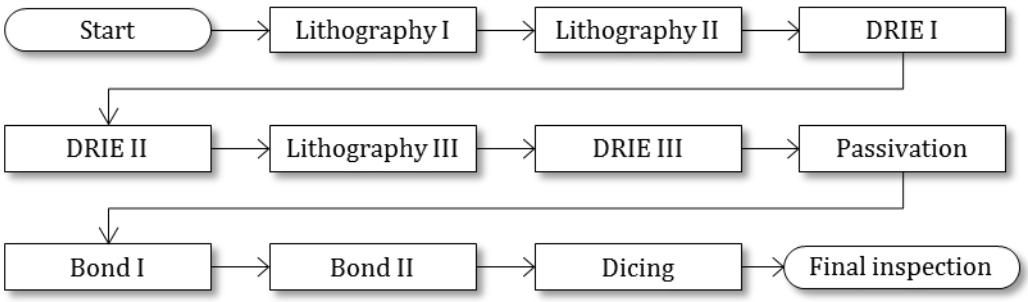

Figure 4-1: Production workflow of the current silicon/glass printheads.

Once the top side processing is completed, thermal oxide is grown on both sides of the silicon wafer. On the bottom side, the oxide layer serves as a mask for the third DRIE step, and on the top side as an etch stop. Due to the well-known feature size dependence and non-uniformity of the etch rate across the wafer diameter, some features experience longer overetch than others. To avoid damage of the structures at the interface with the oxide (notching), the SOI kit from STS is used. The SOI kit helps to avoid notching by reducing the ionic charging at the oxide layer [129]. After the third DRIE step, a thin thermal oxide layer for passivation of the microfluidic structures is grown on both sides of the wafer. Using anodic bonding, the wafer is sandwiched between two semi-finished glass substrates with fluidic access holes. The final thickness of the achieved glass/silicon/glass stack is

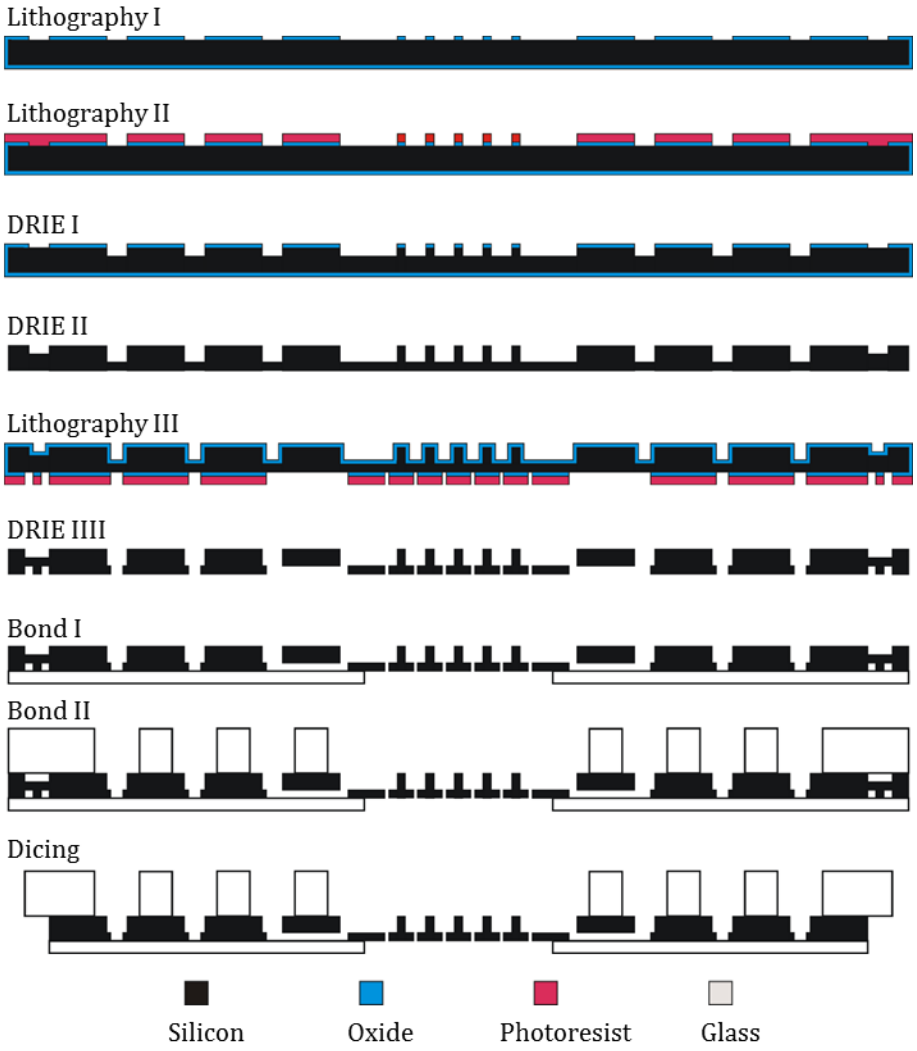

Figure 4-2: Fabrication process for the silicon/glass printheads. A silicon wafer is structured by DRIE and sandwiched between two glass layers by anodic bonding. The individual printheads are separated at the end of the process by dicing through the silicon/glass triple stack.

2.53 mm. The process ends by dicing with a conventional diamond saw blade using a recipe with 48 dicing paths per wafer.

4.2 Lead time and yield

In the context of the thesis, lead time is considered as the period of time between the start and the completion of a production cycle. In manufacturing facilities, the production resources are shared between different products and their availability depends on factors such as product priority, production control and machine maintenance. The lead time analysis in this section is based on the following assumptions:

- The availability of resources and production control does not allow starting more than one process per day.
- Each 8 hours of operator and machine time or a part of thereof result in one day of process duration, i.e. one day lead time. Thermal oxidation is an exception with each 24 hours of machine time resulting in one day.
- A process block is never reworked more than once.

With the above assumptions, three lead times were estimated: optimistic, expected and pessimistic. The optimistic lead time (LT_{OPT}) is an extreme case assuming that all parameters are within the specifications and neither process needs to be reworked. The optimistic lead time for one complete production cycle is the sum of the optimistic lead times of the twelve process blocks:

$$LT_{\mathrm{OPT}} = \sum_{i=1}^{12} LT_{\mathrm{OPT},i} \tag{4.1}$$

Using Equation 4.1, the above assumptions and the machine and operator times from Table A 1 in the Appendix, the optimistic lead time was calculated to be 35 days ($LT_{OPT} = 35$ days).

Another extreme is represented by the pessimistic lead time (LT_{PES}), i.e. the production is so unstable that each process block has to be reworked (with exception of cases where rework is not possible). The pessimistic lead time is given by the sum of the optimistic lead time and the rework duration (RD) of each process block:

$$LT_{\mathrm{PES}} = LT_{\mathrm{OPT}} + \sum_{i=1}^{12} RD_i \tag{4.2}$$

The rework duration depends on the rework strategy of the corresponding process block. A common rework strategy of the process blocks Lithography I-III is to strip the masking layer and repeat the lithography steps. This does not produce a rework of other process blocks and therefore the rework duration for Lithography was considered equal to the corresponding optimistic lead time ($RD_{\text{LITHO I–III}} = LT_{\text{OPT,LITHO I–III}}$). The same applies to the rework duration of the process block Passivation ($RD_{\text{PASS}} = LT_{\text{OPT,PASS}}$). In certain cases, however, a failure might require to rework more than one process block. In this case, the rework duration takes longer than the corresponding optimistic lead time ($RD_i > LT_{\text{OPT},i}$). This situation applies to the process blocks Bonding and Dicing where the rework strategy involves HF dip to remove the inaccurately bonded or diced glass substrates. Since the HF removes all glass substrates and the passivation layer, this rework sets the production back to the process block Passivation. As a consequence, rework of Bonding I/II and Dicing takes longer than the corresponding optimistic lead time. Obviously, when rework is not possible (rework probability $RP = 0\ \%$), the rework duration is 0 days ($RD_{\text{DRIE I–III}} = RD_{\text{INSP}} = 0$). From the above considerations, $LT_{\text{OPT}} = 35$ days and using Equation 4.2, the pessimistic lead time was calculated to be 59 days ($LT_{\text{PES}} = 59$ days). The uncertainty of lead time prediction expressed by the difference between the pessimistic and the optimistic lead time is 24 days.

Both the optimistic and pessimistic lead times are extremes that describe the lower and upper limit of the lead time. A realistic indication of the lead time is given by the expected lead time which is the sum of the optimistic lead time and the weighted rework duration RD_{WEI} of each process block:

$$LT_{\text{EXP}} = LT_{\text{OPT}} + \sum_{i=1}^{12} RD_{\text{WEI},i} \tag{4.3}$$

The weighted rework duration can be expressed to:

$$RD_{\text{WEI},i} = RP_i \cdot RD_i \tag{4.4}$$

where RP_i is the rework probability, an important indicator for the efficiency of a process. The rework probability is a rule of thumb which estimates the chance that a process block will produce a rework. In the current fabrication process, rework is most often caused by lithography related steps where the estimated rework probability is 20 %. Possible failure modes in lithography are air bubbles or radial inhomogeneities (comet-like structures) in the resist layer, partially uncoated wafer areas, sticking between mask and resist layer, insufficient resist adhesion or improper exposure dose. Other process blocks with a relatively high rework proba-

bility of 10 % are Bonding and Dicing. Typical failure modes related to anodic bonding are voids due to particle contamination or trapped air between the substrates. Other failure modes are non-bonded areas due to filmic contamination or insufficient substrate flatness. Particularly critical are bonding failures between microchannels because they represent risk for cross-talk. Among all other process blocks, Dicing has a special significance since it is the step where the wafers have their highest value. Possible failure modes in Dicing are chipping and cracking of the top glass layer and correspondingly inacceptable edge quality.

Process blocks with a low or close to zero rework probability are Passivation, DRIE and Final inspection. The most probable failure mode in Passivation is a deviation from the specified thickness of the oxide layer. The chance for such a deviation is estimated at 5 %. Regarding DRIE, there is no rework strategy because DRIE removes material from the wafer and consequently its rework probability is 0 %. The rework probability of Final inspection is 0 % too, because the process block is performed after dicing and therefore rework is not possible.

Using Equations 4.3 and 4.4 and the above estimates regarding rework probability and duration, the expected lead time was calculated to be 42 days (LT_{EXP} = 42 days), or approx. 20 % longer than the optimistic lead time. In other words, 7 days or more than 15 % of the time required for production of the silicon/glass printheads is caused by rework. An overview of the rework durations and the calculated lead times for all process blocks is presented in Table 4-1.

Table 4-1: Overview of the lead time and yield analysis for the silicon/glass printheads. LT_{OPT}, LT_{EXP} and LT_{PES} are the optimistic, expected and pessimistic lead times. *RD* is the rework duration and *RP* is the rework probability, i.e. the chance that a process block will produce a rework. *FPY* and *Y* are the first pass yield and the process yield after rework. Machine and operator times are taken from Table A 1 in the Appendix. Time units smaller than 24 hours are rounded to one day.

#	Process block	In case of rework	LT_{OPT} [days]	*RD* [days]	*FPY* [%]	*RP* [%]	*Y* [%]	LT_{EXP} [days]	LT_{PES} [days]
1	Start	n/a	2	0	100	0	100	2	2
2	Lithography I	Repeat	5	5	80	20	100	6	10
3	Lithography II	Repeat	1	1	80	20	100	2	2
4	DRIE I	n/a	4	0	95	0	95	4	4
5	DRIE II	n/a	5	0	95	0	95	5	5
6	Lithography III	Repeat	3	3	80	20	100	4	6
7	DRIE III	n/a	5	0	95	0	95	5	5
8	Passivation	Repeat	1	1	95	5	100	2	2
9	Bonding I	Back to #8	2	3	80	10	90	3	5
10	Bonding II	Back to #8	1	4	80	10	90	2	5
11	Dicing	Back to #8	3	7	80	10	90	4	10
12	Final inspection	n/a	3	0	96	0	96	3	3
TOTAL			**35**	**24**	**20**	**n/a**	**60**	**42**	**59**

The yield of a process block was calculated to:

$$Y_i = RP_i + FPY_i \tag{4.5}$$

where FPY is the first pass yield of the process block, i.e. the quotient of number of wafers to specification without rework to the number of wafers entering the process block. The first pass yield, rework probability and waste are linked by the following relation:

$$RP_i + FPY_i + Waste_i = 100\ \% \tag{4.6}$$

Realistic values for the first pass yield based on experience acquired from the serial printhead production are listed in Table 4-1. By substituting these values in Equations 2.1 and 4.5, the total yield was calculated to be 60 %. The most significant contributors to waste are the process blocks Bonding and Dicing. In case of bonding and dicing failures, rework is not always carried out because of the long rework duration and relatively high rework cost. If the failures cause only cosmetic deviations, the affected printheads can still be used for training purposes or experiments but not for sale.

4.3 Cost analysis

Due to the confidentiality of cost data, the cost analysis was performed using the imaginary monetary unit M.U. instead of Euro. The calculation of the manufacturing cost was based on the following assumptions:

- Machine time (machine running without operator intervention) costs 130 M.U. per hour.
- Operator time costs 130 M.U. per hour.
- All processes are performed using equipment for single-wafer processing, except for wet-etching of SiO_2 and thermal oxidation, where the batch size is 25 and 50 wafers, respectively.

Lithography masks, silicon wafers and semi-finished glass substrates with fluidic access holes are purchased from commercial suppliers. The lithography masks are considered as fixed material costs, and both silicon wafers and glass substrates are considered as variable material costs. An overview of the material costs is presented in Table 4-2. Consumables such as photoresists, chemicals, gloves etc. are considered as overhead and are not included in the analysis. Using Equations 2.4 to 2.6, the manufacturing costs per printhead (C_{PH}) can be written as the sum of the fixed ($C_{\mathrm{MAT,FIX}}$) and variable material costs ($C_{\mathrm{MAT,VAR}}$), machine costs (C_{MA}) and operator costs (C_{OP}) divided by the product of wafer lot size (S), number of printheads per wafer (n) and total yield Y_{TOT}:

Table 4-2: Material costs involved in the manufacturing of the silicon/glass printheads.

#	Item	Cost type	Unit	Qty.	Value
1	Lithography mask set	Fixed	M.U.	1	2400
2	Silicon wafers	Variable	M.U.	1	80
3	Semi-finished glass substrates (Top)	Variable	M.U.	1	400
4	Semi-finished glass substrates (Bottom)	Variable	M.U.	1	500

$$C_{\mathrm{PH}} = \frac{C_{\mathrm{MAT,FIX}} + C_{\mathrm{MAT,VAR}} + C_{\mathrm{MA}} + C_{\mathrm{OP}}}{S \cdot n \cdot Y_{\mathrm{TOT}}} \tag{4.7}$$

Substituting $n = 6$ and $Y_{\mathrm{TOT}} = 60$ % in Equation 4.7 and with the processing times from Table A 1 in the Appendix, the manufacturing costs per printhead were calculated for different production volumes. The calculation revealed that the costs per printhead decrease by about 50 % when the production volume is increased from 10 to 100 printheads. For production volumes smaller than 40 printheads, the costs decrease very rapidly with increasing volume. For quantities between 40 and 70, the decrease slows down and for quantities larger than 70 it becomes close to zero, i.e. the effect of economy of scale is practically cancelled out (Figure 4-3(a)).

For more detailed analysis, the cost drivers were divided into two groups. The first group considers all costs related to silicon micromachining, i.e. items #1 and #2 from Table 4-2 and all process blocks up to and including Passivation from Figure 4-1. The second group considers all costs that arise after silicon micromachining is completed, i.e. items #3 and #4 and all process blocks after and including Bond I. This classification showed the high significance of the non-silicon related processes. Depending on the production volume, the second costs group (back-end costs)

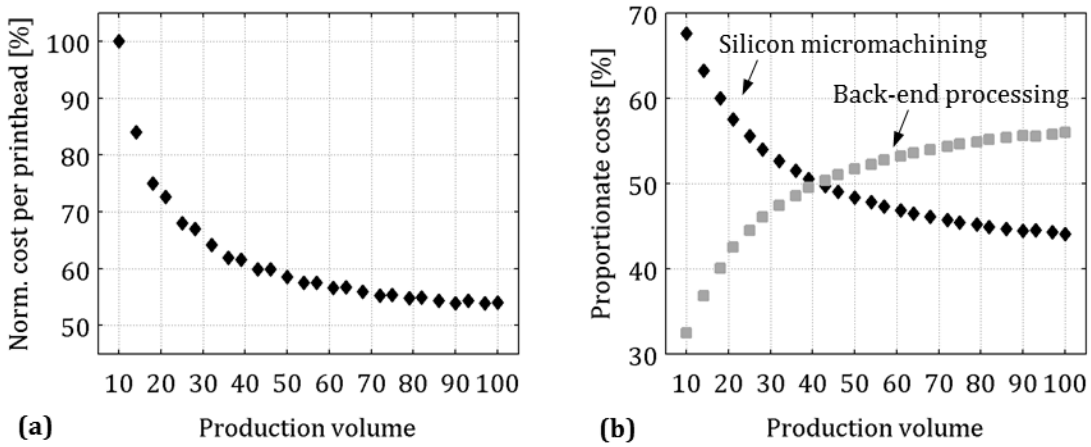

Figure 4-3: Relation between manufacturing costs and production volume. **(a)** Total costs per printhead normalised to the costs per printhead at a production volume of 10. **(b)** Proportionate costs for silicon micromachining and back-end processing for production volumes of 10 to 100.

accounts for approx. 30 % to 55 % of the total manufacturing costs with increasing importance for higher production volumes. By contrast, silicon micromachining has a higher contribution to costs for smaller quantities and its cost fraction decreases from almost 70 % to less than 45 % when the production volume increases from 10 to 100. As shown in Figure 4-3(b), cost optimisation of silicon related processes will have a higher impact for production volumes below 40 and optimisation of back-end costs is more important for production volumes above 40. This relationship suggests that cost optimisation for lot sizes of 10 to 100 requires the consideration of both silicon micromachining and back-end processing.

4.4 Lifetime

Lifetime analysis is usually performed using accelerated testing conditions where stresses that appear in normal operation are "accelerated" in order to accelerate the time to failure. With appropriate acceleration models, the accelerated time to failure can be used to calculate the lifetime under normal operation conditions. Possible failure modes for TopSpot printheads are material fatigue (accelerated by the number of printing cycles), plastic deformation (temperature, mechanical load) and corrosion (humidity, temperature). However, a quantitative lifetime study based on accelerated lifetime models was not a part of the thesis. Instead, the lifetime is discussed based on general material considerations and experience with silicon/glass printheads in the field.

Silicon is well-known for its pure crystalline structure resulting in no mechanical hysteresis and respectively no material fatigue under all possible conditions (one of the reasons for being a perfect material for sensors). Besides, silicon is an elastic material with no plasticity or creep below 800 °C. Similarly, fatigue and plastic deformation of glass are of minor importance as long as the temperature remains below the softening temperature. Thus, it can be concluded that material fatigue and plastic deformation are not lifetime limiting factors for the silicon/glass printheads. Since the anodic bond takes place at temperatures which are well above the maximum operating temperature of the printheads, temperature induced degradation of the bond is not expected. Docmeci et al. reported on accelerated corrosion test of anodically bonded silicon/glass packages in saline and deionised water solutions and predicted a lifetime of 177 years at 37 °C [244]. Based on the above considerations and years of intensive use in the field, it can be concluded that when the silicon/glass printheads are properly used, their lifetime is practically unlimited.

5 DESIGN OPTIMISATION FOR MINIMUM COSTS

The main issue addressed in this chapter is the possibility for cost optimisation of the silicon/glass printheads. The optimisation analysis was based on the requirement that reduced manufacturing costs should have no or only little adverse impact on the functionality of the printheads. The chapter is subdivided into two sections: Section 5.1 explores the possibility for cost reduction by scaling, i.e. cost reduction without technological changes, by just making the printheads smaller and/or moving to larger wafers. The possibilities for cost reduction by technological innovation are described in Section 5.2, where new printhead designs based on alternative fabrication processes and material combinations are presented.

5.1 Cost reduction by scaling

Scaling enables to achieve more printheads from one wafer and reduce the manufacturing costs without changing the fabrication process. The underlying principle is that most operations of the fabrication process presented in Section 4.1 take a fixed amount of time and do not depend on the wafer size or the number of printheads on it. The size of the printheads is limited mainly by the reservoir pitch. In the current design, the reservoir pitch is 4.5 mm, which corresponds to the well spacing of a 384-well microtiter plate. This pitch results in a printhead size of 655 mm^2 and enables to achieve six printheads from one 100mm wafer (Figure 5-1(a)). Reducing the reservoir pitch to 2.25 mm, corresponding to the well spacing of a 1536-well microtiter plate, leads to a printhead size of 310 mm^2, which enables to achieve 13 printheads from the same wafer size. By combining the smaller printheads with the next larger wafer size (150 mm), the number of printheads placed on one wafer can be increased to 35, almost a factor of 6. Possible die arrangements for 100mm and 150mm wafers are depicted in Figure 5-1(b). Even

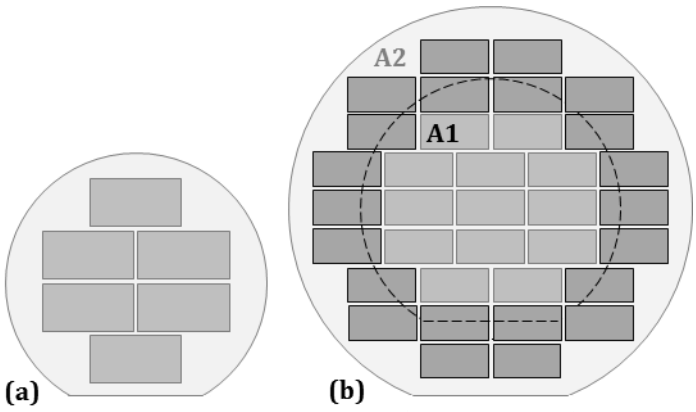

Figure 5-1: (a) Arrangement of the printheads on a 100mm wafer as implemented by the current design. **(b)** Reducing the reservoir pitch without transition to larger wafers enables to achieve 13 printheads per wafer (arrangement A1). By reducing the reservoir pitch and using 150mm wafers, the number of printheads per wafer can be increased up to 35 (arrangement A2).

larger wafer sizes were not considered as they are not supported by the equipment in typical MEMS foundries.

The increased dicing length in A1 and A2 will lower the dicing yield and to some extent compensate for the yield improvement by the smaller printhead size. In a first approximation, it can be assumed that the dicing yield for A1 and A2 will drop to approx. 80 % due to the higher number of dicing paths. The first pass yield in the process blocks Lithography 1 to 3 will increase but without bringing significant improvements in the process yields which are still close to 100 %. Furthermore, it can be assumed that the DRIE process itself does not introduce additional defects and the process yield would remain unaffected by the scaling. In contrast, the smaller printhead size will slightly increase the bonding yield and the yield after final inspection. Based on the above assumptions, the total yield for the arrangements A1 and A2 would remain roughly unchanged with respect to the current design (Table 5-1).

The cost analysis for the arrangement A1 and A2 in Figure 5-1(b) was performed corresponding to Section 4.3 considering appropriate scaling factors for material costs and for the size dependent processes blocks Dicing and Final inspection. The material costs for the arrangement A2 were obtained using the scaling factor 2.25, i.e. the quotient of the area of a 150mm wafer by the area of a 100mm wafer. The time required for the process block Final inspection was adapted using the scaling factors of 2.2 and 5.8 for A1 and A2, respectively. These factors represent the quotients of the number of printheads per wafer (13 and 35) by the current number of printheads per wafer (6). The process time for Dicing was achieved using the fac-

Table 5-1: Expected yield values for A1 and A2. The yield values of the current design are shown for comparison.

#	Process block	Current design			After scaling (A1/A2)		
		FPY	***RP***	***Y***	***FPY***	***RP***	***Y***
1	Start	100	0	100	100	0	100
2	Lithography I	80	20	100	90	10	100
3	Lithography II	80	20	100	90	10	100
4	DRIE I	95	0	95	95	0	95
5	DRIE II	95	0	95	95	0	95
6	Lithography III	80	20	100	90	10	100
7	DRIE III	95	0	95	95	0	95
8	Passivation	95	5	100	95	5	100
9	Bonding I	80	10	90	80	15	95
10	Bonding II	80	10	90	80	15	95
11	Dicing	80	10	90	70	10	80
12	Final inspection	96	0	96	97	0	97
TOTAL		**20**	**n/a**	**60**	**26**	**n/a**	**60**

tors 1.5 and 4.9 for A1 and A2, respectively. 1.5 is the quotient of the number of dicing paths in A1 (72) by the number of dicing paths in the current design (48). 4.9 is the quotient of the number of dicing paths in A2 (156) by the number of dicing paths in the current design, multiplied by 1.5 (quotient of wafer diameters). The used cost scaling factors are depicted in Table 5-2.

Based on a yield of 60 %, the achievable reduction of the manufacturing costs was calculated to be in the range of 25 % to 50 %, depending on the production volume and wafer size (Figure 5-2). Larger production volumes cause higher cost reductions than smaller ones, and the reduction achieved by A2 is higher compared to A1. The reasons for the relatively small cost reduction compared to the highly increased number of printheads are the higher material costs associated with the larger wafer size and the increased process time for Dicing and Final inspection (Figure 5-3). For example, dicing of one A2 wafer takes almost 23 hours (machine and operator), which makes dicing the highest individual cost factor. Expressed in another way, nearly 40 % of the manufacturing costs for a batch size of 3 wafers

Table 5-2: Cost scaling factors for the arrangements A1 and A2 from Figure 5-1(b) with respect to the current design.

Affected cost driver	A1	A2
Material costs	1	2.25
Processing time for Dicing	1.5	4.9
Processing time for Final inspection	2.2	5.8

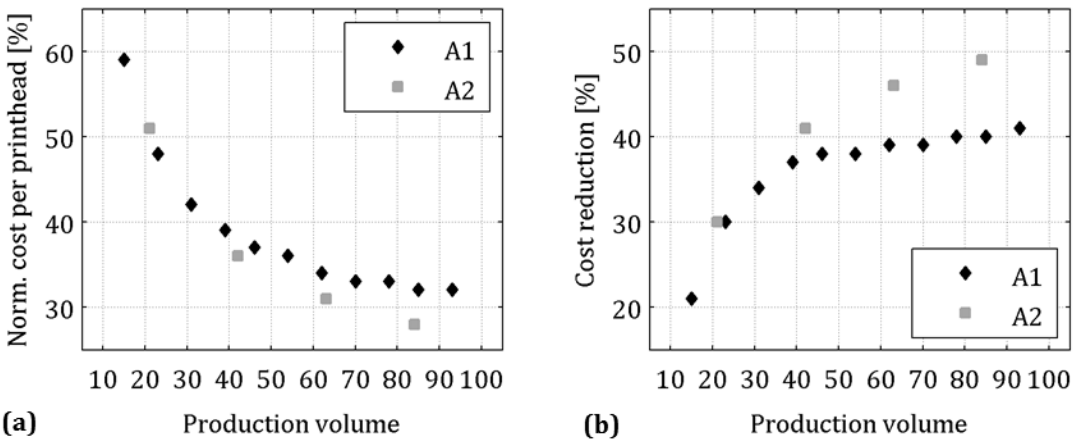

Figure 5-2: Costs behaviour of A1 and A2 for production volumes of 10 to 100. The calculation is based on a yield of 60 %. The considered wafer batch sizes are 2 to 12 for A1 (production volume of 15 to 93) and 1 to 4 for A2 (production volume of 21 to 84). Smaller and larger wafer batches are not considered as the corresponding printhead outcomes are outside the range of interest. **(a)** Costs per printhead normalised to the current costs per printhead at a production volume of 10. **(b)** Achievable cost reduction with respect to the same production volume.

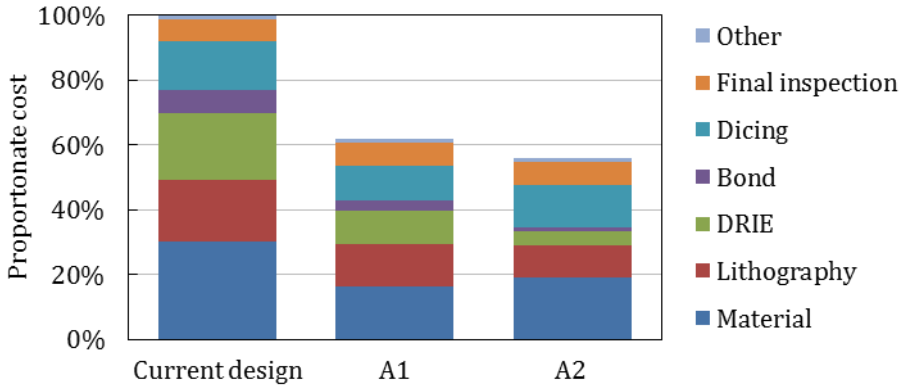

Figure 5-3: Comparison of cost breakdown for a production volume of 60 printheads.

(corresponding to 63 printheads, assuming 35 printheads per wafer and a yield of 60 %) would be caused by dicing. Obviously, the difference between A1 and A2 is almost negligible for the investigated production volume. The reason for this is that for production volumes smaller than 100, the potential of A2 is still far from being exhausted. As the data presented in Figure 5-2 makes clear, cost reduction higher than 50 % requires new designs and alternatives to the established silicon/glass technologies. Such alternatives are presented in the next section.

5.2 Cost reduction by technological innovation

In the last years, increased attention has been given to the role of polymers in microfluidics [111]. Among the most widely used materials are the silicon rubber Poly(dimethylsiloxane) (PDMS) [130], the epoxy based photoresist SU-8 [131] and thermoplastic materials, typically poly(methylmethacrylate) (PMMA) [132], polycarbonate (PC) [133] and cyclic olefin copolymer (COC) [134]. The main reason for the increased use of thermoplastics is the fact that they can be easily shaped by applying heat and pressure, which enables to produce a large number of devices by replicating a master structure.

Another polymer group with increasing importance in microfluidics is that of dry film resists [135]. In contrast to liquid resists which are applied to the substrate by spraying, dipping or spin coating, dry film resists are available in a sheet form and are usually applied in a lamination process.

Using dry film resists, two solutions were identified as the most promising candidates for achieving higher cost-reduction and flexibility beyond what is possible by scaling alone: the hybrid silicon/polymer and the all-polymer approach. Both approaches consider polymers in general, and dry film resists in particular, as a substitute to silicon/glass. The main difference between them is the extent to which

dry film resists are present in the final printheads. In the following sections, an introduction to the use of dry film resists in microfluidics is given, the process of material choice is discussed and the two printhead concepts are presented.

5.2.1 Dry film resists for microfluidics and MEMS

Although relatively new to microfluidics and MEMS, dry film resists are well established as a masking material for the patterning of circuit layouts in the printed circuit board (PCB) industry. Dry film resists were introduced in the 1960s by DuPont as alternative to liquid photoresists and have found wide acceptance, especially for the fabrication of printed circuit boards with plated through holes [136]. Dry film resists provide the photoresist as a very viscous ("dry") liquid sandwiched between two protective sheets and rolled up on a pipe core. To make this very viscous layer conform to the substrate surface, heat and pressure are applied in a lamination step. In this way, the resist can be used to cover cavities without flowing into them (tenting). The thickness uniformity obtained by lamination is high over the wafer diameter and no edge bead removal is required, as this is the case with thick liquid resist. Since dry film resists are not diluted by a solvent, no drying (soft-bake) is required prior to exposure. Even though dry film resists vary in their physical properties, many of them have common features which make them the material of choice for numerous applications (Figure 5-4).

The majority of dry film resists borrowed from the PCB industry is acrylic-based and has only limited chemical resistance. In microfluidics, such resists are not used for their intended purpose and have a very limited efficiency. This is especially the case when the resists are applied as a permanent material and remain a functional part of the final device. Often, acrylic based dry film resists cannot survive in common microfluidic environments. Heuschkel *et al*. reported on the lower chemical resistance and inferior adhesion of Riston dry film compared to SU-8 [137] and Ito *et al*. observed swelling of ME 1050 after a few hours in pure water [138].

In the last years there was an increased interest to overcome these limitations.

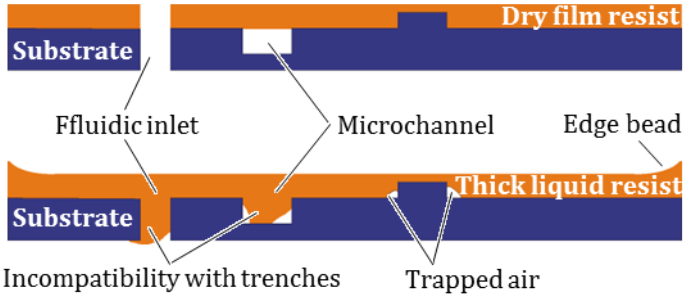

Figure 5-4: Main differences between dry film and thick liquid resists.

This led to the development of epoxy based dry film resists with properties adapted to the requirements of microfluidics and MEMS. Epoxy based resists are designed for permanent applications and have a higher resolution and aspect ratio compared to acrylic-based resists. Besides, it is practically impossible to strip them once they are cross-linked. Kieninger *et al*. first demonstrated self-made epoxy based laminates based on SU-8 [139]. Lately, photoresist laminates have become commercially available. As of today, these are Ordyl SY, an acrylic-epoxy-based dry film resist by Elga Europe, and the epoxy based TMMF by TOK, PerMX by DuPont and SUEX by DJ DevCorp. Other epoxy-based dry film resists are in development [140]. Table 5-3 gives an overview of publications where dry film resists have been used for the fabrication of microsystems and microfluidic devices.

Among the advantages of dry films over thick liquid photoresists is the ability of:

- Realising 3D multilayer structures by repeated lamination and exposure
- Lamination onto substrates with different shapes and sizes
- Tenting over trenches and holes that already exist in the substrate
- Direct sealing of microfluidic channels
- Selective sealing by patterning of the cover lid
- Uniform and reproducible thickness over large areas
- Use as a lithographically patterned adhesive for wafer bonding
- Time saving due to fewer processing steps and simultaneous lamination onto

Table 5-3: Dry film resists in microfluidics and MEMS. In permanent applications, the dry film resist remains in the final device or is used as a replication master. In a non-permanent application, the dry film is used as a sacrificial material, e.g. as a masking layer for etching or sand blasting, and is removed after having served its purpose.

DFR series	Application	References	DFR series	Application	References
Self-made (SU-8 based)	Permanent	[139,141-145]	PerMX	Permanent	[146-155]
	Non-permanent	n/a		Non-permanent	[156]
Ordyl SY	Permanent	[135,157-169]	ME1000	Permanent	[138,170-172]
	Non-permanent	n/a		Non-permanent	n/a
Riston	Permanent	[137,173-175]	SUEX	Permanent	[176-178]
	Non-permanent	[179,180]		Non-permanent	n/a
MX5000	Permanent	n/a	Vacrel	Permanent	[181,182]
	Non-permanent	[183,184]		Non-permanent	n/a
TMMF	Permanent	[185-200]	Other	Permanent	[142,201-208]
	Non-permanent	[209]		Non-permanent	[202,206,210-222]

several substrates

The most commonly reported drawbacks related to dry film resists are:

- Less total thickness
- Limitation of the thickness to multiples of the film thickness
- Smaller aspect ratio
- Lower resolution

Latest results have shown that these limitations have already been successfully addressed by some dry film resist manufacturers. Recently, Wangler *et al*. have reported on a 360 µm thick dry film resist providing an aspect ratio of 14 [140] and Johnson *et al*. have achieved aspect ratios of 15 with a 250 µm thick SUEX dry film resist [176].

5.2.2 Hybrid silicon/polymer printheads

In the scope of the thesis, the term *hybrid* is used as suggested by Gärtner *et al.* to indicate that a given performance parameter (e.g. costs) is provided by a material (e.g. polymer) that is basically different from the main material (e.g. silicon). Gärtner *et al.* predicted that hybrid microfluidic devices will gain in importance and that new fabrication techniques are required in order to expand the number of possible combinations between materials and processes [223].

The concept of the hybrid silicon/polymer printhead is based on a silicon layer with microfluidic structures which is sandwiched between two polymer layers replacing the glass in the current design. Originally, the hybrid printhead design has evolved from the observation that a very significant part of the manufacturing costs is related to back-end processing and especially to glass, i.e. buying ready-to-bond semi-finished glass substrates with fluidic holes, dicing of thick glass substrates etc. Since the properties of glass and the strength of the anodic bond are not necessarily required for the proper printhead operation, it was assumed that the hybrid approach will provide functionality comparable to that of the silicon/glass printheads but at significantly lower costs.

In order to choose appropriate substitute materials, it was important to first consider the functions of the glass components that are to be replaced. Regarding the top glass layer, its main function is to provide the macro-to-micro fluidic interface. In operation, this layer is subjected to a constant mechanical load by the O-ring that seals the actuation chamber (Figure 1-7). Therefore, the mechanical stiffness of the polymer replacing the glass on the top side must be as high as possible to minimise the risk of damage and inacceptable deformation. Other requirements are high chemical and thermal resistance and low water absorption, as the printheads are frequently cleaned with chemical cleaning agents at higher temperatures

and, due to the nature of their application, are frequently exposed to a water environment. Among the polymers commonly used in microfluidics, these requirements are very good met by COC grade 5013. This material has a very high Young's modulus, i.e. mechanical stiffness, of 3.2 GPa and meets the biocompatibility requirements of USP Class VI and ISO 10993. Besides, it withstands all common sterilisation methods and has a high glass transition temperature of 134 °C [224]. Therefore, COC grade 5013 was chosen as a substitute for the top glass layer.

The main function of the glass layer on the bottom side of the printhead is to seal the microchannels and, due to its hydrophilic nature, to support the capillary transport of the samples from the reservoirs to the nozzles. Additionally, the transparency of the lid provides an optical access into the microchannels. In preliminary tests, sealing the channels by gluing a polymer lid to the silicon layer turned out to be inappropriate due to the high risk of channel clogging, alignment failures and leakage. These preliminary tests have revealed that accurate and reproducible sealing of microchannels with such a high density can be provided only by a direct bonding method, i.e. without using an intermediate glue layer. However, since in most cases bonding of heterogeneous materials such as silicon and polymers involves some kind of glue, the number of possible candidates to replace the glass lid was restricted to two: PDMS and dry film resists.

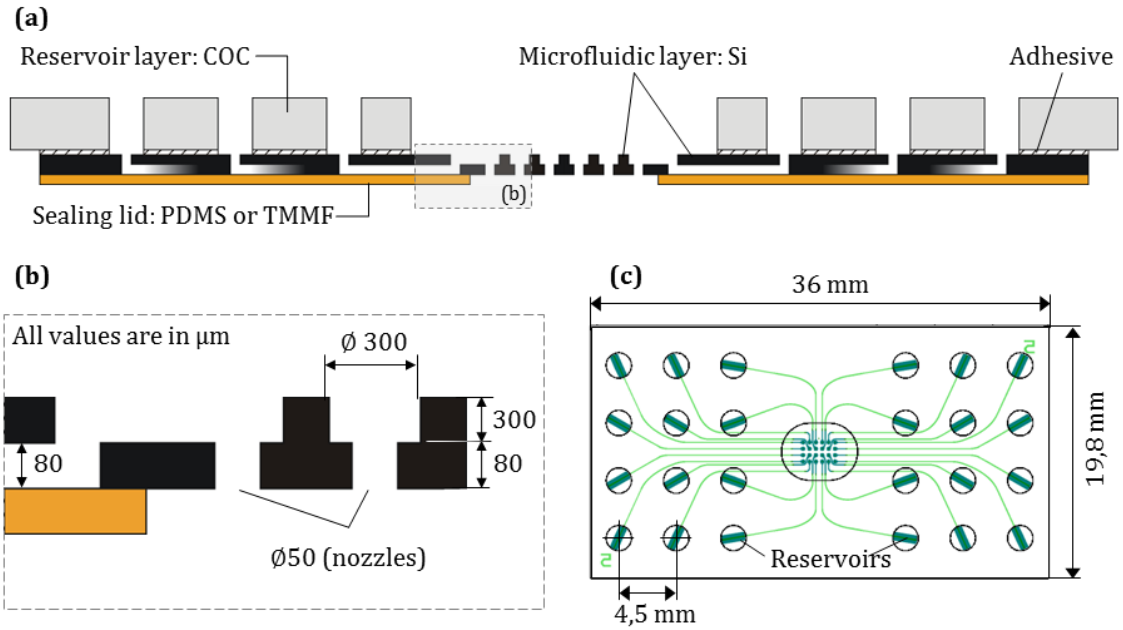

Figure 5-5: (a) Schematic cross-sectional view of the hybrid printhead design: the top glass layer is replaced by COC and the bottom glass layer by PDMS or TMMF. **(b)** and **(c)** All fluidic and outer dimensions are kept unchanged in order to make use of the available lithography masks and microarrayer hardware.

PDMS was selected due to its ability to bond to silicon and silicon oxide after being treated with oxygen plasma [130]. Dry film photoresists were chosen because they can easily be applied for selective or entire sealing of silicon microfluidic channels without an additional adhesive layer. Among the variety of dry film resists, TMMF was used as a first choice while PerMX and Ordyl were considered as a backup. Figure 5-5 shows a cross-sectional and a top view of a hybrid printhead. The outer printhead dimensions and the dimensions of all silicon structures were kept the same as in the silicon/glass design in order to use the available microarrayer hardware and lithography masks.

5.2.3 All-polymer printheads

According to the all-polymer printhead concept, all printhead components consist of polymer materials and therefore polymers are considered not "only" as an interface but as a key factor that determines the printhead performance. The main requirements on the polymer fabrication technology are to:

- Enable homogeneous production of small through holes (nozzle uniformity)
- Provide high stiffness of the nozzle material
- Allow for multilayer structures
- Assure the suitability for small production quantities

In a preliminary material selection, five technologies together with the corresponding materials were considered as possible candidates to realise an all-polymer printhead: (i) injection moulding, (ii) hot embossing, (iii) SU-8, (iv) dry film resists and (v) PDMS. The suitability of these candidates with respect to the above requirements is summarised in Table 5-4, a detailed discussion is given below:

According to the state of the art in the polymer industry, some of the above requirements pose a serious challenge for the moulding of thermoplastics [225]. Injection moulding is not suitable for small production quantities due to the high cost of the mould insert which, for complex devices such as a multichannel printhead, are typically in the range of €100 000 [226]. This makes injection moulding economically feasible for large production quantities but inappropriate for small lot sizes.

For small lot sizes, hot embossing is an established alternative to injection moulding. Hot embossing is well suited for manufacturing microcavities but, since the first description of the process, it has serious limitations when through holes are required [227]. The problem is caused by the characteristic residual layer between the mould and the counter plate. In order to open up the holes, this layer needs to be removed after the moulding process. This involves a demanding finishing that cannot be performed in a precise and reproducible manner as required for a Top-

Table 5-4: Comparison of different processes and materials. (-) indicates that the material fails to meet the minimum level of the corresponding requirement. (○) and (+) indicate a good and, respectively, very good agreement with the requirement.

Requirement	Injection moulding	Hot embossing	PDMS	SU-8	DFR
Production of through holes	○	-	+	+	+
High stiffness	+	+	-	○	○
Multilayer structures	+	+	+	-	+
Small production quantities	-	+	+	+	+

Spot printhead. Currently, hot embossing of microstructured through holes without finishing is under development by several research groups. Mehne *et al.* have adapted the hardness of the mould insert and the counter plate, which allows for complete displacement of the polymer melt between the mould pins and the plate [228]. When the hardness of the mould insert is higher than the hardness of the plate, the pins can penetrate few tens of micrometres into the counter plate without being damaged. The used polymers in this study were PMMA and COC and the manufacturing tolerance was ± 6 µm for a hole diameter of 110 µm. Rapp *et al.* suggested another solution, the so-called hot punching – an adaptation from the macroscopic punching process – and demonstrated the suitability of this technique for the manufacturing of through holes with a diameter of 1 mm on large PMMA substrates [227]. Even though the obtained results are promising, they also show that further research is necessary before hot embossing can provide nozzles at a quality level comparable to that of silicon micromachining. The main concerns related to hot embossing are caused by the lack of accuracy, the presence of burrs and insufficient edge quality. Besides, the accuracy of polymer components manufactured by thermal replication has a physical limit given by the thermal shrinkage of the material as a function of the overall size of the component. Due to the reasons presented above, polymer replication was not further considered as an option for the production of all-polymer printheads.

In a preliminary material selection, PDMS and SU-8 were identified as candidates to replace silicon and glass because they meet basic microfluidic requirements to a large extent. On closer examination, however, several drawbacks were revealed. The limiting factor for PDMS is its low Young's modulus, i.e. low stiffness. Even though the Young's modulus of PDMS can be slightly increased by higher cross linker concentrations and longer baking times, it remains below 4 MPa, which is not compatible with the demand for rigid nozzles [229]. In contrast to PDMS, cross-linked SU-8 has a very high stiffness and its Young's modulus is about three orders of magnitude higher (approx. 4 GPa). Concerning this requirement, SU-8 is even superior to thermoplastic materials such as COC, PMMA and PC. On the other side, SU-8 is liquid before cross-linking, which makes the processing of SU-8 onto

substrates with fluidic access holes (reservoirs) challenging. Therefore, using SU-8 implies that the fluidic layer and the reservoirs are produced separately and attached to each other when SU-8 is cross-linked. This poses a technological challenge due to the lack of established methods for releasing the cross-linked SU-8 from the substrate on which it is processed and for sealing of SU-8 microchannels [230]. In this regard, dry film resists are advantageous over SU-8 because they have comparable stiffness but they are not liquid and therefore can easily be applied on structured substrates.

Among the available dry film resists, TMMF was chosen as TMMF has already been successfully incorporated as a nozzle material into inkjet printheads and has operated successfully for ejecting 2.5 pl droplets at frequencies higher than 60 kHz [200]. PerMX and Ordyl SY were considered as backup options. For the reservoir layer, COC, PMMA and PC were all considered equally because no sufficient data exists in the literature concerning the compatibility of polymer substrates with TMMF, PerMX or Ordyl SY.

A schematic cross-sectional and top view of the all-polymer printhead design is shown in Figure 5-6. The outer dimensions are kept the same as for the silicon/glass printhead in order to use the already available microarrayer hardware. Due to process related limitations, the dimensions of some fluidic features were changed. The height of the fluidic channels was increased from 80 to 110 µm because the achievable thickness of a dry film multilayer can be only a multiple of the

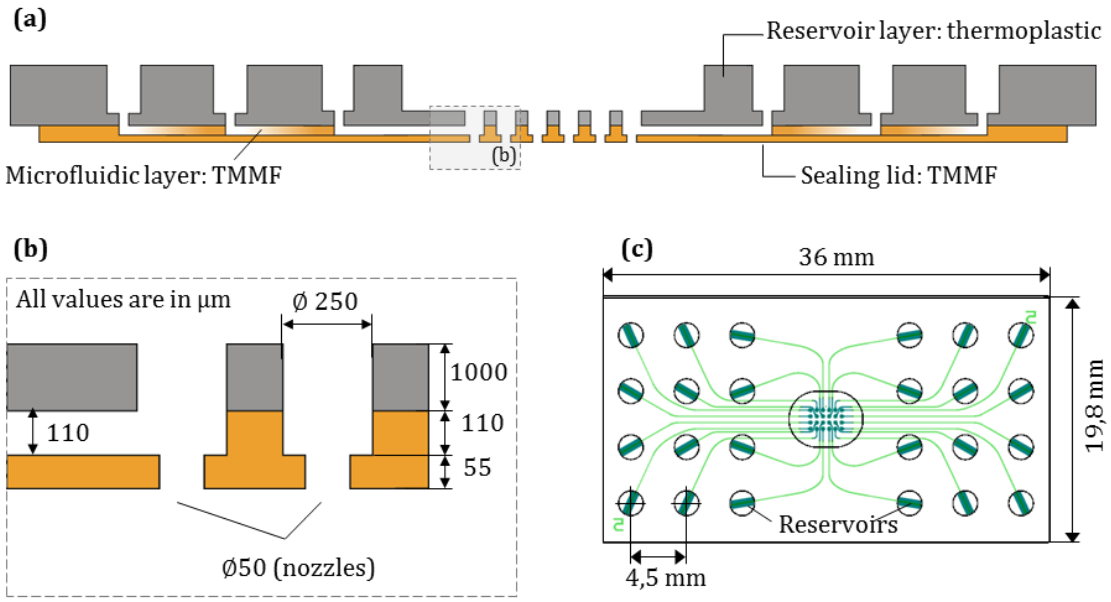

Figure 5-6: Polymer printhead. **(a)** Schematic cross-sectional view. **(b)** Fluidic dimensions. **(c)** Outer dimensions.

thickness of a single layer (55 µm). For the same reason, the nozzle length was reduced from 80 to 55 µm. The diameter of the nozzle inlets was reduced from 300 to 250 µm in order to reduce the risk of adhesion failures by increasing the contact area between the substrate and the dry film resist. The nozzle inlets were incorporated into the bulk layer and their length was increased from originally 300 to 1110 µm. This modification was necessary to provide a rigid support during lamination of the dry film resist.

5.2.4 Summary of the concepts

Two concepts, a hybrid silicon/polymer and an all-polymer concept, were identified as promising candidates to reduce the manufacturing costs and provide higher flexibility beyond what is achievable by scaling and without significant impact on the printing performance. An overview of the material and geometrical parameters of these concepts is presented in Table 5-5. In the hybrid printhead, silicon remains the major functional material and the glass layers are replaced by a rigid COC interface on the top side and a lid of either dry film resist or PDMS on the bottom side. The COC interface can be glued to the silicon, whereas the lid must be applied without a glue layer to avoid failures due to clogging or leakage. In the all-polymer concept, the top glass layer is replaced by a thermoplastic interface, and the silicon and bottom glass layers are both replaced by a multi-layered dry film resist. Due to its tenting properties, the dry film can be applied and processed

Table 5-5: Materials and dimensions of the different printheads. The thermoplastic materials used in the experimental sections are PMMA Plexiglas Gallery UV 100 AR (Evonik Industries), COC grade 5013 (TOPAS advanced polymers), PC grade Makrolon 2805 (Bayer MaterialScience). The used dry film resists are TMMF grade S2055 (55 µm thick, TOK), PerMX grade 3050 (50 µm thick, DuPont) and Ordyl grade SY355 (55 µm thick, Elga Europe). PDMS Sylgard 184 is from Dow Corning.

Materials	**Unit**	**Silicon/glass**	**Hybrid**	**All-polymer**
Reservoir layer	n/a	Glass	COC	PMMA, COC, PC
Bonding type Top	n/a	Anodic	Adhesive	Direct
Microfluidic layer	n/a	Silicon	Silicon	DFR
Bonding type Bottom	n/a	Anodic	Direct	Direct
Sealing layer	n/a	Glass	DFR, PDMS	DFR
Dimensions				
Outer dimensions	mm	36 × 19	36 × 19	36 × 19
Channel height	µm	80	80	110
Channel width	µm	80	80	80
Nozzle diameter	µm	50	50	50
Nozzle length	µm	80	80	55
Nozzle inlet diameter	µm	300	300	250
Nozzle inlet length	µm	300	300	1110

directly onto the interface.

6 DRY FILM RESISTS

The focus of this chapter is on the dry film resists, which were chosen to be a functional component in the hybrid and the all-polymer printheads: TMMF, PerMX and Ordyl SY. The chapter is organised into two sections. Section 6.1 reflects technological issues such as compatibility with polymer substrates and processing. In Section 6.2, relevant properties of TMMF, PerMX and Ordyl SY are discussed, in particular, their wetting behaviour, the possibilities for surface modification by a treatment with oxygen plasma, the optical properties and biocompatibility. The theoretical background of this chapter is based on studies by Karl H. Dietz [231]. Even though his research is focused on dry film resists for printed circuit boards, the reference is recommended for further reading on this topic.

6.1 Processing

The main steps in dry film resist processing are lamination, exposure, post exposure bake (PEB) and development (Figure 6-1). Lamination is used to apply the dry film resist onto a substrate. Four substrate materials were considered: silicon for the hybrid printheads and COC, PMMA and PC for the all-polymer printheads. Exposure to UV light through a lithography mask is used to initiate a crosslinking reaction and transfer the mask pattern to the resist. PEB is used to crosslink the resist at the exposed areas. In the development step, the unexposed areas are dissolved and removed in a developer leaving a cross-linked resist structure which is a negative image of the mask pattern.

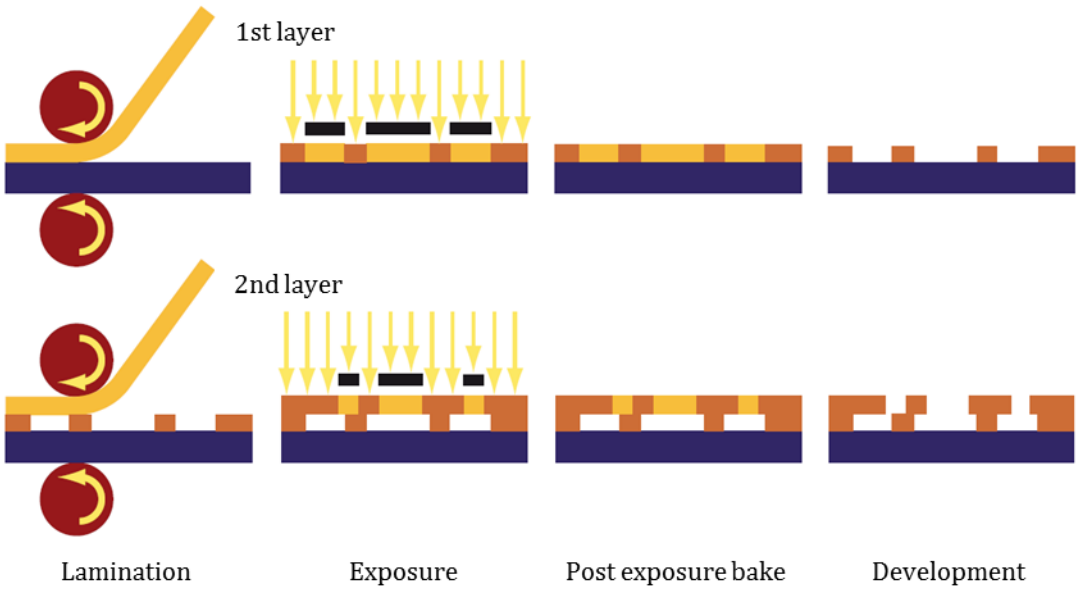

Figure 6-1: The main steps of dry film resist technology.

6.1.1 Dry film resists on polymer substrates

A critical issue for the application of dry film resists onto polymer substrates is the chemical resistance of the substrates to the developer chemistry. Ordyl SY is developed in a mixture of organic solvents which is provided by Elga Europe under the trade name BMR. The ingredients of BMR are xylene, 2-Butoxyethylacetate and ethylbenzene [232]. In the literature there is no data on the compatibility of polymers with BMR. TMMF and PerMX, are developed in propylene glycol monomethyl ether acetate (PGMEA), an organic solvent which is also used as a SU-8 developer.

Several studies have used SU-8 on polymer substrates: Lam *et al*. used the material combination SU-8/PMMA for the fabrication of a microfluidic mixer [233] and Bubendorfer *et al.* demonstrated casting of PDMS microchannels from a SU-8/PMMA mould [234]. In another study, Song *et al.* experimentally verified that PMMA is compatible with SU-8 processing [235]. However, PMMA is not a specific material but rather a general term for a group of materials that partly have different properties. The same applies for PC and COC. Therefore, the degradation of PMMA, PC and COC was studied by immersion of test samples in the developer solutions. The duration of the immersion was 20 minutes which corresponds to the duration of three development cycles, 6-7 minutes each. After immersion, the test samples were rinsed with isopropyl alcohol (IPA) and distilled water, blown dry with nitrogen and inspected for signs of chemical degradation such as softening and cracking. PC showed poor resistance to both PGMEA and BMR: its surface was attacked very shortly after immersion into these developers. COC showed good resistance to PGMEA but it was attacked by BMR. PMMA proved to be the only material with good resistance to both developers being able to survive the time equivalent of three development cycles without obvious chemical degradation. A further quantification of the chemical resistance of the polymer substrates, e.g. by the degree of swelling or mass loss, was not a part of the study.

The next step of the compatibility study was to examine the adhesion of the resists. Polymers with poor resistance against one of the developers were not considered for adhesion testing with the corresponding resist, i.e. the material combinations were limited to five: PMMA with TMMF, PerMX and Ordyl SY, and COC with TMMF and PerMX. Adhesion test series were performed by lamination, exposure and development of the dry films onto the polymer substrates. Values for the process parameters were taken from the data sheets. The resists were patterned by using a lithography mask with test structures. For each substrate/resist combination, it was tested whether ultrasonic agitation during development causes delamination of the resist and whether the adhesion can be improved by treating the substrates with oxygen plasma prior to lamination. Oxygen plasma treatment is a general and well-known method for improving the adhesion by removing organic contaminants and chemical modification of the treated surface. In case of poor adhesion,

Table 6-1: Results of experimental adhesion testing of TMMF, PerMX and Ordyl on polymer substrates. The influence of the development modes (with and without ultrasonic agitation) and the surface treatment (with and without plasma treatment) was investigated. "Y" or "N" means that ultrasonic agitation and plasma treatment were or were not applied. (-) means poor adhesion, i.e. large resist areas easily peel off. (○) indicates that large structures adhere on the substrate but small structures occasionally peel off. (+) means good adhesion, i.e. even thin lines and posts remain on the substrate after development.

Process conditions	**Unit**	**TMMF**				**PerMX**				**Ordyl**			
Roll temperature	°C	80				85				100			
Roll pressure	kPa	approx. 200				approx. 200				approx. 200			
Lamination speed	m/min	1				1				0.5			
Exposure	mJ/cm²	270				1125				160			
PEB	min @ °C	50 @ 150				5 @ 95				5 @ 85			
Ultrasonic	n/a	Y	N	Y	N	Y	N	Y	N	Y	N	Y	N
O_2 plasma	n/a	N	N	Y	Y	N	N	Y	Y	N	N	Y	Y
Adhesion on PMMA	n/a	○	+	○	+	○	+	○	+	○	+	○	○
Adhesion on COC	n/a	-	-	-	-	-	-	-	-	n/a	n/a	n/a	n/a

the tests were repeated by using increased lamination pressure and temperatures of up to about 15 °C below the glass transition temperature of the substrate. The experimental analysis showed that the adhesion of TMMF and PerMX was poor on COC and could not be improved by higher lamination temperatures or plasma treatment. In contrast, all dry film resists had a good adhesion on PMMA with the exception of tiny structures which appeared prone to delamination when the development was supported by an ultrasonic agitation. Oxygen plasma treatment had no noticeable effect on the adhesion properties. The results of the investigation are summarised in Table 6-1.

6.1.2 Lamination

Principle

The main task of the lamination process is to provide intimate contact between the resist and the substrate. Dry film resists are non-Newtonian fluids of very high viscosity, and intimate contact is achieved by lowering the viscosity through heat and by applying pressure to cause flow and make them conform to the substrate. Resist flow is described by the shear rate: heat reduces the viscosity which increases the shear rate at a constant shear force and, respectively, the amount of flow increases per unit time. Usually, heat and pressure are applied by the lamination rolls of a hot roll laminator. In scientific literature, the most common parameters to describe the process are roll pressure, roll temperature and lamination speed. It is important that these parameters are considered in connection with the whole system because neither the force on the resist nor the temperature at the resist/substrate interface or the contact time of the resist with the roll is measured directly. The contact time is a function of the lamination speed and the width of the

roll/substrate contact zone, also called *footprint*. The footprint itself is influenced by the total force, the roll diameter and the hardness and thickness of the roll cover material. The pressure gauge measures the pressure applied to the pneumatic cylinders at some point but the actual pressure applied to the resist depends on the wafer size and the footprint. The temperature at the resist/substrate interface also depends on several factors. These are the roll temperature, the contact time and the heat transfer coefficients of the materials between the roll and the interface. Thus, the lamination parameters, i.e. pressure, temperature and speed, have to be adapted separately for each application taking into account the wafer size, type and thickness of the resist, laminator type and substrate topography.

As a basic rule, substrates without cavities are laminated at the highest possible roll temperature and pressure, as long as there is no wrinkling and thermal polymerisation of the resist, and the roll bending remains within an acceptable range. Particularly, roll bending becomes an issue for thick substrates and when lamination is performed at high pressures. As depicted in Figure 6-2, roll bending results in an irregular pressure distribution and might lead to inhomogeneous resist thickness over the substrate. When dry film resists are used to cover cavities, e.g. microfluidic channels for the purpose of sealing, lamination parameters become more critical due to the challenge to tent over the channels. In this case, the process is a balancing act. On the one hand, high lamination temperatures and pressures are needed for good confirmation and adhesion. On the other hand, high temperatures and pressures may cause the resist to flow into the channel and destroy its cross-section or even completely block it (Figure 6-3). If the lamination temperature is too high, the resist keeps flowing even after lamination has been completed. Another typical failure mechanism is thinning of the lid at the channel rim. Special attention has to be paid to thinning when working with thin resists and soft rolls. An extreme example demonstrating thinning failure at the rim of a microfluidic channel is shown in Figure 6-3(d). The thickness of the resist is important for the sealing of microchannels because the lid strength is proportional to the square of the resist thickness. For example, the comparison of different TMMF grades, S2055 with a thickness of 55 µm and S2030 with a thickness 30 µm, shows

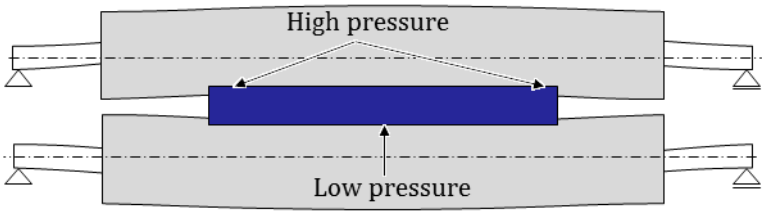

Figure 6-2: Inhomogeneous distribution of the lamination pressure due to roll bending (adapted from [231]).

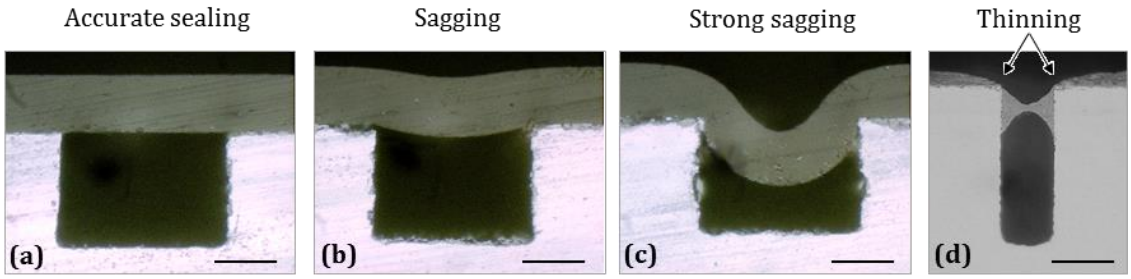

Figure 6-3: Cross-section of microchannels sealed with dry film resist showing the influence of the lamination parameters on the tenting properties of the resist. (**a)** Lamination performed at appropriate parameters. **(b)** and **(c)** Failure caused by too high lamination temperature and pressure **(d)** Thinning at the channel rim and resist flowing. TMMF with a thickness of 55 µm was used for (a-c). PerMX with a thickness of 14 µm was used for (d). Scale bars are 50 µm.

that a lid produced with the thicker resist is more than three times stronger. The strength of the lid is also influenced by the channel geometry and is inversely proportional to the square of the channel width [231]. Thus, for sealing of microfluidic channels, it is preferable to seal narrow channels and use the highest available resist thickness. This helps to avoid thinning failures during lamination and damage of the lid in operation.

Experimental implementation

A hot roll laminator by DuPont with manual substrate loading and resist trimming after lamination was used in the experiments. The parameters that could be set were the roll temperature and speed. The lamination pressure was adjusted indirectly by the roll distance. The substrates were placed on a sheet of cleanroom paper and a piece of resist slightly larger than the wafer was cut and fixed to the cleanroom sheet with a tesa tape. The protective layer that faced the wafer was peeled off and the resist was laminated onto the substrate. During lamination, the film was kept tensioned to avoid wrinkling (Figure 6-4).

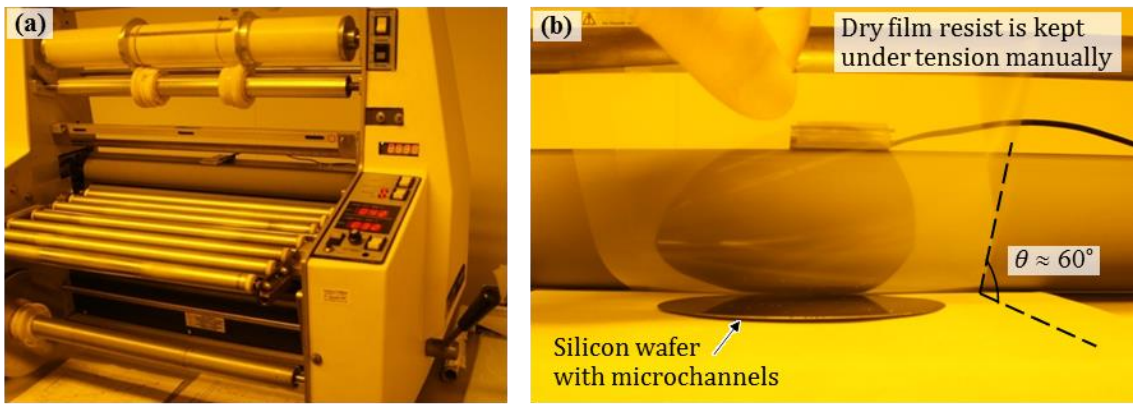

Figure 6-4: The used laminator **(a)** and a detail of the lamination process **(b)**.

Table 6-2: Lamination parameters for sealing of TopSpot microchannels. When tenting was not required, e.g. for the fluidic layer of the all-polymer printheads, the lamination temperature and pressure were increased to 90 °C and approx. 0.2 MPa, respectively.

Parameter	Unit	TMMF	PerMX	Ordyl
Temperature	°C	60	85	55
Speed	m/min	1	1	1
Pressure	MPa	0.1	0.1	0.1

The goal of the experimental work was to find a parameter set suitable to cover 80 µm wide cavities, which corresponds to the microchannel width of a TopSpot printhead. For the purpose of high adhesion, it was necessary to identify a combination of lamination temperature and pressure close to but below the values that would cause tenting failures or clogging. All experiments were performed on silicon wafers with a thickness of 380 µm. It was assumed that the substrate material and thickness have no influence on the tenting performance of the resist. In fact, besides the upper lamination roll that directly heats the resist, the lower lamination roll also heats the wafer and the temperature at the resist/wafer interface depends on the heat conductivity and thickness of the wafer. Assuming a footprint of 5 mm and lamination speed of 1 m/min, the contact time between the rolls and the substrate is 0.3 s, which is too short to allow a noticeable temperature increase at the resist/wafer interface by the lower roll. Thus, the impact of the substrate material on the tenting properties was neglected. The used wafers had microchannels and through holes at the end of each channel which were necessary to allow for venting of the channels during post exposure bake.

The lamination speed and pressure (defined by the gap between the rolls) were kept constant and the temperature was varied, starting with 40 °C and working upwards in 5 °C steps. The lamination speed for all experiments was 1 m/min. The roll gap was set after the rolls had reached their final temperature to compensate for thermal expansion. The gap was set in such a way that the wafer could be moved in between by slightly pushing it forward. By using Pressurex, a pressure sensitive film showing a characteristic colour corresponding to a certain pressure range, it was determined that the lamination pressure was approx. 0.1 MPa. The quality of the lamination was determined by a microscopic analysis of the channel cross-section. Suitable lamination parameters are listed in Table 6-2. When the purpose of the resist was to form a fluidic layer and not to a sealing lid, the lamination temperature and pressure for all resist types were increased to 90 °C and approx. 0.2 MPa, respectively.

6.1.3 Exposure

Exposure was performed on a MA6 aligner by SUSS equipped with a mercury lamp filtered at 360-370 nm (i-line). TMMF, PerMX and Ordyl SY are all negative working resists, i.e. the transfer of the mask into a polymerised resist pattern was obtained by exposure to UV light through the transparent areas of the mask. The UV energy is used by the photoresist to initiate the photopolymerisation. The polymerisation reaction was completed by a post exposure bake on a levelled hotplate. Since the light source had a constant power density of 5 W/cm², the exposure energy was varied via the exposure time and calculated by the relationship: $W/cm^2 \times seconds = mJ/cm^2$. Being a crucial factor for the polymerisation reaction, the exposure energy is thereby important for the tenting and sealing performance of the resist. Generally, higher exposure energies increase the resist strength due to a higher level of polymerisation but, on the other hand, they also increase its brittleness which can cause cracks and sealing failures.

For the exposure process, it is essential that the light is collimated and not scattered. However, these requirements cannot be met perfectly and some amount of the UV light reaches resist areas that are not intended to be exposed. Main factors contributing to this effect are the distance between the mask and the resist (exposure gap), light scattered by the protective coversheet and light reflected from the substrate and the chuck (Figure 6-5). For the hybrid printheads, where the resist is used as a sealing lid, the loss of resolution caused by the above factors was negligible. The same applies for the fluidic layer of the all-polymer printheads where the resist forms the channels that connect the reservoirs with the dispensing nozzles. For these two applications, exposure was performed without special care of scat-

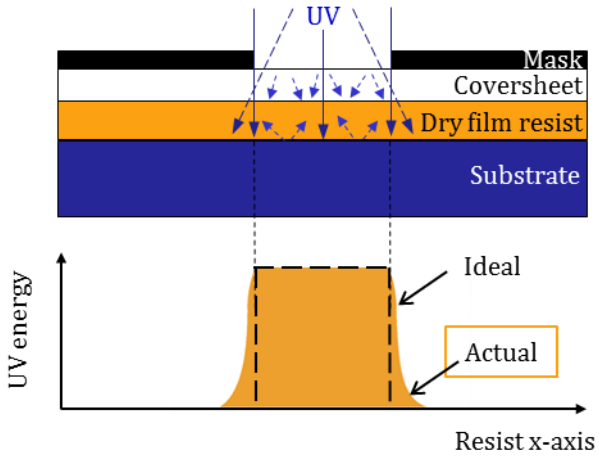

Figure 6-5: Deviation from the ideal UV energy distribution. Major contributors to this deviation are the exposure gap, the protective coversheet and the UV light reflected form the substrate and the chuck.

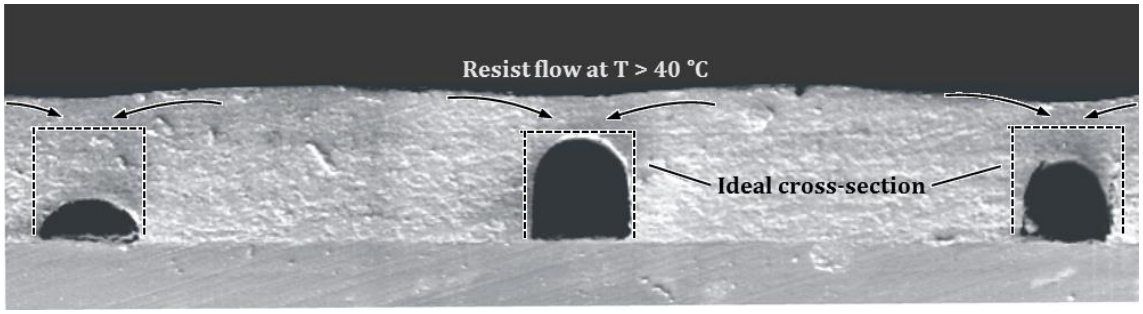

Figure 6-6: Deformation of the channel cross-section caused by flowing of the resist into the channels during soft baking at temperatures above 40 °C. The non-uniformity of flow can be explained by an inhomogeneous temperature distribution inside the resist, e.g. due to an unevenness of the hotplate or warping of the substrate.

tering effects and pushing the resist towards the resolution limit. In contrast, when the resist is applied to form nozzles, the resolution and smoothness of the nozzle edge become critical. Traditionally, unintended exposure of resist areas is minimised by exposure in a contact mode and eliminating sources of scatter along the light path. On the other hand, the standard mode for exposing dry film resists is with the protective coversheet on top. The coversheet has a twofold adverse effect on the resolution: it prevents direct contact between the resist and the mask and acts is a source of scattered light.

The major problem when the coversheet is removed in order to perform exposure in a contact mode is that the resist will stick to the mask. To avoid sticking, the TMMF manufacturer recommends a soft bake at 60 °C. This, however, appeared to be inappropriate when TMMF is used to seal channels because at temperatures above 40 °C TMMF becomes less viscous, which leads to channel clogging by a viscous flow (creeping) of the resist into the channels (Figure 6-6). Therefore, instead through a soft bake, the problem of resist sticking to the mask was avoided by re-

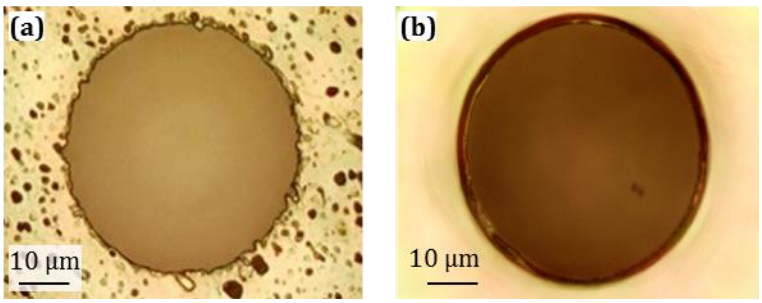

Figure 6-7: Contact exposure with coversheet **(a)** and without coversheet **(b)**. The pockmarks in the left image are caused by particles which are partially embedded in the coversheet to facilitate air escape during vacuum lamination. When exposure is performed without the coversheet, the pockmarks disappear and nozzle edge becomes smoother.

moving the coversheet 24 h prior to exposure to allow for evaporation of the remaining solvent. In this way, the resist loses its sticking surface and contact exposure becomes possible. Figure 6-7 illustrates the improvement achieved by removing the coversheet. The hold time between removing the cover sheet and exposure can be extended to five days without decrease in the adhesion quality or resolution. The exposure energies found to be suitable for the application were 150 mJ/cm² for TMMF, 900 mJ/cm² for PerMX and 125 mJ/cm² for Ordyl. Illumination was performed with discrete energy doses of 25 mJ/cm² with an interval of 10 s between the illuminations.

6.1.4 Post exposure bake and development

Post exposure bake was performed on a levelled hot plate to complete the cross-linking reaction of the dry films. The increasing and decreasing temperature rates were kept low in order to reduce the stress by the CTE mismatch between the dry films and the substrate material. In the development step, the unexposed resist areas were removed by the developer leaving the negative mask pattern on the substrate. Megasonic supported development was used to reduce the risk of delamination of structures with small contact area to the substrate. The megasonic agitation carries away recently dissolved resist and brings fresh developer solution into the narrow structures. After the development step, the substrates were rinsed with IPA and distilled water to remove the developer solution. A final drying step with a nitrogen purge or in an oven was used to remove residual moisture. An overview of the used parameters is shown in Table 6-3.

Table 6-3: Process parameters for post exposure bake and development. Development was carried out by immersion in the developer solution and can be supported by megasonic actuation.

Process	Substrate	TMMF	PerMX	Ordyl
PEB	Silicon	45′ @ 150 °C	5′ @ 95 °C	2′ @ 80 °C
	PMMA	45′ @ 90 °C		
Development	Silicon	7′ in PGMEA		7′ in BMR
	PMMA	Optional: megasonic		Optional: megasonic

6.2 Properties

6.2.1 Wetting behaviour

A crucial factor for the proper performance of the printheads is the capillary transport of reagents from the reservoirs to the dispensing nozzles. The ability for capillary transport depends on the wettability of the channels and, more particularly, on the advancing contact angles of the reagents on the channel walls. Generally, the smaller the contact angles, the greater the ability for capillary transport.

The materials intended to be used as a channel material were analysed in terms of their wetting behaviour, suitability for hydrophilisation by oxygen plasma treatment and degradation of their hydrophilic properties over time. The challenge of hydrophilic degradation was addressed by storing the samples in tightly sealed boxes under nitrogen atmosphere. The influence of this storage condition was studied by comparing the contact angles with samples that were treated the same way but stored at ambient conditions.

The size of the samples was approx. 25 mm × 50 mm. PDMS slabs were prepared by mixing the PDMS prepolymer with a curing agent (Sylgard 184, Dow Corning) at a weight ratio of 10:1, casting the mixture on a petri dish, degasing under vacuum and curing for 1 h at 65 °C [130]. The TMMF, PerMX and Ordyl samples were prepared using the parameters presented in Section 6.1. The glass samples were diced from an anodically bondable borosilicate wafer (Pyrex 7740, Corning). The silicon samples were prepared by etching the surface of a silicon wafer with the same DRIE recipe as for etching the printhead channels and growing a 100 nm thermal oxide on it. This allows for representativeness of the measurements by providing conditions as close as possible to the conditions in the microchannel of a silicon/glass printhead. The PMMA samples were laser cut from a larger PMMA sheet. The initial wetting was determined by measuring the advancing contact angles on untreated samples. A microcontroller driven microsyringe was used to deposit a water droplet onto the sample surface and add additional water to the droplet so its volume gradually increased (Figure 6-8). As the droplet grew, an image was taken and the contact angle was directly measured by the image analysis software (OCA 15+, DataPhysics Instruments). After determining the initial conditions, the samples were exposed to RF oxygen plasma at 100 W for 6 min (Zepto, Diener electronic). The advancing contact angles were measured immediately after the plasma treatment and 1, 2, 4, 9, 14 and 22 days afterwards. During the measure-

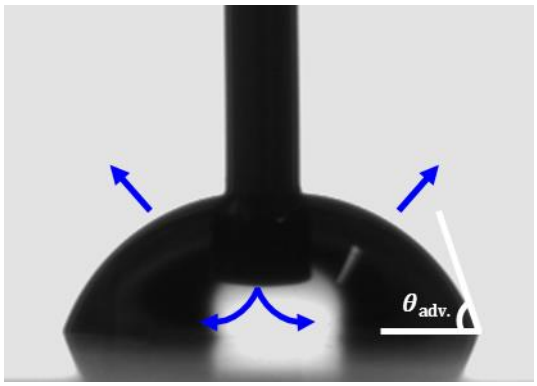

Figure 6-8: Measurement of an advancing contact angle by adding additional water to a sessile droplet.

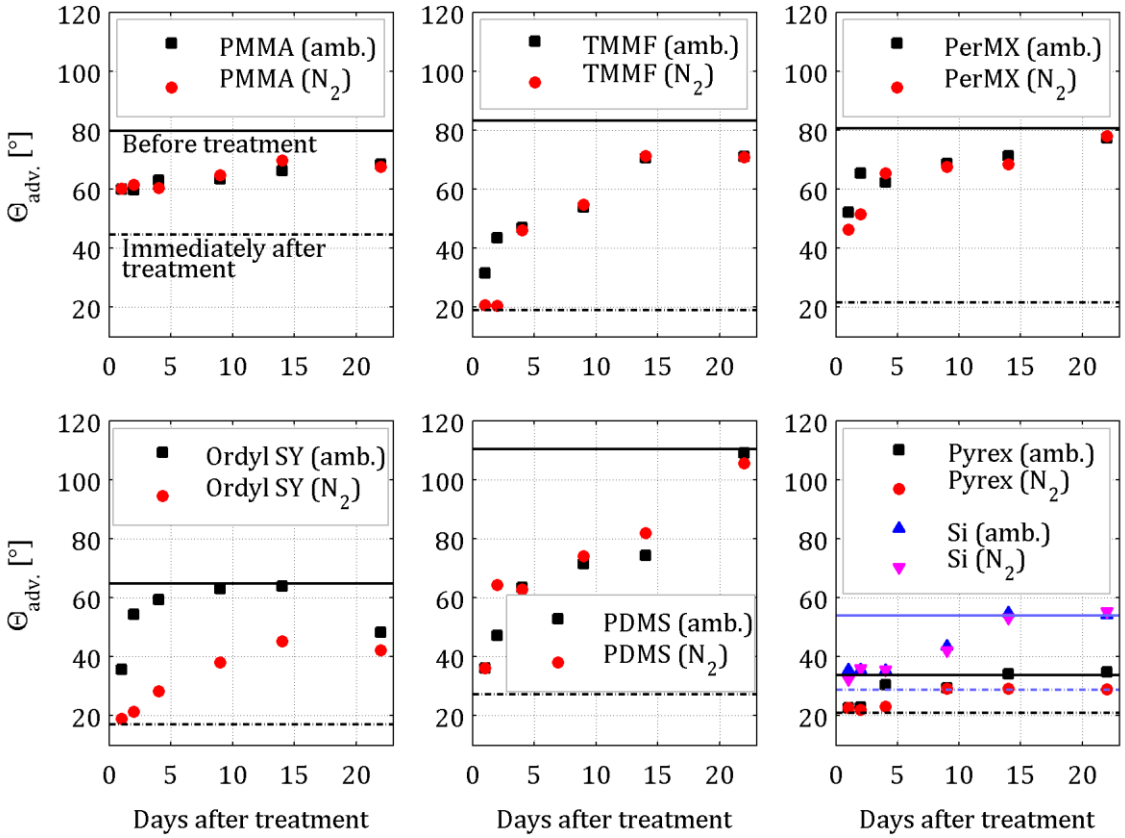

Figure 6-9: Advancing contact angles of water on different materials: initial situation (continuous line), immediately after oxygen plasma treatment (broken line). Each data point is the mean value of 10 measurements.

ment, the samples were exposed to ambient conditions for approx. 10 minutes.

The initial wetting of all polymers was inferior compared to the wetting of Pyrex. Ordyl SY had an initial advancing contact angle of 64.8° ± 1.3°, TMMF and PerMX were both in the range of 80°, and PDMS was clearly hydrophobic with a contact angle of well above 90°. Immediately after the plasma treatment, TMMF, Ordyl SY and PDMS showed wetting behaviour similar to Pyrex, i.e. contact angles in the range of 20°, but a significant part of the plasma-induced wettability got lost within a few days after the treatment. While the degradation of the hydrophilic properties of Pyrex was slow, the wetting characteristics of the polymer materials showed faster degradation over time. Surprisingly, the hydrophilic degradation was largely independent on the storage conditions. The loss of wettability over time is depicted in Figure 6-9 depicts.

6.2.2 Optical properties

The transparency of the lid is a useful property during printhead maintenance and inspection of the microchannels. Besides, clarity is generally preferable over opacity for the lid of a microfluidic device. The transmittance of TMMF, Ordyl SY and

PerMX was measured for the wavelength range of 300 nm to 900 nm and compared to the transmittance of Pyrex 7740, an anodically bondable borosilicate glass with a high optical clarity (Figure 6-10). In the visible range, the dry film resists behaved similar to Pyrex with TMMF having a slightly higher transmittance than PerMX and Ordyl SY. Below 400 nm, the transmittance of all resist materials decreased while the transmittance of Pyrex remained higher than 90 % for the entire wavelength range.

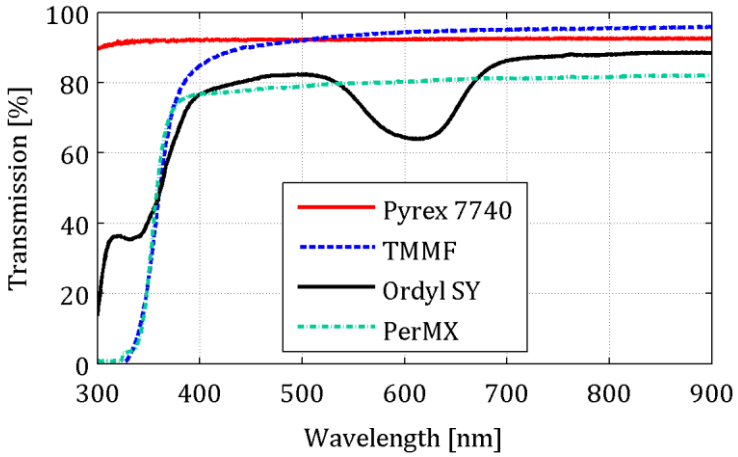

Figure 6-10: Optical transmittance spectra of TMMF (thickness of 55 µm), PerMX (50 µm), Ordyl SY (55 µm) and Pyrex 7740 (150 µm).

6.2.3 Biocompatibility

According to a widely used definition by the European Society for Biomaterials, biocompatibility describes the ability of a material to perform with an appropriate host response in a specific application. This definition implies that a technical device is placed within the body and is suitable for TopSpot printheads only to a limited extend. In microfluidics, the term *biocompatibility* is rather used to describe the compatibility between a given material and bioanalytical assays. Depending on the microfluidic application, the biocompatibility of a material can be verified by different methods, e.g. the degree of cytotoxicity, protein and DNA denaturation etc. A series of standards for evaluating the biocompatibility of a device is given by ISO 10993. One of those standards is dedicated to in vitro cytotoxicity: a test which is usually performed in the very early stages of a biocompatibility study [236].

The cytotoxicity of TMMF was analysed according to ISO 10993 as a first indication for its compatibility with microfluidic applications. TMMF samples were covered with DMEM cell culture medium and incubated at 37 °C for 24 h. The cell culture medium was then placed onto a monolayer of L929 cells replacing the medium that had nourished the cells up to that point. The cells were incubated for 24 h at

37 °C and the amount of lactate dehydrogenase (LDH, an indicator for cell viability) was compared to the LDH amount in the control media. Organotin polyvinyl chloride, a known cytotoxic material, and Thermanox Coverslips were used as positive and negative control media, respectively. The analysis did not show any cytotoxic reaction. This, however, does not mean that TMMF would pass all ISO 10993 standards or that it is compatible with any bioanalytical assay. Besides, it has to be considered that differences in the processing of a material can change the outcome of biocompatibility tests [236]. For the purpose of the above experiment, TMMF was processed on a silicon wafer as described in Section 6.1. The cytotoxicity of the other lid candidates, Ordyl and PDMS, was demonstrated in earlier studies by Vulto *et al.* [135] and Leclerc *et al.* [237], respectively. The cytotoxicity of PerMX was not analysed, because it was not available when the biocompatibility experiments started. Two other materials intended for use in the hybrid printheads – 3M 9965, a polyester tape coated with an acrylate adhesive on both sides, and COC – were also tested for cytotoxicity and both did not show any cytotoxic effects on the proliferation of L929 cells.

7 HYBRID PRINTHEADS

According to the previously described optimisation, the hybrid silicon/polymer printheads were identified as a promising alternative to improve the balance between functional and economic requirements. The term *hybrid* is used to reflect the fact that the printheads are manufactured by combining dissimilar materials to give a stronger emphasis to economic properties such as manufacturing flexibility and costs. This chapter describes the fabrication and experimental characterisation of the hybrid printheads. The flexibility of the technology is demonstrated by scaling up the process to a larger wafer format.

7.1 Fabrication

Similarly to Section 4.1, the fabrication of the hybrid printheads can be represented by a flow chart consisting of process blocks, which allows to easily gain insight into the long process chain. As shown in Table 5-5, two methods were considered to implement the sealing layer of the hybrid printheads: either by a layer of dry film resist or by a PDMS lid. When the microchannels are sealed by a layer of dry film resist, it is convenient to implement the process block Sealing before Dicing (Figure 7-1(a)). In this way, several dies are sealed in one lamination step. In the case of sealing by a PDMS lid, Dicing is performed before Sealing because handling

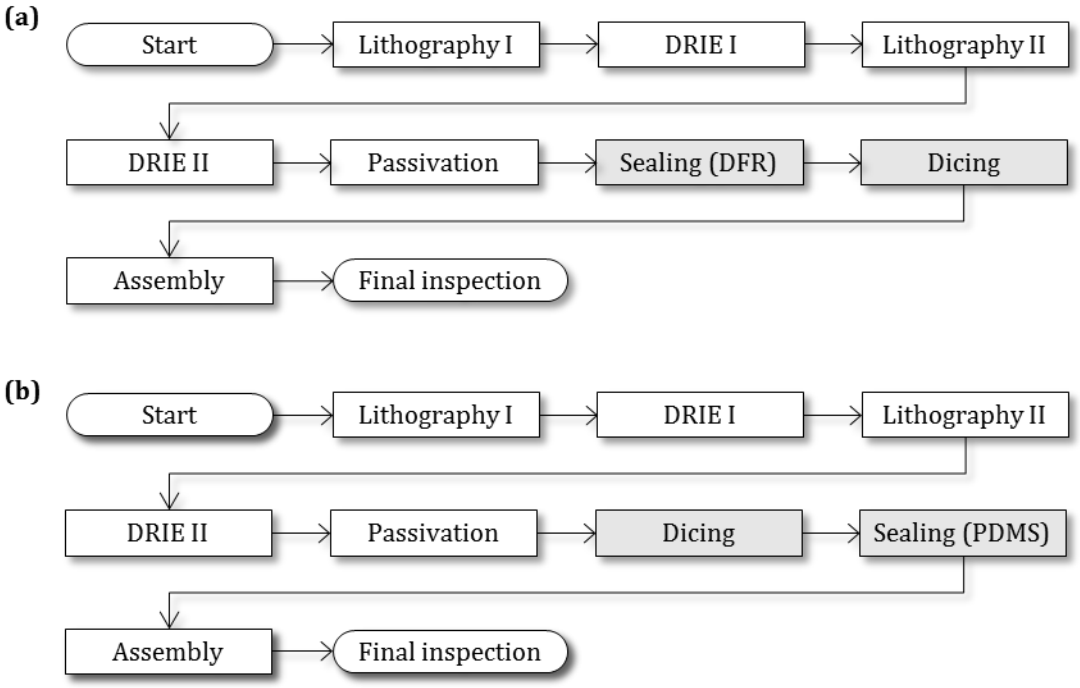

Figure 7-1: Production flow represented by 10 process blocks. **(a)** Sealing by a layer of dry film resist. **(b)** Sealing by a PDMS lid. The only difference between both production flows is the sequence of Sealing and Dicing. In the DRF-based method, Sealing is performed before Dicing. In the PDMS-based method, the silicon wafer is diced first and Sealing is performed on a die by die basis.

and aligning a thin PDMS layer on a wafer level appeared to be challenging and error prone (Figure 7-1(b)). The advantage of the PDMS based method is that it provides higher parallelisation since all individual printhead components can be manufactured in a parallel fashion before being assembled. The only difference between both methods is the sequence of the process blocks Sealing and Dicing. The process chain up to and including Passivation and the execution of the process block Assembly are the same for both methods.

7.1.1 Modification of the silicon micromachining process

Silicon micromachining includes all process blocks up to and including Passivation. Even though the silicon layer in the hybrid printheads remained the same as in the silicon/glass printheads, the process presented in Section 4.1 was modified in several aspects, mainly to use the opportunities for cost reduction provided by the new production sequence.

In the hybrid concept, the most significant factor enabling cost optimisation of the silicon micromachining process is that dicing is performed prior to assembling the reservoirs. Thus, the process blocks required to create the trenches for dicing release can be skipped (Lithography I and DRIE I from Figure 4-1). Further modification was necessary since the SOI kit that is used to avoid notching was not available in the used in-house facilities. Therefore, the oxide layer that is used as etch

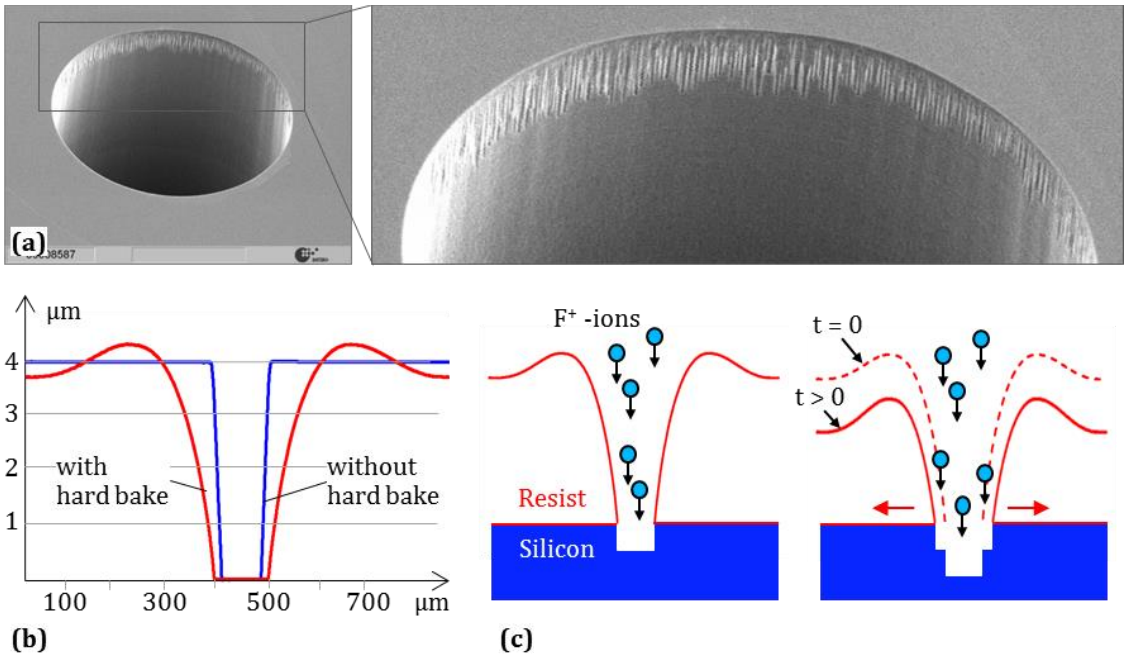

Figure 7-2: Resist as a masking material for DRIE – the influence of hard bake on the etch quality. **(a)** Silicon nozzle with damaged walls caused by reflow of the resist during hard bake. **(b)** Contact measurements of a resist profile before and after hard baking. The used resist for this experiment was AZ 4500 with a thickness of approx. 4 µm; **(c)** Enlargement of the masking layer during etching.

stop for through-hole etch in the process presented in Section 4.1 was replaced by aluminium. Aluminium has been demonstrated to be appropriate for notch-free silicon etching [238]. Since this oxide was at the same time the masking layer for nozzle etching, the oxide mask on the bottom side was replaced by a photoresist mask. The problem with the last modification was damaged nozzle walls. As shown in Figure 7-2(a), in the early development process, nozzles etched with a photoresist mask showed irregularities which may provoke cracking during printhead operation or cleaning. The reason was found to be a thermal softening and rounding of the resist during hard baking. This phenomenon is called reflow and can be observed when the developed resist is heated above its softening temperature of typically 110 °C. Though for some applications reflow of the resist is important and desirable, it may interfere with the required dimensional accuracy when the resist is used as a masking material for DRIE. A characteristic feature of reflow is that the point of contact between resist and substrate remains, while the upper edges of the resist structures become rounded (Figure 7-2(b)). As depicted in Figure 7-2(c), the rounded edges lead to an enlargement of the mask opening during DRIE, which produced dimensional irregularities. The irregularities were avoided by skipping the hard baking step, which in this case appeared to be redundant.

7.1.2 Sealing

This section describes the main steps needed to manufacture the lid and seal the microchannels.

Method A: Dry film resist

The starting point for the sealing process is a fully processed silicon wafer with

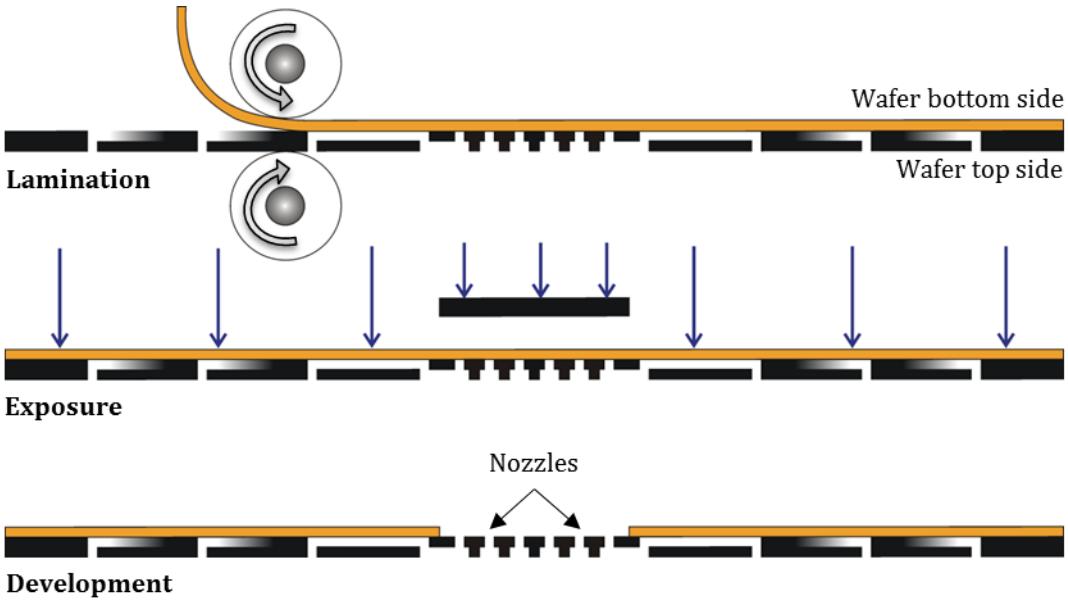

Figure 7-3: Selective sealing of TopSpot microchannels by a layer of dry film resist.

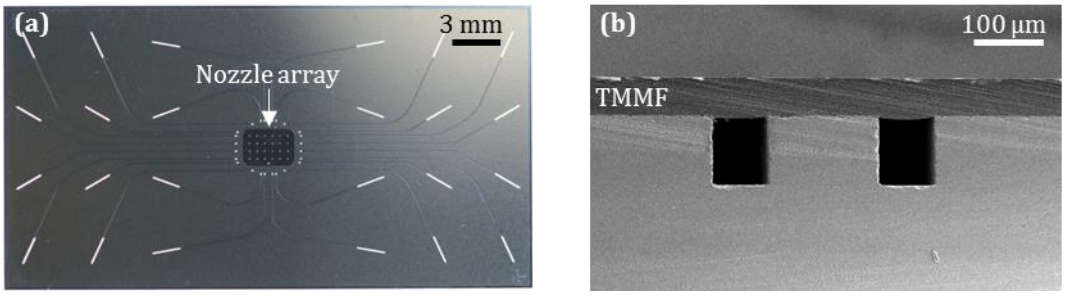

Figure 7-4: Top view **(a)** and cross-section **(b)** of microchannels sealed by a layer of TMMF.

microchannels and nozzles. The main process steps are shown in Figure 7-3, a top view and cross-section of sealed microchannels are shown in Figure 7-4. The processing of the dry film resists was performed using the parameters from Section 6.1. As exposure is performed after the resist is applied onto the wafer, no alignment was required during lamination. Cross-linking was initiated by exposure to UV light with the protective coversheet on top of the resist. A printed mask with a resolution of 800 dpi was used to prevent exposure above the nozzles. Cross-linking was completed on a hotplate at temperature rates of about 2 °C/min. The unexposed resist above the nozzles was removed in the subsequent development step.

Method B: PDMS

This process block comprises casting of the PDMS lid and bonding of the lid to the already separated silicon dies. The mould was fabricated using Ordyl SY dry film resist and allowed for the parallel casting of six lids (Figure 7-5). PDMS was mixed with its curing agent in a 10:1 ratio, casted on the mould, degassed in desiccator for 1 hour and cured over night at 70 °C. Prior to bonding, the surfaces of the PDMS and the silicon were activated by oxygen plasma for 30 s at 80 W (Picollo, Plasma Electronic). The lid was placed on a clean glass slide to obtain mechanical support,

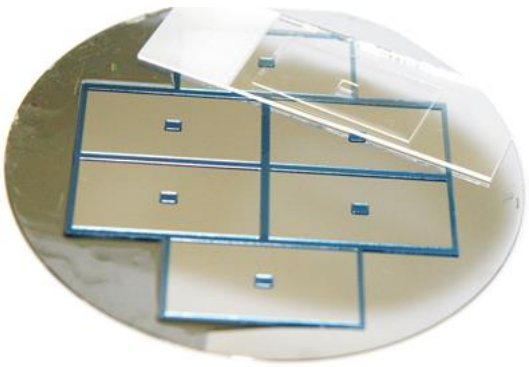

Figure 7-5: Mould for casting of the PDMS lids and a single lid placed on a glass substrate to obtain mechanical stability for the alignment and bonding process.

aligned by hand under a microscope and applied onto the silicon. Since the probability of good bonding decreases with time after activation, the application of the lid was performed within a few minutes after the plasma treatment. The main challenge was to achieve a permanent, irreversible connection for the whole surface. Most susceptible to bonding failures were border areas, where the lid could easily be detached from the silicon. Possible reasons for these failures are surface contamination or inappropriate parameters for plasma treatment. Generally, sealing of the channels by PDMS was less reproducible compared to sealing by dry film resists. In the course of the thesis work, it was decided to no longer pursue the PDMS based approach in order to concentrate on dry film resists, which promised to be considerably more successful for the intended application.

7.1.3 Assembly

In the process block Assembly, the already sealed dies and the COC reservoirs are joined to form the printhead. The COC reservoirs were purchased from an external supplier. Two joining methods were studied: using a two component epoxy adhesive and using a double side coated pressure sensitive adhesive tape.

Method A: Two component epoxy adhesive

The method was based on using Epo-Tek 375, a two-component epoxy adhesive by Polytec-PT. An adhesive layer with a thickness of about 20 µm was transferred onto the reservoirs as described in [239]. Due to the hydrophobic nature of COC, gluing the reservoirs to the silicon core without a surface treatment was not possible. Therefore, before applying the glue, the COC surface was treated with oxygen plasma for 4 minutes at 200 W. This treatment helped to provide a strong bond, however, after curing, the glue became too rigid to compensate the CTE mismatch when the assembly was heated up to the printhead washing temperature of 80 °C. At this temperature, the CTE mismatch between COC (55E-06 K^{-1}) and silicon (3E-06 K^{-1}) caused cracks on the COC surface and damaged the reservoirs.

Method B: Pressure sensitive adhesive tape

The used tape was 3M 9965, a polyester diagnostic tape coated with a pressure sensitive acrylate adhesive on both sides. The thickness of the polyester tape is 50 µm and the thickness of the adhesive layer on each side is 20 µm. The typical applications of this tape are microfluidic devices and sealing consumables for biological assays such as PCR and ELISA. The tape was first laser cut to obtain the required shape (Figure 7-6) and using an alignment tool, it was first applied on the silicon and then on the COC. Bonding was realised by applying slight pressure by hand. In contrast to the epoxy adhesive, the tape provided enough flexibility to compensate the difference in thermal expansion between COC and silicon when the printheads were heated up to the washing temperature. Thus, this method was chosen for production and further characterisation of the hybrid printheads.

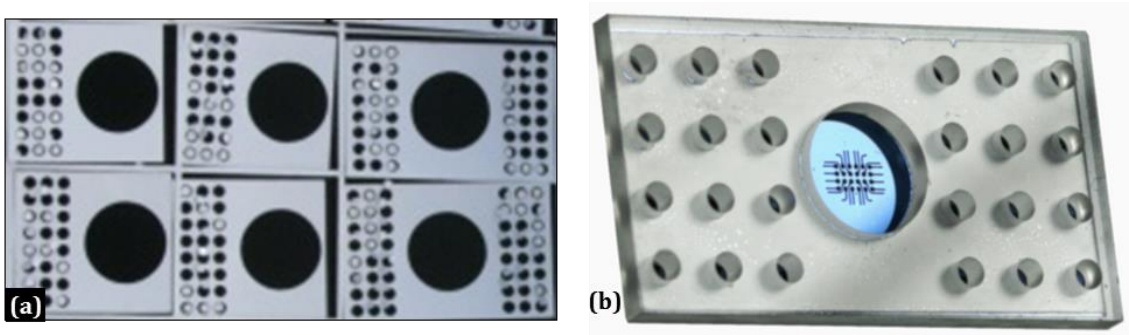

Figure 7-6: (a) Laser cut 3M 9965 adhesive tape. **(b)** Finished hybrid printhead.

7.2 Characterisation

In this section, the following printhead parameters are discussed: priming, delamination, cross-talk and carryover, printing, lead time and yield, manufacturing costs and lifetime.

7.2.1 Printhead priming

Even though several descriptions of capillary liquid transport have been presented in the literature [240,241], it is not possible to analytically predict whether a liquid will definitely spontaneously overcome all geometrical hurdles in the channels, e.g. changing cross-section, changing flow direction and corners. One indirect possibility to analyse whether the hybrid printheads are more prone to priming failures is to compare the capillary pressures in the channels of the hybrid and the silicon/glass printheads. Generally, the higher the capillary pressure, the faster and safer the capillary priming of the printhead. For microchannels with a rectangular cross-section like in the TopSpot printheads, the capillary pressure in the channels can be calculated by [242]:

$$P = \gamma\left(\frac{cos\theta_{\mathrm{B}} + cos\theta_{\mathrm{T}}}{h} + \frac{cos\theta_{\mathrm{L}} + cos\theta_{\mathrm{R}}}{w}\right) \tag{7.1}$$

where γ is the surface tension of the liquid, h and w are the height and width of the channel and $\theta_{\mathrm{B,T,L,R}}$ are the contact angles of the liquid on the bottom, top, left and right channel wall, respectively. According to Equation 7.1, the capacity of a microchannel to provide capillary flow decreases with increased advancing contact angles.

Using Equation 7.1 and the experimental results from Section 6.2.1, the capillary pressure in the microchannels was calculated for different lid materials. The results are presented in Table 7-1. The highest pressure for untreated microchannels was calculated to be 2.36 kPa and was obtained for the silicon/glass printheads.

Table 7-1: Change of the capillary pressure over time for different lid materials. The channel material is silicon. The liquid is water with a surface tension of 72.75 mN/m, the width and height of the channels are 80 µm. The contact angles are taken from Section 6.2.1, using the values achieved for storage under nitrogen atmosphere.

	Untreated					Immediately after plasma treatment				
Lid	TMMF	PerMX	Ordyl	PDMS	Glass	TMMF	PerMX	Ordyl	PDMS	Glass
***P* [kPa]**	1.71	1.75	1.99	1.29	2.36	3.25	3.24	3.26	3.20	3.24
	9 days after plasma treatment					**14 days after plasma treatment**				
Lid	TMMF	PerMX	Ordyl	PDMS	Glass	TMMF	PerMX	Ordyl	PDMS	Glass
***P* [kPa]**	2.55	2.35	2.74	2.27	2.82	1.93	1.97	2.28	1.77	2.43

For microchannels sealed by a dry film resist, the capillary pressure was in the range of 1.71 kPa to 1.99 kPa, depending on the type of the used resist. The initial pressure in microchannels sealed by a PDMS lid was 1.29 kPa or about 45 % lower compared to the silicon/glass printheads. Immediately after plasma treatment, the pressures for all lid materials became comparable. Nine days after the treatment, the priming performance of the hybrid printhead was still comparable to that of the silicon/glass printheads. Generally, the capillary pressures for all printheads drop over time. Even though the calculated capillary pressures are not quantitatively linked to an increased probability for filling failure, Table 7-1 shows that the priming performance of the hybrid printheads will be slightly inferior compared that of the silicon/glass printheads.

7.2.2 Delamination, cross-talk and carryover

Delamination or damage of the lid are potential failure modes that might cause cross-talk between channels or carryover by formerly printed samples and thus distort the results of microarray experiments. Since traditional methods of adhesion evaluation such as tensile or tape test are not fully representative of the operational conditions, the quality of the sealing was verified by alternately pushing 5 % (v/v) RBS cleaning solution and water through the channels for approx. 5 hours. The pressure in the liquid inlet line was 0.2 MPa. The experiment was performed using the printhead cleaning station presented in [243]. During the experiment, the printhead was dipped in a glass beaker filled with pure water and sonicated in a water bath at 80 °C. According to the standard operation procedure for printhead cleaning [244], this load corresponds to more than 30 washing cycles. After the load test, the printhead was dried with nitrogen and examined under the microscope. No delamination or lid damage was observed, even for those areas of the lid where the distance between neighbouring microchannels was only 100 µm. These areas are especially prone to failures as the contact surface between the lid and the silicon is very small and the load required to cause delamination is more easily exceeded.

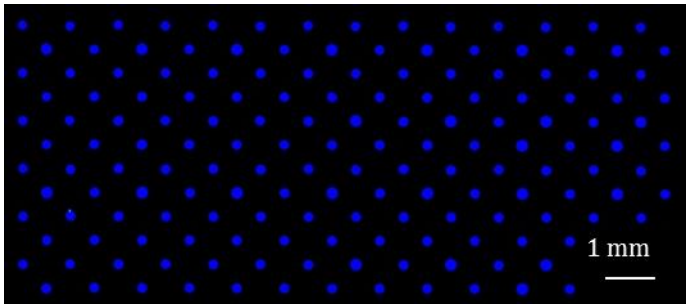

Figure 7-8: Cross-contamination and carryover test by printing a checkerboard pattern of a fluorescent dye and pure water.

The functional absence of cross-talk and carryover was confirmed by the following experiment: A hybrid printhead was first primed with Rhodamine B fluorescent dye at a concentration of 100 nM and water in a checkerboard pattern. Subsequently, the printhead was cleaned according to [244] and the pattern was inverted so that each reservoir that was previously filled with the fluorescent dye was now filled with water and vice versa. The inverted layout was printed onto an epoxy coated glass slide using an E-Vision microarrayer by BioFluidix. Finally, the image of the printed droplets was analysed using a LaVision BioAnalyzer (BioTec), showing that there was no cross-talk or carryover contamination of samples and confirming the high quality of the sealing (Figure 7-8).

7.2.3 Printing

TopSpot hybrid printheads were successfully applied for the printing of DNA and protein microarrays within several research projects and pilot studies, e.g. for HPV detection [245] and sepsis diagnostic [246]. The microarrays for these studies were produced using an E-Vision single slide microarrayer and a multi-slide microarray printer by BioFluidix. Using the SpotCheck camera, the printing perfor-

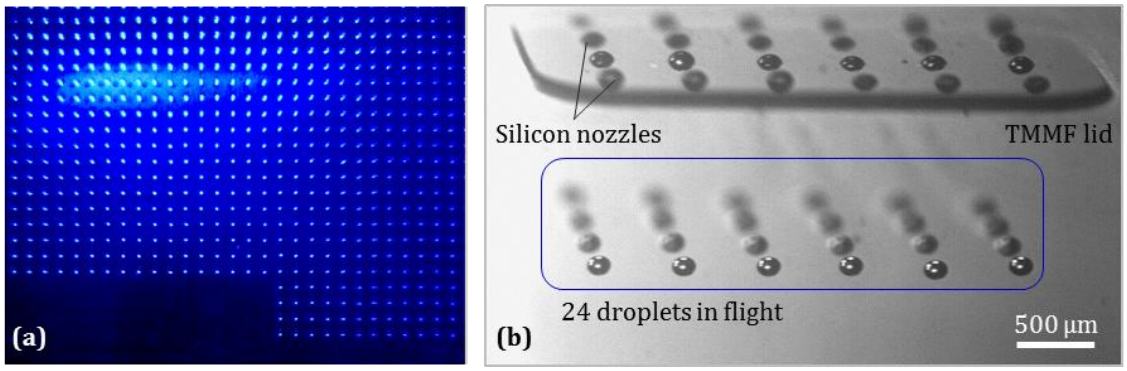

Figure 7-7: Microarray printing with hybrid printheads. **(a)** Image of an oligonucleotide microarray taken by the DropCheck camera of an E-Vision microarrayer during the microarray fabrication process. **(b)** Stroboscopic image of droplets in flight.

mance was monitored during the microarray fabrication process (Figure 7-7(a)). The printing performance was further analysed by stroboscopic observation of the droplets in flight (Figure 7-7(b)). The focus of the analysis was on possible failures such as satellite droplets, wetting of the nozzles or tilted droplet trajectories. Such failures can occur due to filmic contamination by the chemistry of the dry film resist or by resist residues on the nozzles. The stroboscopic analysis provided a good quantitative insight into the printing process and showed that the droplet formation and droplet flight are well comparable to that of the silicon/glass printheads. Since the dispensing quality is defined mostly by the quality of the nozzles (which is identical for both concepts) it is expected that the printing reproducibility of both concepts is nearly equal, as well.

7.2.4 Lead time and yield

Lead time and yield analysis was carried out analogously to Section 4.2. The yield of the individual process blocks and their rework probability were considered the same as for the silicon/glass concept, except for the process block Dicing and the newly introduced Sealing and Assembly. The dicing yield could be increased from 90 % to 95 % due to the reduced thickness of the substrate being diced (from 2.48 mm to 0.38 mm) and the reduced number of dicing paths per wafer (from 48 to 16). Due to the reduced thickness, the dicing feed rate could be increased by a factor of 2, which together with the reduced number of dicing paths caused a total reduction of the processing time for dicing by a factor of 6. The sealing by dry film resist is more tolerant to particle contamination, and the yield of Sealing could be increased from 90 % to 95 % (compared to the process blocks Bond in the silicon/glass technology). The rework probability of Sealing was 20 %, the same as for Lithography. The most probable failure in Sealing was wrinkling of the dry film during lamination caused by the high number of manual operations involved in this process. In case of lamination failure, the dry film was removed by immersion in the developer and the lamination was repeated. Even though the adhesive tape is more tolerant to particles and surface inhomogeneities, the yield of the process block Assembly could not be increased compared to the yield of Anodic bonding. The main part of the failures during assembly was caused by the manual implementation of the assembly procedure which proved to be prone to misalignment and mechanical damage of the silicon. A drawback of the new assembly procedure is that there is no feasible rework strategy. In contrast to the silicon/glass concept where bonding failures can be reworked, the rework probability for the process block Assembly was 0 %.

An overview of the lead times, yield and rework probability is presented in Table 7-2. Using the processing times from Table A 2 and Equations 4.1 to 4.4, the optimistic, pessimistic and expected lead times were calculated to be 24, 28 and 30 days, respectively. In other words, the uncertainty of lead time prediction ex-

Table 7-2: Lead time and yield analysis. LT_{OPT}, LT_{EXP} and LT_{PES} are the optimistic, expected and pessimistic lead times. RD is the rework duration and RP the rework probability, i.e. the chance that a process block will produce a rework. FPY and Y are the first pass yield and the process yield after rework. Machine and operator times are taken from Table A 2 in the Appendix. Time units smaller than 24 hours are rounded to one day.

#	Process block	In case of rework	LD_{OPT} [days]	RD [days]	FPY [%]	RP [%]	Y [%]	LT_{EXP} [days]	LD_{PES} [days]
1	Start	n/a	2	0	100	0	100	2	2
2	Lithography I	Repeat	1	1	80	20	100	2	2
3	DRIE I	n/a	6	0	95	0	95	6	6
4	Lithography II	Repeat	2	2	80	20	100	3	4
5	DRIE II	n/a	5	0	95	0	95	5	5
6	Passivation	Repeat	1	1	95	5	100	2	2
7	Sealing	Repeat	2	2	75	20	95	3	4
8	Dicing	n/a	1	0	95	0	95	1	1
9	Assembly	n/a	1	0	90	0	90	1	1
10	Final inspection	n/a	3	0	96	0	96	3	3
TOTAL			**24**	**6**	**34**	**n/a**	**70**	**28**	**30**

pressed by the difference between the pessimistic and the optimistic lead time was decreased by a factor 4, and the expected lead time was decreased by more than 35 % compared to the silicon/glass printheads. Using Equations 2.1 and 4.5, the yield was calculated to be 70 %, i.e. a yield improvement by 10 %.

7.2.5 Costs analysis

Cost analysis was performed analogously to Section 4.3, using the material costs presented in Table 7-3 and the process times from Table A 2 in the Appendix. The cost reduction compared to the silicon/glass printheads is presented in Figure 7-9. The mean cost reduction was calculated to be 59 %. The most significant contributors to this saving are the reduced workload for machine and operator and the replacement of cost-intensive semi-finished glass substrates by low cost polymer materials (Figure 7-10). Additionally, polymers allow for sealing and assembly techniques which are faster and have higher yields than anodic bonding. Significant cost reduction is also achieved by simplification of the dicing strategy, reducing the number of dicing paths and increasing the dicing speed.

Table 7-3: Material costs involved in the manufacturing of the hybrid printheads.

#	Item	Cost type	Unit	Qty.	Value
1	Lithography mask set for silicon DRIE	Fixed	M.U.	1	1600
2	Lithography mask for Sealing	Fixed	M.U.	1	100
3	Silicon wafers	Variable	M.U.	1	80
4	Semi-finished COC reservoirs	Variable	M.U.	4	80
5	TMMF sheet (size suitable for one wafer)	Variable	M.U.	1	40

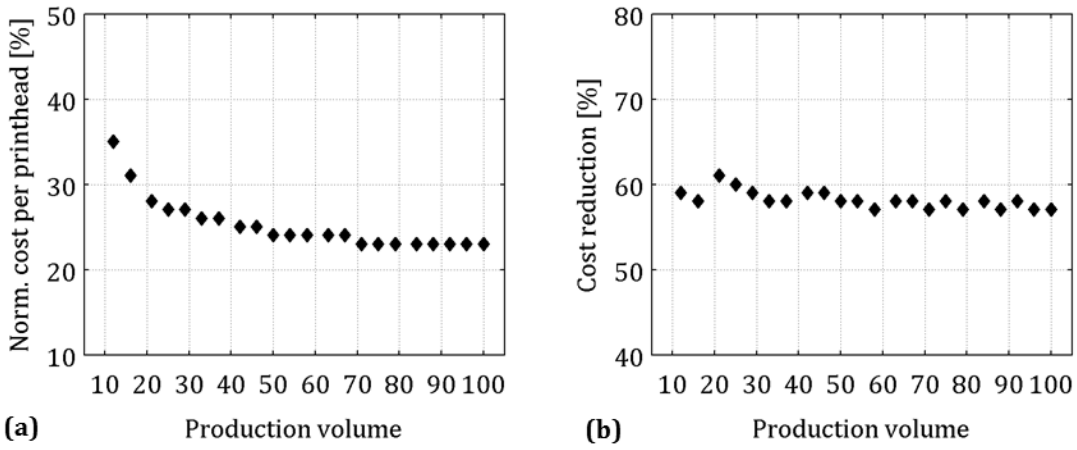

Figure 7-9: Manufacturing cost behaviour for different production volumes. **(a)** Manufacturing costs per printhead normalised to the costs per silicon/glass printhead assuming a production volume of 10. **(b)** Costs reduction with respect to the current silicon/glass technology. The mean cost reduction is 59 %.

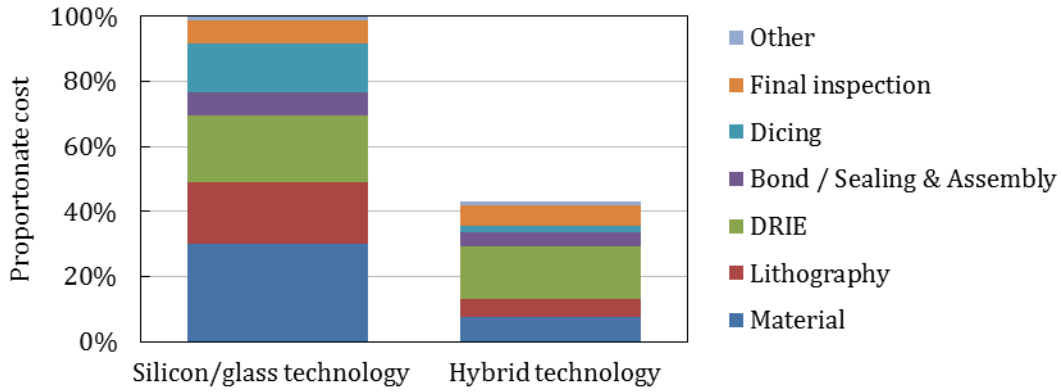

Figure 7-10: Comparison of cost breakdown for a production volume of 60 printheads.

7.2.6 Lifetime

Generally, polymer materials are more prone to aging and degradation than glass. The same applies for adhesive bonds when compared to anodic bonding. The most relevant types of degradation which the polymer materials implemented in the hybrid printheads undergo are mechanical, chemical and thermal. Even though the hybrid printheads were intensively used over the course of months without obvious degradation, it is expected that their lifetime will be shorter than the lifetime of the silicon/glass printheads.

7.3 Process transfer to a 150-mm wafer

The motivation for transferring to a larger wafer format was to determine whether it would weaken the silicon wafer and make it more susceptible to mechanical damage during lamination. In the course of the process transfer, the printheads were redesigned in order to reduce the reservoir pitch and make the nozzle grid conform to the well arrangement of the corresponding microtiter plates, i.e. 8×3 for the 24-channel and 16×6 for the 96-channel printhead, respectively. Besides, the new mask layout considered an additional intermediate printhead format with 48-channels and a nozzle grid of 8×6. When creating the masks, the emphasis was on placing the highest possible number of printheads and using one set of lithography masks to cover all printhead formats. The most appropriate option to meet

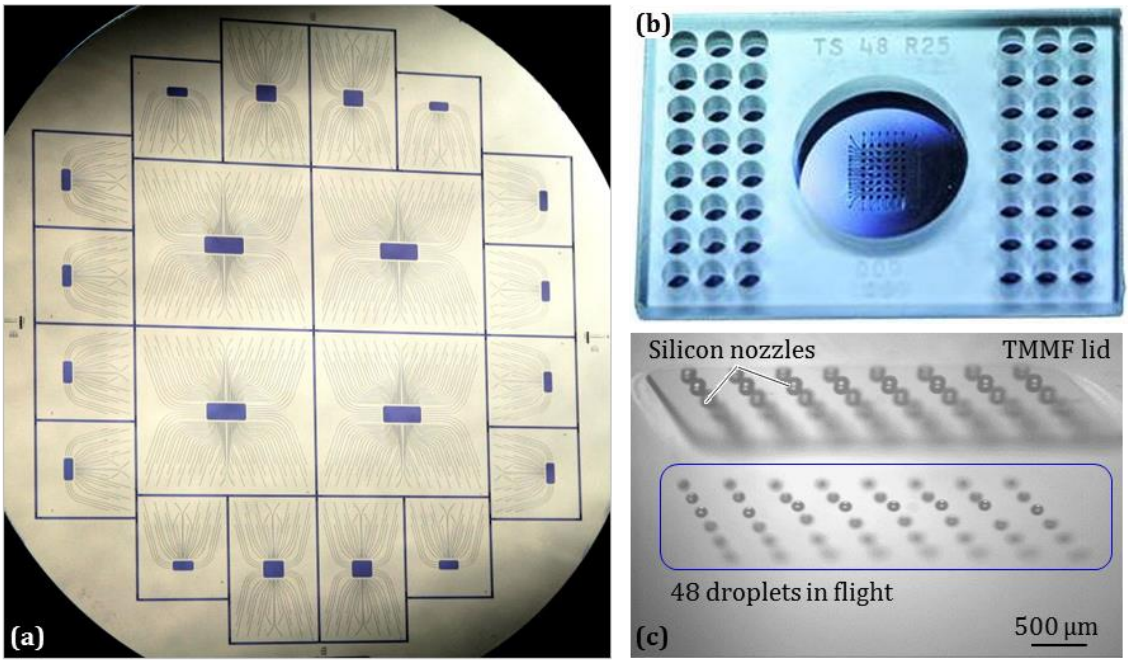

Figure 7-11: (a) 150-mm silicon wafer after lamination and completing the process block Sealing. The implemented design enables the production of different printheads on the same wafer. **(b)** 48-channel hybrid printhead. **(c)** Stroboscopic image of the droplets in flight.

these requirements was a wafer with four 96-channel, four 48-channel and twelve 24-channel printheads (Figure 7-11(a)). The processing of 150mm wafers showed that they are well comparable to 100mm wafers in terms of manufacturing yield and rework probability. The functionality of the 48-channel printheads was proven in preliminary experiments by stroboscopic inspection of the droplets in flight. An assembled 48-channel hybrid printhead and a stroboscopic image of the droplets in flight are shown in Figure 7-11(b-c).

8 All-POLYMER PRINTHEADS

This chapter demonstrates the manufacturing feasibility and the general functionality of the all-polymer printheads. The fabrication process is described and the properties of the printheads are discussed based on priming and printing experiments. As the polymer technology is not yet fully developed, yield and lead time analysis are based on both proof of principle studies and estimations regarding possible improvements until the technology is ready to go into serial production.

8.1 Fabrication

The starting point of the fabrication process were semi-finished PMMA substrates with a size of Ø100 mm × 3 mm featuring reservoirs, nozzle inlets and alignment marks. The semi-finished PMMA substrates were produced by an outside supplier by means of standard CNC machining. As shown in Figure 8-1, the fabrication process can be represented by five process blocks. The fabrication process is illustrated in Figure 8-2, the detailed process chain is presented in Table A 3 in the Appendix.

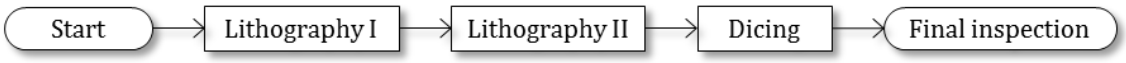

Figure 8-1: Production workflow represented by five process blocks.

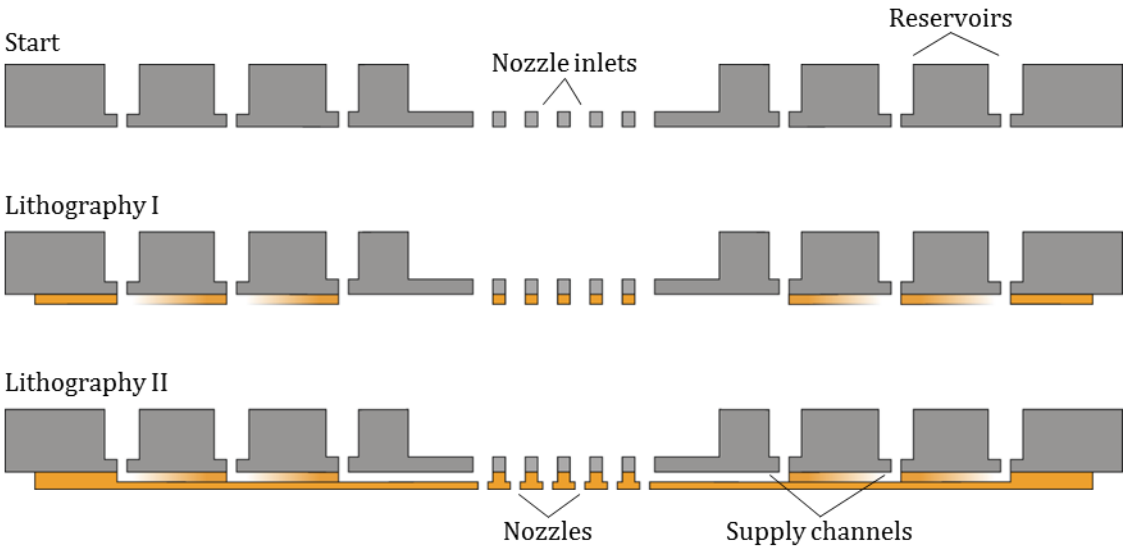

Figure 8-2: Fabrication process of the all-polymer printheads. Starting point is a semi-finished PMMA substrate with fluidic access holes purchased from an outside supplier. The nozzles and the supply channels connecting the nozzles with the reservoirs are fabricated in a multilayer dry film process.

In the process block Lithography I, two TMMF layers were laminated onto the PMMA substrate to obtain a fluidic layer with a thickness of 110 µm. Microchannels running from each reservoir to the corresponding nozzle inlet in the centre of the printheads were patterned by photolithography. After exposure, the wafer was placed on a hotplate to complete the cross-linking reaction, followed by development, rinse with IPA and deionised water and dried under a nitrogen stream. Figure 8-3 shows a PMMA wafer after the process block Lithography I was completed.

The process block Lithography II comprises the production of the sealing layer. TMMF was applied by means of lamination and exposed to UV light through a mask to initiate cross-linking and pattern a nozzle at the end of each channel. In contrast to Lithography I, the exposure of TMMF was performed without the protective coversheet in order to achieve homogeneous nozzles and enable proper droplet break-up. During exposure, sticking between TMMF and the mask was prevented by removing the coversheet 24 hours prior to the exposure, as described in Section 6.1.3. The cross-linking reaction was finalised by PEB on a hotplate, followed by development, rinse with IPA and water and drying with nitrogen purge. Figure 8-4(a) shows a cross-section of an all-polymer printhead. A detailed view of the nozzle array is presented in Figure 8-4(b-c). The printheads were separated from the substrate using a rotating diamond blade. Due to a limitation of the achievable dicing depth, the substrate was not diced completely through: First, 2.2 mm deep grooves were diced along the dicing paths and finally the printheads were separated manually along the grooves (Figure 8-4(d)).

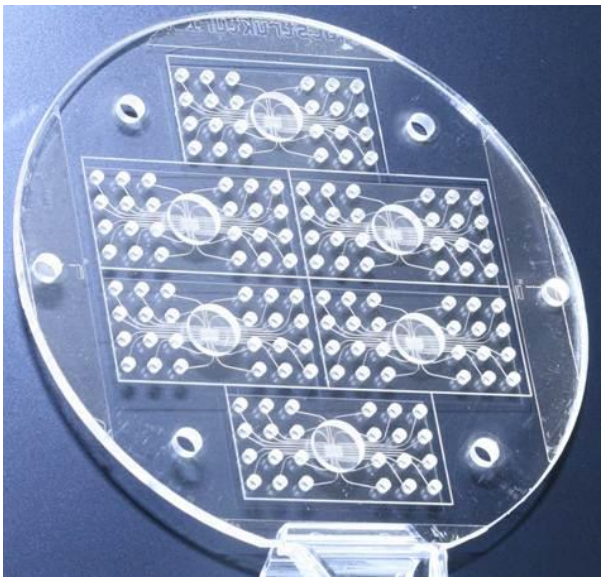

Figure 8-3: PMMA substrate after patterning the first fluidic layer. The six holes in the outer area are for holding the substrate during machining of the fluidic access holes.

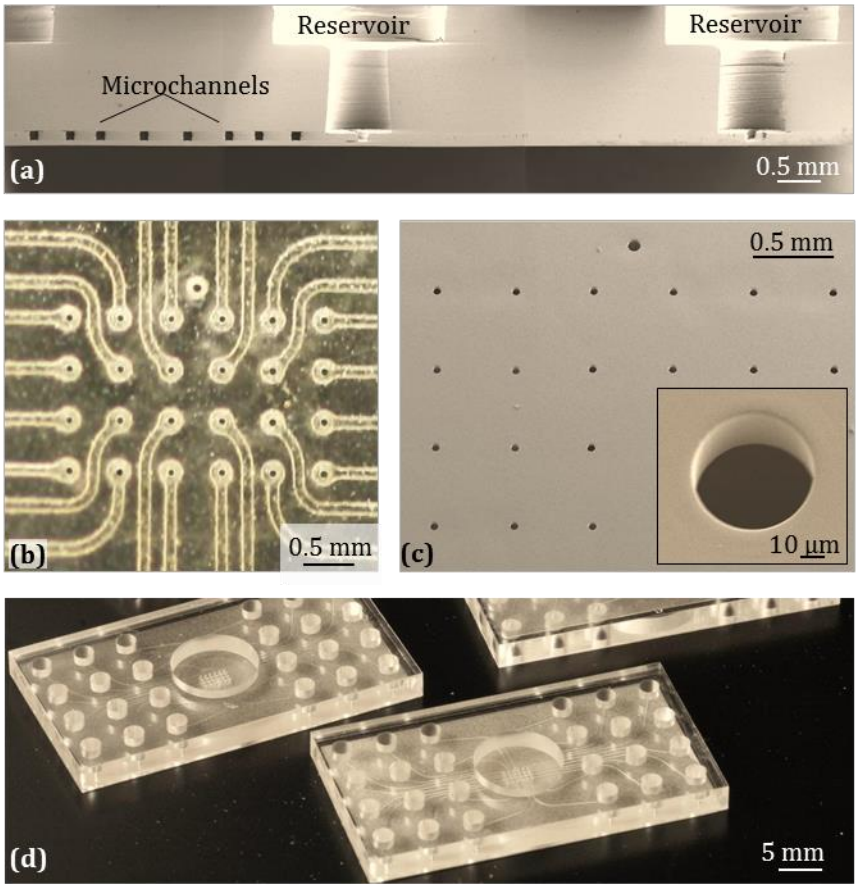

Figure 8-4: All-polymer printheads. **(a)** Cross sectional view showing the reservoirs and sealed microchannels. **(b)** Top view and **(c)** bottom view of the nozzle array. **(c)** Finished polymer printheads after dicing.

8.2 Characterisation

8.2.1 Printhead priming

The priming properties of the printheads were examined experimentally by pipetting dyed water into the reservoirs. The experiment was performed before and after oxygen plasma treatment. The number of tested channels was 419, using 19 different printheads. 37 channels were not considered because they were damaged and did not contribute to the priming study.

Two interfaces were identified to be prone to priming failures: Reservoir/Channel and Channel/Nozzle (Figure 8-5). Even though both TMMF and PMMA are hydrophilic, only 14.8 % of the untreated channels could be filled by capillary forces. In 40.6 % of the channels, the liquid stopped at the interface Reservoir/Channel, and in 44.6 % of the channels a filling stop occurred at the interface Channel/Nozzle. One possible reason for these malfunctions is burrs from the CNC process which

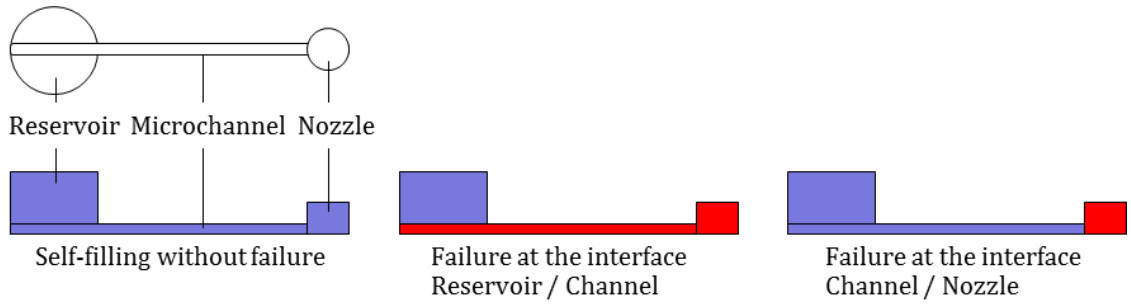

Figure 8-5: Classification of failure modes with respect to priming.

Table 8-1: Priming performance of the all-polymer printheads with untreated channels and immediately after the oxygen plasma treatment.

Failure type	Unit	Untreated	After treatment
Self-filling without failure	[%]	14.8	100
Failure at the interface Reservoir/Channel	[%]	40.6	0.0
Failure at the interface Channel/Nozzle	[%]	44.6	0.0

may cause a stop of the liquid flow. After the plasma treatment, the self-filling properties were significantly improved and 100 % of the channels were filled without any failure. This can be explained by the improved wetting behaviour and increased capillary pressure in the channels. Substituting the measured contact angles from Section 6.2.1 into Equation 7.1, the capillary pressure before and after the treatment was calculated to be 0.44 and 3.06 kPa, respectively. The results of the self-filling study are summarised in Table 8-1.

8.2.2 Delamination, cross-talk and carryover

The initial leak-tightness of the channels was confirmed by the priming study (Figure 8-6). Additionally, the printheads were subjected to a pressure test at

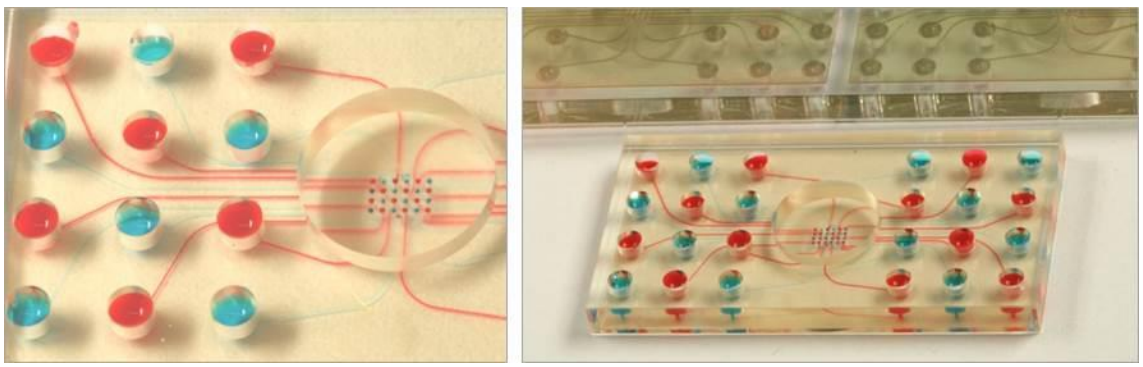

Figure 8-6: Polymer printhead filled with died water to verify the initial leak tightness.

0.8 MPa for 5 min which confirmed that they can withstand this load without delamination or lid damage. However, when the printheads were sonicated in a heated water bath at 80 °C (in addition to the pressure load of 0.8 MPa), delamination at the PMMA/TMMF interface occurred. The delamination was restricted to the centre of the printheads and can be explained by the very small substrate-resist contact area. Even though cross-talk and carryover of samples were not particularly analysed, it can be concluded that combined loads of pressure (0.8 MPa), temperature (80 °C) and ultrasonic actuation weaken the sealing and pose a risk of cross-talk and carryover contamination. Thus, especially when the printheads are not intended to be used as disposable devices, the all-polymer printheads are inferior compared to the hybrid and the silicon/glass printheads.

8.2.3 Printing

Since the standard hydrophobisation procedure for silicon nozzles [247] appeared to be inappropriate for TMMF, the printing performance was studied with uncoated nozzles. The suitability of the all-polymer printheads for printing of single droplets was verified by stroboscopic observation of the droplets in flight. The main challenge was wetting of the nozzles after some period of operation and, as a consequence, missing and satellite droplets (Figure 8-7). Based on the diameter of the droplets in flight, the dispensed volume was calculated to be in the range of 745 pl, which is less than the droplet volume of the silicon/glass printheads (Figure 8-8, Equation 8.1). This can be explained with the changed geometrical dimensions of nozzles and nozzle inlets, which in a previous study were found to have a great influence on the dispensed volume [243]. The accuracy in determining the droplet diameter from the stroboscopic image was found to be $\pm$ 3 px, i.e. approx. $\pm$ 6 µm, which corresponds to a volume error of approx. $\pm$ 115 pl. The homogeneity of droplet volumes was not explicitly analysed because such an analysis is more reasonable after implementing a hydrophobic nozzle coating and optimising the printing parameters. However, it can be assumed that the variation of the droplet vol-

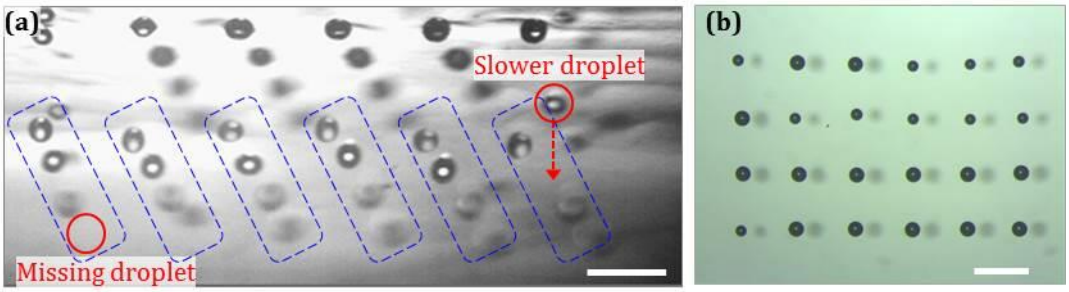

Figure 8-7: Printing performance of polymer printheads with unmodified TMMF nozzles. **(a)** Water droplets in flight. **(b)** Printed droplets on a hydrophobic coated glass slides. Scale bars represent 500 µm.

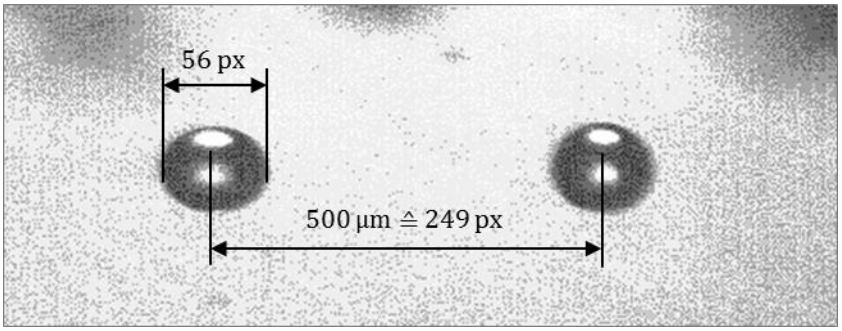

Figure 8-8: Calculation of the droplet volume based on stroboscopic images of the droplets in flight.

$$V = \frac{\pi \times d^3}{6} = \frac{\pi \times (56 \times \frac{500}{249})^3}{6} = 745 \text{ pl} \tag{8.1}$$

ume will be higher as compared to the silicon/glass and the hybrid printheads. The main reasons for this are the lower stiffness of TMMF (2.1 GPa [197]) compared to silicon (130 GPa [248]) and the lower resolution of TMMF (10 µm [191]) compared to the photoresist used as a masking material for etching of the silicon nozzles (1 µm [249]).

The printing experiments demonstrated the general feasibility of the polymer approach. At this development stage, however, the droplet homogeneity and reliability of the all-polymer printheads are not sufficient to compete to the state-of-the-art microarrayers presented in Section 1.3.

8.2.4 Lead time and yield

The optimistic, expected and pessimistic lead times were calculated similarly to Section 4.2 and using the processing times from Table A 3 in the Appendix. The results of the analysis are summarised in Table 8-2. A specific characteristic of the polymer approach is that there is no possibility of rework after the process block Lithography has taken place. The reason for this is that after post exposure bake, the dry film resist cannot be removed from the substrate in a convenient way. The lack of the possibility of rework decreases the total yield, but it is also the reason why the optimistic, expected and pessimistic lead times are identical. This enables a high precision in lead time prediction and adherence to committed delivery dates. Another characteristic of the polymer approach is the shorter lead time. The expected lead time takes about 30 % of the lead time of the hybrid printheads and 20 % of the lead time of the silicon/glass printheads.

To provide honest comparisons between the different concepts, the first pass yield of the process blocks Lithography I/II was adopted from the hybrid and the sili-

Table 8-2: Summary of the lead time and yield analysis. . LT_{OPT}, LT_{EXP} and LT_{PES} are the optimistic, expected and pessimistic lead times. RD is the rework duration and RP the rework probability, i.e. the chance that a process block will produce a rework. FPY and Y are the first pass yield and the process yield after rework. Machine and operator times are taken from Table A 2 in the Appendix. Time units smaller than 24 hours are rounded to one day.

#	Process block	In case of rework	LD_{OPT} [days]	RD [days]	FPY [%]	RP [%]	Y [%]	LT_{EXP} [days]	LD_{PES} [days]
1	Start	n/a	1	0	100	0	100	1	1
2	Lithography I	n/a	2	0	80	0	80	2	2
3	Lithography II	n/a	2	0	80	0	80	2	2
8	Dicing	n/a	1	0	100	0	100	1	1
10	Final inspection	n/a	2	0	84	0	84	2	2
TOTAL			**8**	**0**	**54**	**n/a**	**54**	**8**	**8**

con/glass printheads (80 %). Separation of the printheads with a conventional diamond saw blade proved to work without chipping, cracking or other defects that cause rework or scrap. Therefore, the first pass yield of dicing was assumed to be 100 %.

Since the technology is not yet fully developed, the percentage of good printheads after the final inspection will be significantly lower compared to the hybrid and the silicon/glass concepts. Lower yields are common with new manufacturing processes, and as the process is further developed, the yield will increase. In the early development stage, the most significant contributing factor to yield loss was the production of the nozzle array. The root cause analysis showed that most likely during exposure light is scattered from the wafer chuck and the substrate, thus causing undesirable exposure of masked resist regions. Moreover, the used substrate material had a matte surface finish with a diffuse light reflection which additionally supported light scattering and unwanted polymerisation of the nozzles. A similar problem with SU-8 on glass substrates has been reported in the literature, and different counteractions have already been successfully implemented [250]. In this early development stage, it was assumed that the percentage of printheads that do not pass the final inspection and testing will be 4 times higher compared to the printheads with silicon nozzles. Based on this assumption, the first pass yield of the process block Final inspection was considered to be 84 %. The yield values of all process blocks are summarised in Table 8-2. Using Equation 2.1, the total yield was calculated to be 54 %.

8.2.5 Costs analysis

Cost analysis was performed based on the same assumptions as for the silicon/glass printheads (Section 4.3). Using Equations 2.4-2.6, the material costs from Table 8-3 and the processing times from Table A 3 in the Appendix, the man-

Table 8-3: Material costs involved in the manufacturing of the all-polymer printheads.

#	Item	Cost type	Unit	Qty.	Value
1	Lithography mask set	Fixed	M.U.	1	1600
2	Semi-finished PMMA substrates	Variable	M.U.	1	80
3	TMMF sheet (size suitable for one wafer)	Variable	M.U.	1	40

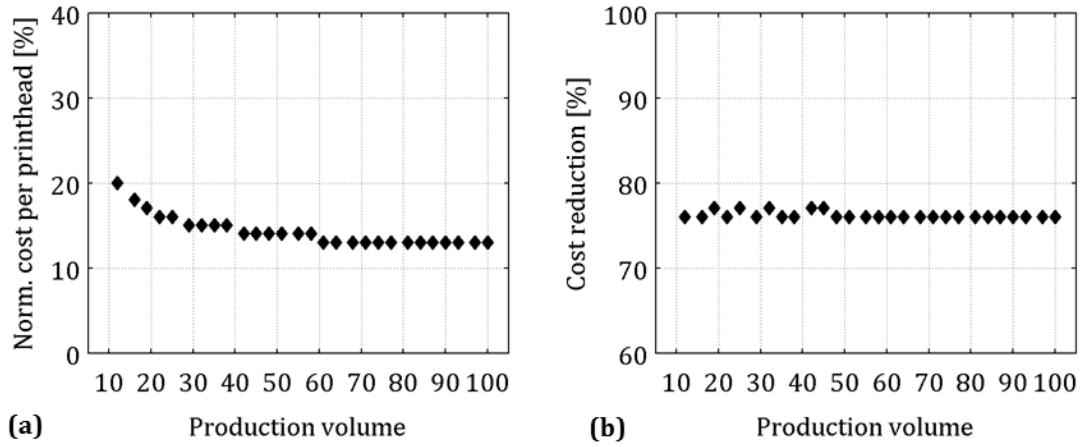

Figure 8-9: Manufacturing cost behaviour for different production volumes. **(a)** Manufacturing costs per printhead normalised to the costs per silicon/glass printhead assuming a production volume of 10. **(b)** Costs reduction with respect to the current silicon/glass technology. The mean cost reduction is 76 %.

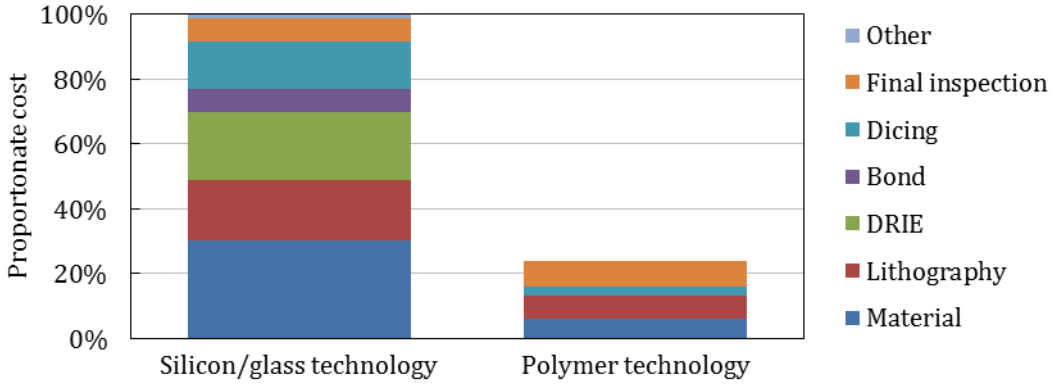

Figure 8-10: Comparison of cost breakdown for a production volume of 60 printheads.

ufacturing costs were calculated for a production volume of 10 to 100 printheads (Figure 8-9). The cost reduction compared to the silicon/glass printheads was calculated to be 76 % for the entire production volume range. The most important factors for cost reduction were the reduction of the processing costs, particularly by eliminating the process blocks DRIE and Bonding, and lower material costs (Figure 8-10).

8.2.6 Lifetime

The lifetime considerations for the hybrid printheads in Section 7.2.6 also hold true for the all-polymer printheads. Since not only the sealing lid but also functional fluidic components such as microchannels and nozzles were implemented in TMMF, it is expected that the lifetime of the all-polymer printheads will be lower than the lifetime of the hybrid and the silicon/glass printheads. The most significant contributor to the reduced lifetime is expected to be delamination of the resist close to the nozzles, promoted by the very small contact area with the substrate. The risk of delamination can be reduced by design adaptation, e.g. decreasing the channel width, increasing the nozzle pitch or a combination of both, and by further process improvement in terms of resist adhesion.

9 TECHNOLOGY SELECTION USING THE ANALYTICAL HIERARCHY PROCESS

There are few applications where the most suitable fabrication technology can be determined without deeper analysis of the specific requirements. In most cases, however, the decision is a balancing act between economic and functional criteria. The process of technology selection can therefore be considered as a multi-criteria decision-making problem. This chapter employs the analytical hierarchy process presented in Chapter 3 with the aim of evaluating different printhead alternatives and selecting the printhead that is most appropriate based on a given set of criteria.

9.1 Hierarchical framework

The hierarchical framework used for the evaluation of the printheads is shown in Figure 9-1. The first level of the framework is the goal, which in this case was the technology selection for TopSpot printheads. The second level comprises the criteria upon which the evaluation is based. The criteria assigned to this level were *performance* (C_1), *lifetime* (C_2), *lead time* (C_3) and *costs* (C_4). In order to enable a deeper analysis without increasing the rank of the comparison matrix, four performance related sub-criteria were arranged in a lower hierarchical level: *printhead priming* (C_{11}), *cross-talk avoidance* (C_{12}), *carryover avoidance* (C_{13}) and *printing quality* (C_{14}). In this way it was also possible to avoid comparing performance related with operational and economic criteria such as lead time and costs. The lowest level of the hierarchical framework represents the different technologies for fabrication of the printheads: the standard silicon/glass technology (A_1), the

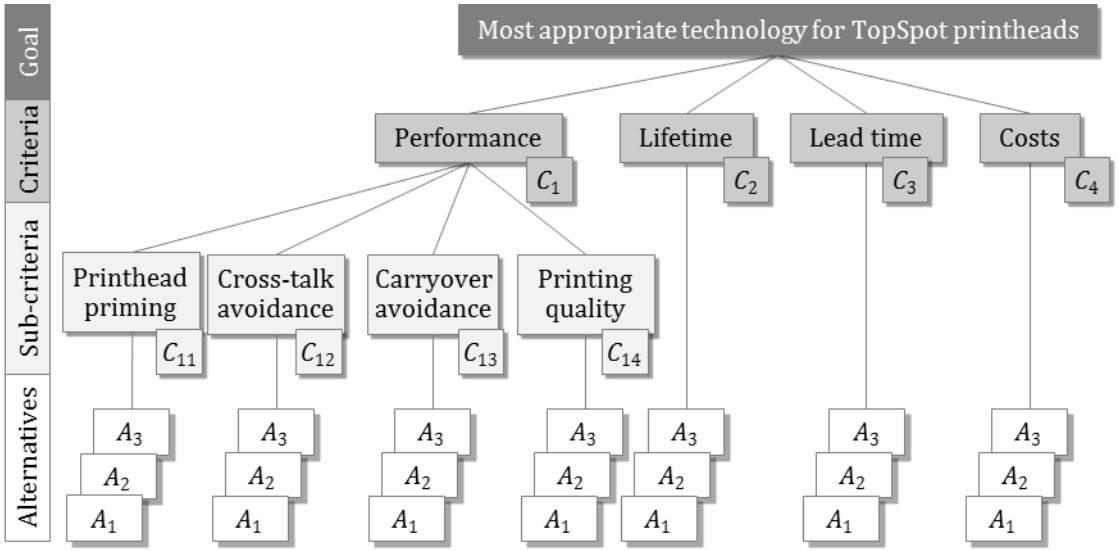

Figure 9-1: The hierarchical framework for evaluating the printhead alternatives.

hybrid silicon/polymer technology based on COC and TMMF (A_2) and the all-polymer technology based on PMMA and TMMF (A_3).

9.2 Comparison, consistency analysis and prioritisation

The pairwise comparison process was accomplished according to the hierarchical framework in Figure 9-1. First, the criteria C_1 to C_4 were compared to each other in order to quantify their importance with respect to the goal. Since the degree of importance of one criterion over another is strongly customer dependent, there is more than one possible priority vector. Common customer needs are represented by the comparison matrices ***A*** and ***B*** in Table 9-1.

The corresponding priority vectors are obtained by the eigenvector method and are the normalised principal eigenvectors of ***A*** and ***B***. The matrix ***A*** represents a typical customer whose buying decision depends mostly on the criteria *performance* ($w_{C1} = 0.589$) and *lifetime* ($w_{C2} = 0.292$) with *lead time* ($w_{C3} = 0.055$) and *costs* ($w_{C4} = 0.064$) being less important. The comparison matrix ***B*** represents a customer paying highest attention to performance ($w_{C1} = 0.439$), followed by *costs* ($w_{C4} = 0.269$), *lead time* ($w_{C3} = 0.229$) and *lifetime* ($w_{C2} = 0.062$). The consistency ratio of ***A*** and ***B*** was calculated using Equations 3.5 and 3.6. For both matrices, the consistency ratio was below 0.1, which means that they satisfy the consistency criterion of the AHP:

$$CR_{\boldsymbol{A}} = \frac{CI_{\boldsymbol{A}}}{RI_{n=4}} = \frac{\frac{\lambda_{\max,\boldsymbol{A}} - n}{n-1}}{RI_{n=4}} = \frac{\frac{4.09-4}{4-1}}{0.9} = 0.03 \tag{9.1}$$

$$CR_{\boldsymbol{B}} = \frac{CI_{\boldsymbol{B}}}{RI_{n=4}} = \frac{\frac{\lambda_{\max,\boldsymbol{B}} - n}{n-1}}{RI_{n=4}} = \frac{\frac{4.18-4}{4-1}}{0.9} = 0.07 \tag{9.2}$$

The four sub-criteria from the third hierarchical level C_{11} to C_{14} were assigned

Table 9-1: Two possible prioritisations representing common customer needs. The priorities are the normalised principal eigenvectors of the matrices ***A*** and ***B***. λ_{max} and CR are the corresponding maximal eigenvalue and the consistency ratio, respectively.

		Matrix *A*					**Matrix *B***				
		C_1	C_2	C_3	C_4	Priority	C_1	C_2	C_3	C_4	Priority
Performance	C_1	**1**	3	9	7	0.589	**1**	7	3	1	0.439
Lifetime	C_2	1/3	**1**	7	5	0.292	1/7	**1**	1/5	1/3	0.062
Lead time	C_3	1/9	1/7	**1**	1	0.055	1/3	5	**1**	1	0.229
Costs	C_4	1/7	1/5	1	**1**	0.064	1	3	1	**1**	0.269
		$\lambda_{\max} = 4.09$; $CR = 0.03$					$\lambda_{\max} = 4.18$; $CR = 0.07$				

Table 9-2: Pairwise comparison matrix for the sub-criteria with respect to their common parent.

		C_{11}	C_{12}	C_{13}	C_{14}	Local priority
Printhead priming	C_{11}	**1**	1	1	1	0.250
Cross-talk avoidance	C_{12}	1	**1**	1	1	0.250
Carryover avoidance	C_{13}	1	1	**1**	1	0.250
Printing quality	C_{14}	1	1	1	**1**	0.250

$\lambda_{\max} = 4;\ CR = 0$

equal importance with respect to their parent C_1. This most appropriate represents a common range of applications where printhead priming, the avoidance of cross-talk and carryover and the printing quality share the same level of importance (Table 9-2).

Since the three technologies are to be evaluated with respect to seven criteria and sub-criteria, seven comparison matrices in the order of 3×3 were necessary for the evaluation (Table 9-3). The entries in the matrices were obtained by comparing the technologies A_1 (silicon/glass), A_2(hybrid) and A_3(all-polymer) with each other and are explained in more detail in Sections 9.2.1 to 9.2.7. The judgment a_{ij} indicates whether the technology i is superior or inferior to the technology j with respect to a given criterion. In accordance to the fundamental scale of the AHP, $a_{ij} > 1$ indicates a superiority of i over j, and $a_{ij} < 1$ indicates a superiority of j over i (the higher the number the stronger the superiority). The diagonal elements of the matrices, i.e. when one technology is compared to itself, are always 1 ($a_{ii} = 1$), and the elements below the diagonal are the reciprocal mirror image of the elements above it ($a_{ij} = 1/a_{ji}$).

9.2.1 Printhead priming

The priming properties of the silicon/glass (A_1) and the hybrid printheads (A_2) are dominated by the wetting behaviour of the silicon channels. Although the channels are fabricated using the same DRIE process and consequently have the same wetting behaviour, a higher priority was given to the silicon/glass technology due to the higher native hydrophilicity of the glass lid and consequently higher capillary pressure in the channels: $a_{12} = 3$. When compared to the all-polymer printheads (A_3) , the silicon/glass and the hybrid printheads were judged strongly and slightly superior, respectively: $a_{13} = 5$ and $a_{23} = 3$.

9.2.2 Cross-talk avoidance

Concerning the risk of cross-talk, the hybrid technology (A_2) and the silicon/glass technology (A_1) were judged to be of equal quality: $a_{12} = 1$. This judgment was based on the experimental results obtained in Section 7.2.2. Even though the all-polymer printheads (A_3) demonstrated initial leak tightness when applied to a

Table 9-3: Pairwise comparison matrices for the printhead alternatives with respect to the seven criteria. The values in the brackets represent the normalised priorities obtained by dividing each priority by the highest priority. In this way, the priority of the most preferred alternative becomes "ideal" and receives the value of 1.

Printhead priming (C_{11})

	A_1	A_2	A_3	Priority	
A_1	**1**	3	5	0.637	(1.000)
A_2	1/3	**1**	3	0.258	(0.405)
A_3	1/5	1/3	**1**	0.105	(0.165)

Cross-talk avoidance (C_{12})

	A_1	A_2	A_3	Priority	
A_1	**1**	1	7	0.467	(1.000)
A_2	1	**1**	7	0.467	(1.000)
A_3	1/7	1/7	**1**	0.067	(0.143)

Carryover avoidance (C_{13})

	A_1	A_2	A_3	Priority	
A_1	**1**	1	5	0.455	(1.000)
A_2	1	**1**	5	0.455	(1.000)
A_3	1/5	1/5	**1**	0.091	(0.200)

Printing quality (C_{14})

	A_1	A_2	A_3	Priority	
A_1	**1**	1	9	0.474	(1.000)
A_2	1	**1**	9	0.474	(1.000)
A_3	1/9	1/9	**1**	0.053	(0.112)

Lifetime (C_2)

	A_1	A_2	A_3	Priority	
A_1	**1**	3	9	0.655	(1.000)
A_2	1/3	**1**	7	0.290	(0.443)
A_3	1/9	1/7	**1**	0.055	(0.084)

Lead time (C_3)

	A_1	A_2	A_3	Priority	
A_1	**1**	1/3	1/5	0.105	(0.165)
A_2	3	**1**	1/3	0.258	(0.405)
A_3	5	3	**1**	0.637	(1.000)

Costs (C_4)

	A_1	A_2	A_3	Priority	
A_1	**1**	1/5	1/7	0.072	(0.111)
A_2	5	**1**	1/3	0.279	(0.430)
A_3	7	3	**1**	0.649	(1.000)

constant pressure load, they are characterised by a significantly higher risk of cross-talk due to possible degradation of the sealing properties. Thus, the polymer technology was judged very strongly inferior to both the hybrid and the silicon/glass technologies: $a_{31} = a_{32} = 1/7$.

9.2.3 Carryover avoidance

In experimental studies, the hybrid printheads (A_2) demonstrated high reliability with no evidence of sample-to-sample carryover and were therefore judged as being equivalent to the silicon/glass printheads (A_1): $a_{12} = 1$. The all-polymer printheads (A_3) were judged strongly inferior to both the hybrid and the silicon/glass printheads: $a_{31} = a_{32} = 1/5$. This judgment was motivated by the minor robustness of the all-polymer printheads which might require gentler cleaning in order to avoid mechanical damage and delamination of the nozzle layer. As a consequence, this might decrease the efficiency of the cleaning process and poses a higher risk of carryover contaminations.

9.2.4 Printing quality

The printing performance is mostly defined by the fabrication accuracy and homogeneity of the nozzles. Since the nozzles of the silicon/glass (A_1) and the hybrid printheads (A_2) are both fabricated using the same silicon DRIE process, the two technologies have nearly equal printing performance and were accordingly assigned equal priority: $a_{12} = 1$. The appropriateness of this judgment was confirmed by the printing experiments in Section 7.2.3 and by the fact that both printheads use the same coating method to avoid wetting of the nozzles. The hybrid and the silicon/glass printheads were assigned the highest possible advantage over the all-polymer printheads (A_3): $a_{13} = a_{23} = 9$. The reasons for this judgment are manifold. From more general perspective, the all-polymer technology is in the early development stage and is therefore more prone to deviations from target parameters, especially regarding tightly tolerated features like dispensing nozzles. Besides, the nozzles of the all-polymer printheads suffer from lower mechanical strength (compared to silicon) and lower resolution of TMMF (compared to the photoresist used as a masking material for silicon etching). In addition, the efficiency of the hydrophobic coating on TMMF, a crucial factor in terms of high printing quality, is still insufficient and needs to be further improved in order to be competitive with the silicon/glass and the hybrid printheads.

9.2.5 Lifetime

The highest priority in terms of lifetime is assigned to the silicon/glass technology. The printheads manufactured with this technology have the longest (and practically unlimited) lifetime and can be damaged only by inappropriate operation. The lowest priority is assigned to the all-polymer technology, because the printheads manufactured with this technology were prone to mechanical damage when exposed to operational-like conditions. In terms of lifetime, the entries in the corresponding comparison matrix were based on the following judgements: the silicon/glass technology (A_1) is slightly favoured over the hybrid technology (A_2) and extremely favoured over the polymer technology (A_3): $a_{12} = 3$ and $a_{13} = 9$. The hybrid technology is very strongly favoured over the polymer technology: $a_{23} = 7$.

9.2.6 Lead time

The comparisons regarding lead time were based on an expected time of 42 days for the silicon/glass printheads, 28 days for the hybrid printheads and 8 days for the all-polymer printheads. These durations were transferred into entries of the comparison matrix using the following verbal judgments: The silicon/glass printheads (A_1) are slightly inferior to the hybrid printheads (A_2) and strongly inferior to the all-polymer printheads (A_3): $a_{12} = 1/3,\ a_{13} = 1/5$. The all-polymer printheads are slightly superior to the hybrid printheads: $a_{32} = 3$.

9.2.7 Costs

The comparison of the three techniques in terms of costs was based on the cost analyses in Section 1.1 (silicon/glass), Section 7.2.5 (hybrid) and Section 8.2.5 (all-polymer). The highest priority was given to the polymer technology (A_3) according to the verbal judgments "very strongly favoured over the silicon/glass technology (A_1)": $a_{31} = 7$) and "slightly favoured over the hybrid technology (A_2)": $a_{32} = 3$. The hybrid technology was considered to be strongly favoured over the silicon/glass technology: $a_{21} = 5$.

9.3 Synthesis

In this final evaluation step, the three technologies were evaluated using the ideal synthesis mode according to Section 3.5.2. The ideal mode was preferred over the distributive mode because the purpose of the decision process was to select the technology that best meets a given set of criteria and the priorities of the not chosen technologies were of no relevance.

The first step of the synthesis process was to obtain the global priorities of the sub-criteria C_{11} to C_{14}. This is done by multiplying their local priorities by the priority of their parent C_1, which is 0.589 for the customer needs represented by the matrix $\boldsymbol{A}$, and 0.439 for the customer needs represented by $\boldsymbol{B}$:

$$\begin{pmatrix} w_{C11} \\ w_{C12} \\ w_{C13} \\ w_{C14} \end{pmatrix}_{GLO,\boldsymbol{A}} = \begin{pmatrix} w_{C11} \\ w_{C12} \\ w_{C13} \\ w_{C14} \end{pmatrix}_{LOK} \cdot w_{C1,\boldsymbol{A}} = \begin{pmatrix} 0.250 \\ 0.250 \\ 0.250 \\ 0.250 \end{pmatrix} \cdot 0.589 = \begin{pmatrix} 0.147 \\ 0.147 \\ 0.147 \\ 0.147 \end{pmatrix} \tag{9.3}$$

$$\begin{pmatrix} w_{C11} \\ w_{C12} \\ w_{C13} \\ w_{C14} \end{pmatrix}_{GLO,\boldsymbol{B}} = \begin{pmatrix} w_{C11} \\ w_{C12} \\ w_{C13} \\ w_{C14} \end{pmatrix}_{LOK} \cdot w_{C1,\boldsymbol{B}} = \begin{pmatrix} 0.250 \\ 0.250 \\ 0.250 \\ 0.250 \end{pmatrix} \cdot 0.439 = \begin{pmatrix} 0.110 \\ 0.110 \\ 0.110 \\ 0.110 \end{pmatrix} \tag{9.4}$$

According to Equation 3.10, the priority of each technology with respect to the overall goal was calculated as the sum of the product of each criterion's global priority (7 criteria) times the priority of the technology with respect to that criterion:

$$p_{Ai} = \sum_{j=1}^{7} w_j \cdot a_{Ai(j)} \tag{9.5}$$

In the following example, the priority of the silicon/glass technology is calculated with respect to the customer needs represented by the comparison matrix $\boldsymbol{A}$:

$$p_{A1} = (0.147 \cdot 1) + (0.147 \cdot 1) + (0.147 \cdot 1) + (0.147 \cdot 1) + (0.292 \cdot 1) + (0.055 \cdot 0.165) + (0.064 \cdot 0.111) = 0.896 \quad (9.6)$$

Similarly, the priorities of all technologies were calculated with respect to ***A*** and ***B***. The corresponding values are shown in Table 9-4. For the customer needs represented by ***A***, the first rank was obtained by the silicon/glass technology (A_1) which yielded the highest priority value of 0.896. The second and third ranks are taken by the hybrid and the all-polymer technologies whose priorities were calculated to 0.680 and 0.235, respectively. Given the customer needs represented by matrix ***B***, the most appropriate technology is the hybrid silicon/polymer technology which yielded a priority value of 0.610, followed by the all-polymer and the silicon/glass technologies with very close priorities of 0.571 and 0.570, respectively.

Under certain conditions, this situation may change and the polymer technology might become a stronger competitor to the silicon/glass and the hybrid technologies. This might be the case when the all-polymer technology is further developed or when the intention is to provide printheads with costs and lead time having higher priority than performance and lifetime.

Table 9-4: Synthesis according to the criteria prioritisation in Table 9-1. A_1, A_2 *and* A_3 are the technologies to be evaluated (silicon/glass, hybrid and all-polymer, respectively). C_{11} to C_4 are the criteria upon which the evaluation is based, together with their corresponding global priorities. The elements in the decision matrices indicate the priority of each technology with respect to the above criterion.

According to the prioritisation in matrix ***A***

	C_{11}	C_{12}	C_{13}	C_{14}	C_2	C_3	C_4		
	0.147	0.147	0.147	0.147	0.292	0.055	0.064	Priority	**Rank**
A_1	1.000	1.000	1.000	1.000	1.000	0.165	0.111	0.896	1st
A_2	0.405	1.000	1.000	1.000	0.443	0.405	0.430	0.680	2nd
A_3	0.165	0.143	0.200	0.112	0.084	1.000	1.000	0.235	3rd

According to the prioritisation in matrix ***B***

	C_{11}	C_{12}	C_{13}	C_{14}	C_2	C_3	C_4		
	0.110	0.110	0.110	0.110	0.062	0.229	0.269	Priority	**Rank**
A_1	1.000	1.000	1.000	1.000	1.000	0.165	0.111	0.570	3rd
A_2	0.405	1.000	1.000	1.000	0.443	0.405	0.430	0.610	1st
A_3	0.165	0.143	0.200	0.112	0.084	1.000	1.000	0.571	2nd

10 CONCLUSIONS

In this thesis two alternatives to the established silicon/glass micromachining technology were investigated by using TopSpot microarray printheads as a case study. The investigated alternatives were TopSpot printheads fabricated in hybrid silicon/polymer technology and all-polymer printheads. The criteria for selecting the most appropriate technology were “performance”, “life time”, “lead time” and “costs”.

The main conclusion of the work is that the manufacturing costs per printhead can be reduced by approximately 60 % without affecting the printing performance and without changing any dimensional parameters. The cost reduction applies to the whole studied production volume range of 10 to 100 printheads and was achieved by the hybrid silicon/polymer technology. With the hybrid printheads, the advantage of uniform and precise nozzles fabricated by silicon micromachining is retained and material and processing costs are reduced by replacing glass components with polymer ones. The hybrid process enables an increase of the manufacturing yield from 60 % to 70 % and reduction of the production lead time by more than 30 %. It also renders expensive micromachining of glass unnecessary and in combination with shorter lead times enables to react faster to changing customer requirements.

Further cost reduction and even shorter lead times can be achieved with all-polymer printheads in which both glass and silicon components are replaced by polymers. However, commonly used polymer technologies such as injection moulding, hot embossing, PDMS and/or SU-8 technology turned out to be inappropriate due to requirements such as small production quantities (excludes injection moulding), homogeneous production of through holes (excludes hot embossing), high nozzle stiffness (excludes PDMS) and multilayer structures (excludes SU-8). In order to avoid these limitations, a novel technology utilising the processing of TMMF dry film resist on a semi-finished polymer substrates was developed and proof-of-principle experiments with all-polymer printheads were carried out. The manufacturing costs of the all-polymer printheads were about 80 % lower compared to the silicon/glass printheads without changing the overall size. Similarly to the hybrid technology, the cost reduction applies to the whole production volume range of 10 to 100 printheads. The expected lead time was reduced by approximately 76 %, which is another clear advantage over the silicon/glass and the hybrid technologies. However, experimental results showed that the polymer technology is not yet mature and further research and development is needed to make it ready for industrial exploitation. Major drawbacks are the inferior printing accuracy due to the lack of appropriate methods for hydrophobisation of the nozzles, the short lifetime and the higher risk of cross-talk and carry over due to the lower bonding quality.

The evaluation of the technologies using a method for multi criteria decision making showed that the silicon/glass technology is still superior as long as the highest importance is paid to the requirements “performance” and “life time”. Considering a different customer profile assigning the highest importance to “performance” and “costs” leads to a different ranking with the highest priority assigned to the hybrid technology. The all-polymer technology is not yet competitive to state-of-the-art devices for printing of microarrays, but is extremely promising in terms of “cost” and “lead-time” reduction. Based on the obtained results, another important conclusion is that, depending on the requirements, silicon based solutions can add value to microfluidic devices and justify the higher costs compared to all-polymer solutions.

APENDIX

Table A 1: Expenditure of time for the processes involved in the manufacturing of the silicon/glass printheads [251]. Time variation is due to rework and operator dependency. The number of the considered wafers is 10.

Process block	Step	Process	Processing time in minutes	
			Operator	Machine
Start	1	Fabrication start	10	10
	2	Wafer measurement	15	15
Lithography I	3	Thermal oxidation I	60	1770
	4	Lithography I	80	290
	5	RIE	60	230
	6	Plasma ashing	10	60
Lithography II	7	Lithography II	140	410
DRIE I	8	DRIE I	300	1200
	9	Plasma ashing	20	90
DRIE II	10	DRIE II	240	600
	11	Plasma ashing	30	90
	12	Collection of yield data	5	5
	13	Wet etching SiO_2	60	90
Lithography III	14	Thermal oxidation	100	450
	15	Lithography III	140	310
	16	RIE	30	90
DRIE III	17	DRIE III	120	700
	18	Plasma ashing	5	30
	19	Collection of yield data	5	5
	20	Wet etching SiO_2	30	30
Passivation	21	Thermal oxidation	60	240
Bond I	22	Anodic bonding (bottom)	180	450
	23	Collection of yield data	10	10
Bond II	24	Anodic bonding (top)	120	450
Dicing	25	Dicing	1200	1370
Final Inspection	26	Final inspection and test	600	600
	27	Fabrication end	5	5

Table A 2: Fabrication process and processing time for the hybrid printheads. The number of the considered wafers is 10.

Process block	Step	Process	Processing time in minutes	
			Operator	Machine
Start	1	Fabrication start	10	10
	2	Wafer measurement	15	15
Lithography I	3	Lithography I	140	410
DRIE I	4	DRIE I	300	1800
	5	Plasma ashing	20	90
	6	Collection of yield data	5	5
Lithography II	7	Aluminium coating	20	70
	8	Lithography II	140	310
DRIE II	9	DRIE II	120	700
	10	Plasma ashing	5	30
	11	Collection of yield data	5	5
	12	Aluminium etching	30	30
Passivation	13	Thermal oxidation	60	240
Sealing	14	Lithography III	120	410
	15	Collection of yield data	10	10
Dicing	16	Dicing	200	230
Assembly	17	Assembly	300	0
Final inspection	18	Final inspection and test	600	600
	19	Fabrication end	5	5

Table A 3: Fabrication process and processing time for the all-polymer printheads. The number of the considered wafers is 10.

Process block	Step	Process	Processing time in minutes	
			Operator	Machine
Start	1	Fabrication start	10	10
Lithography I	2	Lithography I	120	410
	3	Collection of yield data	5	5
Lithography II	4	Lithography II	120	410
	5	Collection of yield data	5	5
Dicing	6	Dicing	200	230
Final inspection	7	Final inspection and test	600	600
	8	Fabrication end	5	5

BIBLIOGRAPHY

[1] M. Weller. Classification of protein microarrays and related techniques. *Anal. Bioanal. Chem.*, 375:15–17, 2003.

[2] H. Zhu and M. Snyder. Protein chip technology. *Curr. Opin. Chem. Biol.*, 7:55–63, 2003.

[3] R. P. Ekins. Multi-analyte immunoassay. *J. Pharmaceut. Biomed.*, 7:155–168, 1989.

[4] R. Ekins, F. Chu, and E. Biggart. Multispot, Multianalyte, Immunoassay. *Ann. Biol. Clin.*, 48:655–666, 1990.

[5] S. P. A. Fodor, J. L. Read, M. C. Pirrung, L. Stryer, A. T. Lu, and D. Solas. Light-Directed, Spatially Addressable Parallel Chemical Synthesis. *Science*, 251:767–773, 1991.

[6] T. Lenoir and E. Giannella. The emergence and diffusion of DNA microarray technology. *J. Biomed. Discov. Collab.*, 1:11, 2006.

[7] A. C. Pease, D. Solas, E. J. Sullivan, M. T. Cronin, C. P. Holmes, and S. P. Fodor. Light-generated oligonucleotide arrays for rapid DNA sequence analysis. *Proc. Natl. Acad. Sci.*, 91:5022–5026, 1994.

[8] M. Schena, D. Shalon, R. W. Davis, and P. O. Brown. Quantitative Monitoring of Gene Expression Patterns with a Complementary DNA Microarray. *Science*, 270:467–470, 1995.

[9] A. Bernal, U. Ear, and N. Kyrpides. Genomes OnLine Database (GOLD): a monitor of genome projects world-wide. *Nucleic Acids Res.*, 29:126–127, 2001.

[10] J. C. et al. Venter. The sequence of the human genome. *Science*, 291:1304–1351, 2001.

[11] F. S. Collins, E. S. Lander, J. Rogers, R. H. Waterston, and Int. Human Genome Sequencing Consortium. Finishing the euchromatic sequence of the human genome. *Nature*, 431:931–945, 2004.

[12] J. Glökler and P. Angenendt. Protein and antibody microarray technology. *J. Chromatogr. B*, 797:229–240, 2003.

[13] I. I. Garibay. *The Proteomics Approach to Evolutionary Computation: An Analysis of Proteome-Based Location Independent Representations based on the Proportional Genetic Algorithm*. PhD thesis, School of Computer Science at the University of Central Florida, 2004.

[14] R. E. Banks, M. J. Dunn, D. F. Hochstrasser, J.-C. Sanchez, W. Blackstock, D. J. Pappin, and P. J. Selby. Proteomics: new perspectives, new biomedical opportunities. *The Lancet*, 356:1749–1756, 2000.

[15] V. Espina, E. C. Woodhouse, J. Wulfkuhle, H. D. Asmussen, E. F. Petricoin, and L. A. Liotta. Protein microarray detection strategies: focus on direct detection technologies. *J. Immunol. Methods*, 290:121–133, 2004.

[16] N. L. Anderson and N. G. Anderson. Proteome and proteomics: New technologies, new concepts, and new words. *Electrophoresis*, 19:1853–1861, 1998.

[17] G. C. Adam, E. J. Sorensen, and B. F. Cravatt. Chemical strategies for functional proteomics. *Mol. Cell. Proteomics*, 1:781–790, 2002.

[18] B. D. Martin, B. P. Gaber, C. H. Patterson, and D. C. Turner. Direct protein microarray fabrication using a hydrogel “stamper”. *Langmuir*, 14:3971–3975, 1998.

[19] G. MacBeath and S. L. Schreiber. Printing proteins as microarrays for high-throughput function determination. *Science*, 289:1760–1763, 2000.

[20] H. Zhu, M. Bilgin, R. Bangham, D. Hall, A. Casamayor, P. Bertone, N. Lan, R. Jansen, S. Bidlingmaier, T. Houfek, T. Mitchell, P. Miller, R. A. Dean, M. Gerstein, and M. Snyder. Global analysis of protein activities using proteome chips. *Science*, 293:2101–2105, 2001.

[21] R. P. Huang. Detection of multiple proteins in an antibody-based protein microarray system. *J. Immunol. Methods*, 255:1–13, 2001.

[22] J. Ziauddin and D. M. Sabatini. Microarrays of cells expressing defined cDNAs. *Nature*, 411:107–110, 2001.

[23] M. L. Yarmush and K. R. King. Living-cell microarrays. *Annu. Rev. Biomed. Eng.*, 11:235–257, 2009.

[24] A. R. Liberski, J. T. Delaney, and U. S. Schubert. "one cell - one well": A new approach to inkjet printing single cell microarrays. *ACS. Comb. Sci.*, 13:190–195, 2011.

[25] European research project PASCA - Platform for Advanced Single Cell Manipulation and Analysis. http://www.pasca.eu/pasca/ (2012).

[26] S. Lindstrom and H. Andersson-Svahn. Overview of single-cell analyses: microdevices and applications. *Lab Chip*, 10:3363–3372, 2010.
[27] A. Yusof, H. Keegan, C. D. Spillane, O. M. Sheils, C. M. Martin, J. J. O'Leary, R. Zengerle, and P. Koltay. Inkjet-like printing of single-cells. *Lab Chip*, 11:2447–2454, 2011.
[28] R. A. Irizarry, D. Warren, F. Spencer, I. F. Kim, S. Biswal, B. C. Frank, E. Gabrielson, J. G. N. Garcia, J. Geoghegan, G. Germino, C. Griffin, S. C. Hilmer, E. Hoffman, A. E. Jedlicka, E. Kawasaki, F. Martinez-Murillo, L. Morsberger, H. Lee, D. Petersen, J. Quackenbush, A. Scott, M. Wilson, Y. Q. Yang, S. Q. Ye, and W. Yu. Multiple-laboratory comparison of microarray platforms. *Nat. Methods*, 2:345–349, 2005.
[29] T. Bammler et al. Standardizing global gene expression analysis between laboratories and across platforms. *Nat. Methods*, 2:351–356, 2005.
[30] M. Barnes, J. Freudenberg, S. Thompson, B. Aronow, and P. Pavlidis. Experimental comparison and cross-validation of the affymetrix and illumina gene expression analysis platforms. *Nucleic Acids Res.*, 33:5914–5923.
[31] A. de Reynies, D. Geromin, J.-M. Cayuela, F. Petel, P. Dessen, F. Sigaux, and D. Rickman. Comparison of the latest commercial short and long oligonucleotide microarray technologies. *BMC Genomics*, 7:51, 2006.
[32] A. Brazma, P. Hingamp, J. Quackenbush, G. Sherlock, P. Spellman, C. Stoeckert, J. Aach, W. Ansorge, C.A. Ball, H.C. Causton, T. Gaasterland, P. Glenisson, F.C.P. Holstege, I.F. Kim, V. Markowitz, J.C. Matese, H. Parkinson, A. Robinson, U. Sarkans, S. Schulze-Kremer, J. Stewart, R. Taylor, J. Vilo, and M. Vingron. Minimum information about a microarray experiment (MIAME) - toward standards for microarray data. *Nat. Genet.*, 29:365–371, 2001.
[33] Frost & Sullivan. Strategic analysis of the European DNA microarrays market. Technical report, 2010.
[34] Research and Markets. Global DNA & Gene Chip (Microarray) Market (2010-2015). http://www.researchandmarkets.com/reportinfo.asp?report_id=1788763&t=d&cat_id= (2011).
[35] Hoffmann-La Roche. Amplichip® cyp450. http://www.roche.com/de/products/product-details.htm?type=product&id=17 (2011).
[36] Medical Coverage Policy of CIGNA Health Insurance. http://www.cigna.com/customer_care/healthcare_professional/coverage_positions/medical/mm_0381_coveragepositioncriteria_AmpliChip.pdf (2011).
[37] Genomic Health. Oncotype dx. http://www.oncotypedx.com/en-US/Breast/PatientCaregiver/OncoOverview.aspx (2011).
[38] Agendia - MammaPrint genomic test. http://www.agendia.com/pages/mammaprint/21.php (2011).
[39] G. Walsh. *Pharmaceutical biotechnology: concepts and applications*. Wiley-VCH, 2007.
[40] D. Kambhampati. *Protein Microarray Technology*. Wiley-VCH, 2004.
[41] P. Mitchell. A perspective on protein microarrays. *Nat. Biotechnol.*, 20:225–229, 2002.
[42] W. Weber and M. Fussenegger. The impact of synthetic biology on drug discovery. *Drug Discov. Today*, 14:956–963, 2009.
[43] Y. Kasper and C. Lenz. Stable 8-year storage of DNA purified with the QIAamp DNA Blood Mini Kit. *Qiagen News*, page e10, 2004.
[44] www.invitrogen.com (2011).
[45] X. Yu, N. Schneiderhan-Marra, and T. O. Joos. Protein microarrays for personalized medicine. *Clin. Chem.*, 56:376–387, 2010.
[46] marketsandmarkets.com. Biochips Market (DNA Microarrays, Lab-on-Chip, Protein Microarrays, Tissue & Cell Arrays) Trends & Global Forecast (2010-2015), 2011.
[47] T. O. Joos and H. Berger. The long and difficult road to the diagnostic market: protein microarrays. *Drug Discov. Today*, 11:959–961, 2006.
[48] S. N. Bailey, R. Z. Wu, and D. M. Sabatini. Applications of transfected cell microarrays in high-throughput drug discovery. *Drug Discov. Today*, 7:113 – 118, 2002.
[49] D. B. Wheeler, A. E. Carpenter, and D. M. Sabatini. Cell microarrays and RNA interference chip away at gene function. *Nat. Genet.*, 37:25–30, 2005.
[50] J. B. Delehanty, K. M. Shaffer, and B. Lin. A comparison of microscope slide substrates for use in transfected cell microarrays. *Biosens. Bioelectron.*, 20:773–779, 2004.

[51] T. Martinsky. Printing technologies and microarray manufacturing techniques: making the perfect microarray. In E. Blalock, editor, *A beginner's guide to microarrays*, pages 93–122. Kluwer Academic Publishers, 2003.
[52] G. Hardiman. Microarray platforms - comparisons and contrasts. *Pharmacogenomics*, 5:487–502, 2004.
[53] M. B. Miller and Y.-W. Tang. Basic concepts of microarrays and potential applications in clinical microbiology. *Clin. Microbiol. Rev.*, 22:611–633, 2009.
[54] I. Barbulovic-Nad, M. Lucente, Y. Sun, M. Zhang, A. R. Wheeler, and M. Bussmann. Bio-microarray fabrication techniques–a review. *CRC Cr. Rev Biotechn.*, 26:237–259, 2006.
[55] Y. Xia, J. A. Rogers, K. E. Paul, and G. M. Whitesides. Unconventional Methods for Fabricating and Patterning Nanostructures. *Chem. Rev.*, 99:1823–1848, 1999.
[56] B. D. Martin, B. P. Gaber, C. H. Patterson, and D. C. Turner. Direct protein microarray fabrication using a hydrogel "stamper". *Langmuir*, 14:3971–3975, 1998.
[57] M. Dufva. Fabrication of high quality microarrays. *Biomol. Eng.*, 22:173–184, 2005.
[58] M. Schena. *Microarray biochip technology*. Eaton Publishing, 2000.
[59] Chris Steinert. *TopSpot Vario: A Novel Microarrayer System for Highly Parallel Picoliter Dispensing*. PhD thesis, IMTEK - University of Freiburg, 2005.
[60] Arrayit. Stealth technology. http://arrayit.com/Products/Microarray_Printing/Microarray_Pins_Stealth_Techno/microarray_pins_stealth_technology.html (2011).
[61] Arrayit. Spotbot printhead. http://arrayit.com/Products/Microarrayers/Arrayer/arrayer.html (2011).
[62] P. J. Park, Y. A. Cao, S. Y. Lee, J.-W. Kim, M. S. Chang, R. Hart, and S. Choi. Current issues for DNA microarrays: platform comparison, double linear amplification, and universal RNA reference. *J. Biotechnol.*, 112:225–245, 2004.
[63] R. A. George. The printing process: Tips on tips. *Method. Enzymol.*, 410:121–135, 2006.
[64] J. Hager. Making and using spotted DNA microarrays in an academic core laboratory. *Method. Enzymol.*, 410:135–168, 2006.
[65] B. Derby. Inkjet printing of functional and structural materials: Fluid property requirements, feature stability, and resolution. *Annu. Rev. Mater. Res.*, 40:395–414, 2010.
[66] Functional Genomics Center Zurich. http://www.fgcz.ch/applications/microarraying/printing/CustomArray.jpg?hires (2011).
[67] A. Asai, S. Hirasawa, and I. Endo. Bubble Generation Mechanism in the Bubble Jet Recording Process. *J. Imaging Technol.*, 14:120–124, 1988.
[68] D. I. Stimpson, P. W. Cooley, S. M. Knepper, and D. B. Wallace. Parallel production of oligonucleotide arrays using membranes and reagent jet printing. *Biotechniques*, 25:886–890, 1998.
[69] T. Okamoto, T. Suzuki, and N. Yamamoto. Microarray fabrication with covalent attachment of DNA using Bubble Jet technology. *Nat. Biotechnol.*, 18:438–441, 2000.
[70] A. Roda, M. Guardigli, C. Russo, P. Pasini, and M. Baraldini. Protein microdeposition using a conventional ink-jet printer. *Biotechniques*, 28:492–496, 2000.
[71] L.R. Allain, M. Askari, D.L. Stokes, and T. Vo-Dinh. Microarray sampling-platform fabrication using bubble-jet technology for a biochip system. *Anal. Bioanal. Chem.*, 371:146–150, 2001.
[72] Q. Zheng, J. Lu, H. Chen, L. Huang, J. Cai, and Z. Xu. Application of inkjet printing technique for biological material delivery and antimicrobial assays. *Anal. Biochem.*, 410:171–176, 2011.
[73] L. Setti, C. Piana, S. Bonazzi, B. Ballarin, D. Frascaro, A. Fraleoni-Morgera, and S. Giuliani. Thermal inkjet technology for the microdeposition of biological molecules as a viable route for the realization of biosensors. *Anal. Lett.*, 37:1559–1570, 2004.
[74] T. Xu, J. Jin, C. Gregory, J. J. Hickman, and T. Boland. Inkjet printing of viable mammalian cells. *Biomaterials*, 26:93–99, 2005.
[75] D. D. Dalma-Weiszhausz, J. Warrington, E. Y. Tanimoto, and C. G. Miyada. The Affymetrix GeneChip Platform: An Overview. *Method. Enzymol.*, 410:3–28, 2006.
[76] S. Singh-Gasson, R. D. Green, Y. J. Yue, C. Nelson, F. Blattner, M. R. Sussman, and F. Cerrina. Maskless fabrication of light-directed oligonucleotide microarrays using a digital micromirror array. *Nat. Biotechnol.*, 17:974–978, 1999.

[77] Roche NimbleGen. Roche NimbleGen - array synthesis. http://www.nimblegen.com/company/technology/ (2011).
[78] A. P. Blanchard, R. J. Kaiser, and L. E. Hood. High-density oligonucleotide arrays. *Biosens. Bioelectron.*, 11:687–690, 1996.
[79] T. R. Hughes, M. Mao, A.R. Jones, J. Burchard, M.J. Marton, K.W. Shannon, S.M. Lefkowitz, M. Ziman, J.M. Schelter, M.R. Meyer, S. Kobayashi, C. Davis, H.Y. Dai, Y.D.D. He, S.B. Stephaniants, G. Cavet, W.L. Walker, A. West, E. Coffey, D.D. Shoemaker, R. Stoughton, A.P. Blanchard, S.H. Friend, and P.S. Linsley. Expression profiling using microarrays fabricated by an ink-jet oligonucleotide synthesizer. *Nat. Biotechnol.*, 19:342–347, 2001.
[80] Roland Zengerle, Nicolaus Hey, Holger Gruhler, Michael Freygang, and Martin Mueller. Fluids manipulation device with format conversion, February 15 2005. US Patent 6,855,293.
[81] O. Gutmann, R. Niekrawietz, R. Kuehlewein, C. P. Steinert, B. de Heij, R. Zengerle, and M. Daub. Impact of medium properties on droplet release in a highly parallel nanoliter dispenser. *Sensor Actuat. A-Phys.*, 116:187–194, 2004.
[82] O. Gutmann, R. Niekrawietz, R. Kuehlewein, C. P. Steinert, S. Reinbold, B. de Heij, M. Daub, and R. Zengerle. Non-contact production of oligonucleotide microarrays using the highly integrated TopSpot nanoliter dispenser. *Analyst*, 129:835–840, 2004.
[83] O. Gutmann, R. Kuehlewein, S. Reinbold, R. Niekrawietz, C. P. Steinert, B. de Heij, R. Zengerle, and M. Daub. Fast and reliable protein microarray production by a new drop-in-drop technique. *Lab Chip*, 5:675–681, 2005.
[84] O. Gutmann, M. K. Wintermantel, R. Niekrawietz, B. de Heij, R. Zengerle, and M. Daub. Dispensing of cells for highly parallel production of living cell microarrays. In *Proc. of TRANSDUCERS*, pages 449–452, 2005.
[85] C. P. Steinert, K. Kalkandjiev, R. Zengerle, and P. Koltay. TopSpot Vario: a novel microarrayer system for highly flexible and highly parallel picoliter dispensing. *Biomed. Microdevices*, 11:755–761, 2009.
[86] C. P. Steinert, H. Sandmaier, M. Daub, B. de Heij, and R. Zengerle. Bubble-free priming of blind channels. In *Proc. of IEEE MEMS*, pages 224–228, 2004.
[87] K. Ehrlenspiel, U. Lindemann, A. Kiewert, and M. S. Hundal. Cost responsibility of the product developers. In *Cost-efficient design*, chapter 2, pages 5–16. Springer, 2010.
[88] G. E. Moore. Cramming more components onto integrated circuits. *Electronics*, 86:114–117, 1965.
[89] H. Becker. One size fits all? *Lab Chip*, 10:1894–1897, 2010.
[90] Number of matches on "microfluidics" on Google Scholar, 5 2014.
[91] H. Becker. It's the economy ... *Lab Chip*, 9:2759–2762, 2009.
[92] Yole Developpement. Emerging market for microfluidic applications. Technical report, 2009.
[93] M. A. Huff, S. F. Bart, and P. Lin. The Economic Realities of MEMS Process Development. In R. Ghodssi and P. Lin, editors, *MEMS Materials and Processes Handbook*, pages 1161–1175. Springer, 2011.
[94] J.L. Hennessy and D.A. Patterson. Trends in Costs. In *Computer Architecture: A Quantitative Approach*, The Morgan Kaufmann Series in Computer Architecture and Design, pages 27–33. Elsevier Science, 2011.
[95] J. Sasserath and D. Fries. Rapid Prototyping and Development of Microfluidic and BioMEMS Devices. *IVD Technology*, June:8–11, 2002.
[96] A. Waldbaur, H. Rapp, K. Lange, and B. E. Rapp. Let there be chip-towards rapid prototyping of microfluidic devices: one-step manufacturing processes. *Anal. Methods*, 3:2681–2716, 2011.
[97] R. Zengerle. Microsystem technologies. IMTEK - University of Freiburg. Lecture, 2010.
[98] Technical specifications of ASML's TWINSCAN NXE platform. http://www.asml.com/asml/show.do?lang=EN&ctx=46772&dfp_product_id=842 (2013).
[99] R. Peeters, S. Lok, E. van Alphen, N. Harned, P. Kuerz, M. Lowisch, H. Meijer, D. Ockwell, E. van Setten, G. Schiffelers, et al. ASML's NXE platform performance and volume introduction. In *Proc. of SPIE Advanced Lithography*, pages 86791F–86791F, 2013.
[100] M. van den Brink. Continuing to shrink: Next-generation lithography-progress and prospects. In *Proc. of IEEE ISSCC*, pages 20–25, 2013.

[101] D. K. de Vries. Investigation of gross die per wafer formulas. *Trans. Semiconduct. Manufact.*, 18:136–139, 2005.
[102] http://www.iisb.fraunhofer.de/de/abteilungen/halbleiterfertigungsgeraeteund-methoden/gadest_2011.html (2013).
[103] D. P. Webb, P. P. Conway, D. A. Hutt, B. J. Knauf, and C. Liu. Processes for integration of microfluidic based devices. In *Proc. of IEEE EMPC*, pages 1–7, 2009.
[104] R. Zengerle, J. Newman, H. Ernst, S. Messner, and G. Andrieux. *FlowMap: Microfluidics Roadmap for the Life Sciences*. Books on Demand, 2004.
[105] S. Haeberle and R. Zengerle. Microfluidic platforms for lab-on-a-chip applications. *Lab Chip*, 7:1094–1110, 2007.
[106] H. Becker. Mind the gap! *Lab Chip*, 10:271–273, 2010.
[107] R. Zengerle, D. Mark, D. Kosse, G. Roth, and F. von Stetten. Microfluidic solutions for miniaturization, integration, automation and parallelization of tests on commercially available instruments. In *Proc. of TRANSDUCERS*, 2011.
[108] Society for Laboratory Automation and Screening. Microplate standards: ANSI/SBS 1-4 (2004).
[109] International Organization for Standardization. ISO 8037-1 - Optics and optical instruments - Microscopes - Slides - Part 1: Dimensions, optical properties and marking, 1986.
[110] MEMS Industry Group. A Glossary of MEMS terms, February 2012.
[111] H. Becker and Claudia G. Polymer microfabrication technologies for microfluidic systems. *Anal. Bioanal. Chem.*, 390:89–111, 2008.
[112] D. Tolfree and R. Mehalso. The Path to Commercialization. In D. Tolfree and M. J. Jackson, editors, *Commercializing Micro-Nanotechnology Products*, pages 1–28. CRC Press, 2010.
[113] IC Knowledge LCC. MEMS Cost Model Manual. http://www.icknowledge.com/our_products/MEMS%20Model%201201%20Manual.pdf (2012).
[114] R. Lawes. Manufacturing costs for microsystems/MEMS using high aspect ratio microfabrication techniques. *Microsyst. Technol.*, 13:85–95, 2007.
[115] K. Ehrlenspiel, U. Lindemann, A. Kiewert, and M. S. Hundal. Cost management for product development. In *Cost-efficient design*, chapter 3, pages 17–30. Springer, 2010.
[116] L. D. Miles. *Techniques of value analysis and engineering*. McGraw-Hill, 1972.
[117] VDI -Gesellschaft Produkt und Prozessgestaltung / Fachbereich Wertanalyse. VDI guideline 2800 Part 1 - Value Management, 2010.
[118] H. Krehl. Erfolgreiche produkte durch value management. In *Proc. of ICED*, pages 246–253, 1981.
[119] M. Pauwels. Einleitung. In *Wertanalyse - Das Tool Im Value Management*, pages 1–11. VDI-Gesellschaft Produkt- und Prozessgestaltung, 6th edition, 2011.
[120] R. Wiest. Der Wertanalyse-Arbeitsplan. In *Wertanalyse - Das Tool Im Value Management*, pages 39–53. VDI-Gesellschaft Produkt- und Prozessgestaltung, 6th edition, 2011.
[121] S. Ansari, J. Bell, and H. Okano. Target Costing: Uncharted Research Territory. In C.S. Chapman, A.G. Hopwood, and M.D. Shields, editors, *Handbook of Management Accounting Research*, Handbooks of Management Accounting Research, pages 507–530. Elsevier Science, 2011.
[122] T. L. Saaty. *The analytic hierarchy process: planning, priority setting, resource allocation*. McGraw-Hill, 1980.
[123] O. S. Vaidya and S. Kumar. Analytic hierarchy process: An overview of applications. *Eur. J. Oper. Res.*, 169:1–29, 2006.
[124] T. L. Saaty and M. S. Ozdemir. Why the magic number seven plus or minus two. *Math. Comput. Model.*, 38:233–244, 2003.
[125] T. L. Saaty. Decision-making with the AHP: Why is the principal eigenvector necessary. *Eur. J. Oper. Res.*, 145:85–91, 2003.
[126] I. Millet and T. L. Saaty. On the relativity of relative measures - accommodating both rank preservation and rank reversals in the AHP. *Eur. J. Oper. Res.*, 121:205–212, 2000.
[127] Alessio I. and Ashraf L. Review of the main developments in the analytic hierarchy process. *Expert Syst. Appl.*, 38:14336–14345, 2011.
[128] T. L. Saaty. How to make a decision: The analytic hierarchy process. *Eur. J. Oper. Res.*, 48:9–26, 1990.

[129] J. Hopkins, I. R. Johnston, J. K. Bhardwaj, H. Ashraf, A. M. Hynes, and L. M. Lea. Method and apparatus for etching a substrate, 2001. US Patent 6,187,685.
[130] D. C. Duffy, J. C. McDonald, O. J. Schueller, and G. M. Whitesides. Rapid prototyping of microfluidic systems in poly(dimethylsiloxane). *Anal. Chem.*, 70:4974–4984, 1998.
[131] H. Lorenz, M. Despont, N. Fahrni, N. LaBianca, P. Renaud, and P. Vettiger. SU-8: a low-cost negative resist for MEMS. *J. Micromech. Microeng.*, 7:121, 1997.
[132] Y. Chen, L. Zhang, and G. Chen. Fabrication, modification, and application of poly (methyl methacrylate) microfluidic chips. *Electrophoresis*, 29:1801–1814, 2008.
[133] Y. Liu, D. Ganser, A. Schneider, R. Liu, P. Grodzinski, and N. Kroutchinina. Microfabricated polycarbonate CE devices for DNA analysis. *Anal. Chem.*, 73:4196–4201, 2001.
[134] J. Steigert, S. Haeberle, T. Brenner, C. Müller, C. P. Steinert, P. Koltay, N. Gottschlich, H. Reinecke, J. Rühe, R. Zengerle, and J. Ducrée. Rapid prototyping of microfluidic chips in COC. *J. Micromech. Microeng.*, 17:333, 2007.
[135] P. Vulto, N. Glade, L. Altomare, J. Bablet, L. Del Tin, G. Medoro, I. Chartier, N. Manaresi, M. Tartagni, and R. Guerrieri. Microfluidic channel fabrication in dry film resist for production and prototyping of hybrid chips. *Lab Chip*, 5:158–162, 2004.
[136] R. S. Khandpur. *Printed Circuit Boards: Design, Fabrication, Assembly and Testing*. T. McGraw-Hill, 2005.
[137] M. O. Heuschkel, L. Guerin, B. Buisson, D. Bertrand, and P. Renaud. Buried microchannels in photopolymer for delivering of solutions to neurons in a network. *Sensor Actuat. B-Chem.*, 48:356–361, 1998.
[138] T. Ito, T. Kawaguchi, H. Miyoshi, K. Maruyama, S. Kaneko, S. Ohya, Y. Iwasaki, O. Niwa, and K. Suzuki. Characterization of a microfluidic device fabricated using a photosensitive sheet. *J. Micromech. Microeng.*, 17:432, 2007.
[139] J. Kieninger, G. Jobst, G. Igel, I. Moser, and G. Urban. 3D polymer microstructures by laminating SU-8 films. In *Proc. of μTAS*, pages 363–365, 2004.
[140] N. Wangler, S. Beck, G. Ahrens, A. Voigt, G. Grützner, C. Müller, and H. Reinecke. Ultra thick epoxy-based dry-film resist for high aspect ratios. *Microelectron. Eng.*, 2012.
[141] P. Abgrall, C. Lattes, V. Conédéra, X. Dollat, S. Colin, and A.M. Gué. A novel fabrication method of flexible and monolithic 3D microfluidic structures using lamination of SU-8 films. *J. Micromech. Microeng.*, 16:113, 2005.
[142] G. Mottet, J. Villemejane, L.M. Mir, and B. Le Pioufle. A technique to design complex 3D lab on a chip involving multilayered fluidics, embedded thick electrodes and hard packaging—application to dielectrophoresis and electroporation of cells. *J. Micromech. Microeng.*, 20:047001, 2010.
[143] S. Charlot, A.M. Gué, J. Tasselli, A. Marty, P. Abgrall, and D. Estève. A low cost and hybrid technology for integrating silicon sensors or actuators in polymer microfluidic systems. *J. Micromech. Microeng.*, 18:017003, 2007.
[144] I. El Gmati, P. Calmon, R. Fulcrand, P. Pons, A. Boukabache, H. Boussetta, M.A. Kallala, and K. Besbes. Variable RF MEMS fluidic inductor incorporating lamination process. *Micro Nano Lett.*, 5:370–373, 2010.
[145] R. Fulcrand, D. Jugieu, C. Escriba, A. Bancaud, D. Bourrier, A. Boukabache, and A. M. Gué. Development of a flexible microfluidic system integrating magnetic micro-actuators for trapping biological species. *J. Micromech. Microeng.*, 19:105019, 2009.
[146] J. Courbat, D. Briand, and N. F. De Rooij. Foil level packaging of a chemical gas sensor. *J. Micromech. Microeng.*, 20:055026, 2010.
[147] A. Chen and T. Pan. Fit-to-flow (f2f) interconnects: Universal reversible adhesive-free microfluidic adaptors for lab-on-a-chip systems. *Lab Chip*, 11:727–732, 2010.
[148] K. Hsiung, C. Tsai, L. Chen, and G. Yen. A novel high resolution epoxy based dry film material for wafer level packaging application. In *Proc. of IEEE IMPACT*, pages 235–238, 2008.
[149] D. Nußbaum, D. Herrmann, T. Knoll, and T. Velten. Micromixing structures for lab-on chip applications: fabrication and simulation of 90 zigzag microchannels in dry film resist. In *Proc. of 4M/ICOMM*, 2009.
[150] R.C. Meier, V. Badilita, J. Brunne, U. Wallrabe, and J.G. Korvink. Complex three-dimensional high aspect ratio microfluidic network manufactured in combined PerMX dry-resist and SU-8 technology. *Biomicrofluidics*, 5:034111, 2011.

[151] J. Kim, S. Seok, N. Rolland, and PA Rolland. Low-temperature, low-loss zero level packaging techniques for RF applications by using a photopatternable dry film. *J. Micromech. Microeng.*, 22:065032, 2012.
[152] A. Banerjee, E. Kreit, Y. Liu, J. Heikenfeld, and I. Papautsky. Reconfigurable virtual electrowetting channels. *Lab Chip*, 12:758–764, 2012.
[153] Z. Gao, S. Gong, C. S. Kim, and D. B. Henthorn. Optofluidic glucose sensor utilizing an epoxy-based, transparent dry film resist. In *Proc. of IEEE Sensors*, pages 284–287, 2011.
[154] M. Dhindsa, J. Heikenfeld, S. Kwon, J. Park, P. D. Rack, and I. Papautsky. Virtual electrowetting channels: electronic liquid transport with continuous channel functionality. *Lab Chip*, 10:832–836, 2010.
[155] R. C. Meier, V. Badilita, U. Wallrabe, and J. G. Korvink. Processing of 3D multilevel SU-8 fluidic network assisted by PerMX dry-photoresist lamination. In *Proc. of IEEE NEMS*, pages 308–311, 2012.
[156] M. Aljada and A. Asthana. Fabrication of multilayer microstructures using dry film resist and deep reactive ion etcher. *Micro Nano Lett.*, 5:121–124, 2010.
[157] P. Vulto, G. Medoro, L. Altomare, G. A. Urban, M. Tartagni, R. Guerrieri, and N. Manaresi. Selective sample recovery of DEP-separated cells and particles by phaseguide-controlled laminar flow. *J. Micromech. Microeng.*, 16:1847, 2006.
[158] P. Vulto, G. Dame, U. Maier, S. Makohliso, S. Podszun, P. Zahn, and G.A. Urban. A microfluidic approach for high efficiency extraction of low molecular weight RNA. *Lab Chip*, 10:610–616, 2010.
[159] T. Lemke, J. Kloeker, G. Biancuzzi, T. Huesgen, F. Goldschmidtboeing, and P. Woias. Fabrication of a normally-closed microvalve utilizing lithographically defined silicone micro O-rings. *J. Micromech. Microeng.*, 21:025011, 2011.
[160] S. Y. Leigh, A. Tattu, J. S. B. Mitchell, and E. Entcheva. M 3: Microscope-based maskless micropatterning with dry film photoresist. *Biomed. Microdevices*, 13:375–381, 2011.
[161] P. Muller, N. Spengler, H. Zappe, and W. Mooench. An optofluidic concept for a tunable micro-iris. *J. Microelectromech. Syst.*, 19:1477–1484, 2010.
[162] N. A. Md Yunus and N. G. Green. Fabrication of microfluidic device channel using a photopolymer for colloidal particle separation. *Microsyst. Technol.*, 16:2099–2107, 2010.
[163] R. D. Henderson, R. M. Guijt, P. R. Haddad, E. F. Hilder, T. W. Lewis, and M. C. Breadmore. Manufacturing and application of a fully polymeric electrophoresis chip with integrated polyaniline electrodes. *Lab Chip*, 10:1869–1872, 2010.
[164] P. Vulto, T. Huesgen, B. Albrecht, and G. A. Urban. A full-wafer fabrication process for glass microfluidic chips with integrated electroplated electrodes by direct bonding of dry film resist. *J. Micromech. Microeng.*, 19:077001, 2009.
[165] R.M. Guijt, E. Candish, and M.C. Breadmore. Dry film microchips for miniaturised separations. *Electrophoresis*, 30:4219–4224, 2009.
[166] R.M. Guijt and M.C. Breadmore. Maskless photolithography using UV LEDs. *Lab Chip*, 8:1402–1404, 2008.
[167] T. Huesgen, G. Lenk, B. Albrecht, P. Vulto, T. Lemke, and P. Woias. Optimization and characterization of wafer-level adhesive bonding with patterned dry-film photoresist for 3D MEMS integration. *Sensor Actuat. A-Phys.*, 162:137–144, 2010.
[168] D. Paul, A. Pallandre, S. Miserere, J. Weber, and J. L. Viovy. Lamination-based rapid prototyping of microfluidic devices using flexible thermoplastic substrates. *Electrophoresis*, 28:1115–1122, 2007.
[169] D. Paul, L. Saias, J. C. Pedinotti, M. Chabert, S. Magnifico, A. Pallandre, B. De Lambert, C. Houdayer, B. Brugg, J. M. Peyrin, et al. A “dry and wet hybrid” lithography technique for multilevel replication templates: Applications to microfluidic neuron culture and two-phase global mixing. *Biomicrofluidics*, 5, 2011.
[170] T. Ito, M. Kunimatsu, S. Kaneko, S. Ohya, and K. Suzuki. Microfluidic device for the detection of glucose using a micro direct methanol fuel cell as an amperometric detection power source. *Anal. Chem.*, 79:1725–1730, 2007.
[171] N. Nashida, W. Satoh, J. Fukuda, and H. Suzuki. Electrochemical immunoassay on a microfluidic device with sequential injection and flushing functions. *Biosens. Bioelectron.*, 22:3167–3173, 2007.

[172] T. Ito, K. Maruyama, S. Ohya, and K. Suzuki. Easy fabrication of microfluidic device using photosensitive sheet. *ECS Trans.*, 3:417–425, 2006.
[173] J. Zhu, A. S. Holmes, J. Arnold, R. A. Lawes, and P. D. Prewett. Laminated dry film resist for microengineering applications. *Microelectron. Eng.*, 30:365–368, 1996.
[174] Y. M. Huang, M. Uppalapati, W. O. Hancock, and T. N. Jackson. Microfabricated capped channels for biomolecular motor-based transport. *Trans. Adv. Packag.*, 28:564–570, 2005.
[175] A.D. Radadia, L. Cao, H.K. Jeong, M.A. Shannon, and R.I. Masel. A 3D micromixer fabricated with dry film resist. In *Proc. of IEEE MEMS*, pages 361–364, 2007.
[176] D. Johnson, J. Goettert, V. Singh, and D. Yemane. SUEX for High Aspect Ratio Micro-Nanofluidic Applications. *Proc. Microtech.*, 2012.
[177] D. Johnson, A. Voigt, G. Ahrens, and W. Dai. Thick epoxy resist sheets for MEMS manufactuing and packaging. In *Proc. of IEEE MEMS*, pages 412–415, 2010.
[178] D. W. Johnson, J. Goettert, V. Singh, and D. Yemane. Opportunities for SUEX dry laminate resist in microfluidic MEMS applications, 2012. Annual Report, CAMD, Louisiana State University.
[179] H. Lorenz, L. Paratte, R. Luthier, N. F. de Rooij, and P. Renaud. Low-cost technology for multilayer electroplated parts using laminated dry film resist. *Sensor Actuat. A-Phys.*, 53:364–368, 1996.
[180] M.A. McClain, I.P. Clements, R.H. Shafer, R.V. Bellamkonda, M.C. LaPlaca, and M.G. Allen. Highly-compliant, microcable neuroelectrodes fabricated from thin-film gold and PDMS. *Biomed. Microdevices*, 13:361–373, 2011.
[181] G. Jobst, I. Moser, P. Svasek, M. Varahram, Z. Trajanoski, P. Wach, P. Kotanko, F. Skrabal, and G. Urban. Mass producible miniaturized flow through a device with a biosensor array. *Sensor Actuat. B-Chem.*, 43:121–125, 1997.
[182] I. Moser, G. Jobst, and G. A. Urban. Biosensor arrays for simultaneous measurement of glucose, lactate, glutamate, and glutamine. *Biosens. Bioelectron.*, 17:297–302, 2002.
[183] F. Jacquet, D. Henry, J. Charbonnier, N. Bouzaida, N. Sillon, C. Tsai, C. Balut, and J. S. Raine. Low cost lithography solution for advanced packaging and application to through silicon via process. In *Proc. of IEEE-EPTC*, pages 51–57, 2008.
[184] R. Leib and M. Topper. New wafer-level-packaging technology using silicon-via-contacts for optical and other sensor applications. In *Proc. of IEEE ECTC*, pages 843–847, 2004.
[185] J.H. Kuypers, S. Tanaka, and M. Esashi. Imprinted laminate wafer-level packaging for SAW ID-tags and SAW delay line sensors. *Trans. Ultrason., Ferroelect., Freq. Contr.Control*, 58(2):406–413, 2011.
[186] U. Stöhr, A. Dohse, P. Hoppe, M. Thomas, K. Kadel, C. P. Klages, and H. Reinecke. Multilayer photoresist stamps for selective plasma treatment in micrometer scales. *Plasma Process. Polym.*, 6:228–233, 2009.
[187] U. Stöhr, A. Dohse, P. Hoppe, A. Gehringer, M. Thomas, C.P. Klages, and H. Reinecke. Porous photoresist stamps for selective plasma treatment. *Plasma Process. Polym.*, 7:9–15, 2010.
[188] U. Stöhr, P. Vulto, P. Hoppe, G. Urban, and H. Reinecke. High-resolution permanent photoresist laminate for microsystem applications. *J. Micro-Nanolith. MEM*, 7:033009–033009, 2008.
[189] K. Misumi, K. Saito, A. Yamanouchi, T. Senzaki, and H. Honma. Minute tunnel structure formation with permanent film photoresist. *J. Photopolym. Sci. Tec.*, 19:57–62, 2006.
[190] K. Kalkandjiev, L. Riegger, D. Kosse, M. Welsche, L. Gutzweiler, R. Zengerle, and P. Koltay. Microfluidics in silicon/polymer technology as a cost-efficient alternative to silicon/glass. *J. Micromech. Microeng.*, 21:025008, 2011.
[191] N. Wangler, L. Gutzweiler, K. Kalkandjiev, C. Müller, F. Mayenfels, H. Reinecke, R. Zengerle, and N. Paust. High-resolution permanent photoresist laminate TMMF for sealed microfluidic structures in biological applications. *J. Micromech. Microeng.*, 21:095009, 2011.
[192] N. Wangler, M. Welsche, M. Blazek, M. Blessing, M. Vervliet-Scheebaum, R. Reski, C. Müller, H. Reinecke, J. Steigert, G. Roth, et al. Bubble jet agent release cartridge for chemical single cell stimulation. *Biomed. Microdevices*, pages 1–8, 2012.
[193] J.A.M. Sondag-Huethorst, S. de Jager, C. de Nooijer, R.B.R. van Silfhout, and M.H. van Kleef. Dry film package for system in package molding process. In *Proc. of TRANSDUCERS*, pages 2071–2074, 2007.

[194] V. Mokkapati, L. Zhang, R. Hanfoug, J. Mollinger, J. Bastemeijer, and A. Bossche. Fabrication and testing of a TMMF S2030 based micro fluidic device for single cell analysis. In *Proc. of IEEE ICQNM*, pages 86–89, 2009.

[195] K. Kalkandjiev, L. Gutzweiler, M. Welsche, R. Zengerle, and P. Koltay. A novel approach for the fabrication of all-polymer microfluidic devices. In *Proc. of IEEE MEMS*, pages 1079–1082, 2010.

[196] C. Shen, V. Mokkapati, H. T. M. Pham, and P. M. Sarro. Micromachined nanofiltration modules for lab-on-a-chip applications. *J. Micromech. Microeng.*, 22:025003, 2012.

[197] N. B. Palacios Aguilera, V. R. S. S. Mokkapati, H. A. Visser, J. Bastemeijer, J. R. Mollinger, R. Akkerman, and A. Bossche. Low-cost technology for the integration of micro-and nanochips into fluidic systems on printed circuit board: Fabrication challenges. *International Journal On Advances in Systems and Measurements*, 5:11–21, 2012.

[198] Y. Hirai, A. Uesugi, Y. Makino, H. Yagyu, K. Sugano, T. Tsuchiya, and O. Tabata. Negative-photoresist mechanical property for nano-filtration membrane embedded in microfluidics. In *Proc. of TRANSDUCERS*, pages 2706–2709, 2011.

[199] N. B. Palacios Aguilera, V. R. S. S. Mokkapati, J. Bastemeijer, J. R. Mollinger, and A. Bossche. Dry film resist microfluidic channels on printed circuit board and its application as fluidic interconnection for nanofluidic chips: fabrication challenges. In *Proc. of IEEE ICQNM*, pages 71–76, 2011.

[200] J. A. Lebens, W. Zhang, and C. N. Delametter. A printhead having self-aligned holes, 2011. EP Patent 2,374,621.

[201] M. Y. Jung, W. I. Jang, C. A. Choi, M. R. Lee, C. H. Jun, and Y. T. Kim. Novel lithography process for extreme deep trench by using laminated negative dry film resist. In *Proc. of IEEE MEMS*, pages 685–688, 2004.

[202] M. E. Sandison and H. Morgan. Rapid fabrication of polymer microfluidic systems for the production of artificial lipid bilayers. *J. Micromech. Microeng.*, 15:S139, 2005.

[203] Y. Tsai, S. Yang, H. Lee, H. Jen, and Y. Hsieh. Fabrication of a flexible and disposable microreactor using a dry film photoresist. *J. Chin. Chem. Soc.*, 53:683, 2006.

[204] Y. C. Tsai, H. P. Jen, K. W. Lin, and Y. Z. Hsieh. Fabrication of microfluidic devices using dry film photoresist for microchip capillary electrophoresis. *J. Chromatogr. A*, 1111:267–271, 2006.

[205] S. Zhao, H. Cong, and T. Pan. Direct projection on dry-film photoresist (DP2): do-it-yourself three-dimensional polymer microfluidics. *Lab Chip*, 9:1128–1132, 2009.

[206] K.S. Kiang, H.M.H. Chong, and M. Kraft. A novel low cost spring-less RF MEMS switch prototype. *Procedia Engineering*, 5:1462–1465, 2010.

[207] K. Stephan, P. Pittet, L. Renaud, P. Kleimann, P. Morin, N. Ouaini, and R. Ferrigno. Fast prototyping using a dry film photoresist: microfabrication of soft-lithography masters for microfluidic structures. *J. Micromech. Microeng.*, 17:N69, 2007.

[208] Y. C. Tsai, H. P. Jen, K. W. Lin, and Y. Z. Hsieh. Fabrication of microfluidic devices using dry film photoresist for microchip capillary electrophoresis. *J. Chromatogr. A*, 1111:267–271, 2006.

[209] A. Yusof, R. Zengerle, and P. Koltay. TMMF dry film resist as masking layer in deep etching of Pyrex-glass for microfluidic chip fabrication. *Procedia Engineering*, 25:827–830, 2011.

[210] E. Kukharenka, M. M. Farooqui, L. Grigore, M. Kraft, and N. Hollinshead. Electroplating moulds using dry film thick negative photoresist. *J. Micromech. Microeng.*, 13:S67, 2003.

[211] L. T. Jiang, T. C. Huang, C. Y. Chang, J. R. Ciou, S. Y. Yang, and P. H. Huang. Direct fabrication of rigid microstructures on a metallic roller using a dry film resist. *J. Micromech. Microeng.*, 18:015004, 2007.

[212] P. Dixit, J. Salonen, H. Pohjonen, and P. Monnoyer. The application of dry photoresists in fabricating cost-effective tapered through-silicon vias and redistribution lines in a single step. *J. Micromech. Microeng.*, 21:025020, 2011.

[213] P. W. Leech, N. Wu, and Y. Zhu. Application of dry film resist in the fabrication of microfluidic chips for droplet generation. *J. Micromech. Microeng.*, 19:065019, 2009.

[214] V. L. Spiering, J. W. Berenschot, and M. Elwenspoek. Planarization and fabrication of bridges across deep grooves or holes in silicon using a dry film photoresist followed by an etch back. *J. Micromech. Microeng.*, 5:189, 1999.

[215] P. J. Slikkerveer, P. C. P. Bouten, and F. C. M. De Haas. High quality mechanical etching of brittle materials by powder blasting. *Sensor Actuat. A-Phys.*, 85:296–303, 2000.
[216] E. Koukharenko, M. Kraft, G.J. Ensell, and N. Hollinshead. A comparative study of different thick photoresists for MEMS applications. *J. Mater. Sci. - Mater. El.*, 16:741–747, 2005.
[217] D. S. Lee, H. C. Yoon, and J. S. Ko. Fabrication and characterization of a bidirectional valveless peristaltic micropump and its application to a flow-type immunoanalysis. *Sensor Actuat. B-Chem.*, 103:409–415, 2004.
[218] S.J. Ok, C. Kim, and D.F. Baldwin. High density, high aspect ratio through-wafer electrical interconnect vias for MEMS packaging. *Trans. Adv. Packag.*, 26:302–309, 2003.
[219] S.X. Chuan, J. Yufeng, L. Haijing, and W.C. Khuen. Process development of negative tone dry film photoresist for MEMS applications. In *Proc. of IEEE ICSICT*, pages 575–578, 2004.
[220] M. Kubota, Y. Mita, K. Ito, F. Marty, T. Bourouina, and T. Shibata. A contour-lithography method for rapid and precise deep-etched nano-MEMS structure fabrication. In *Proc. of TRANSDUCERS*, pages 1449–1452, 2005.
[221] Y. Jeong, Y. Han, S. Kim, H. Lee, J. K. Chang, D. D. Cho, D. S. Chung, and K. Chun. Channel flow network at low electric field with high flow resistance compensation pattern. In *Proc. of IEEE MEMS*, pages 431–434, 2003.
[222] Y. Hirono-Hara, H. Noji, and S. Takeuchi. Single-biomolecule observation with micro one-way valves for rapid buffer exchange. *J. Appl. Phys.*, 105:102016–102016, 2009.
[223] C. Gärtner, S. Kirsch, B. Anton, and H. Becker. Hybrid microfluidic systems: combining a polymer microfluidic toolbox with biosensors. In *Proc. of SPIE Micro and Nanofabrication*, pages 64650F–64650F, 2007.
[224] TOPAS Advanced Polymers. COC grade 5013 - Technical datasheet, 2007.
[225] M. Heckele and W. K. Schomburg. Review on micro molding of thermoplastic polymers. *J. Micromech. Microeng.*, 14:R1, 2004.
[226] H. Becker. Microfabrication technologies for microfluidic devices. http://microfluidicchipshop.com/files.php?dl_mg_id=36&file=dl_mg_1117904546.pdf (2014).
[227] B. E. Rapp, M. Schneider, and M. Worgull. Hot punching on an 8 inch substrate as an alternative technology to produced holes on a large scale. In *Proc. of IEEE DTIP*, pages 136–139, 2009.
[228] C. Mehne, R. Steger, P. Koltay, D. Warkentin, and M. P. Heckele. Large-area polymer microstructure replications through the hot embossing process using modular moulding tools. *Proc. Inst. Mech. Eng., B J. Eng. Manuf.*, 222:93–99, 2008.
[229] D. Fuard, T. Tzvetkova-Chevolleau, S. Decossas, P. Tracqui, and P. Schiavone. Optimization of poly-di-methyl-siloxane (PDMS) substrates for studying cellular adhesion and motility. *Microelectron. Eng.*, 85:1289–1293, 2008.
[230] P. Abgrall, V. Conedera, H. Camon, A.M. Gue, and N.T. Nguyen. SU-8 as a structural material for labs-on-chips and microelectromechanical systems. *Electrophoresis*, 28:4539–4551, 2007.
[231] K. H. Dietz. *Dry Film Photoresist Processing Technology*. Electrochemical Publications Limited, 2001.
[232] Paul Vulto. *A Lab-on-a-Chip for automated RNA extraction from bacteria*. PhD thesis, IMTEK - University of Freiburg, 2008.
[233] R. H. W. Lam, K. F. Lei, J. H. M. Lam, and W. J. Li. Digitally controllable large-scale integrated microfluidic systems. In *Proc. of IEEE ROBIO*, pages 301–306, 2004.
[234] A. Bubendorfer, X. Liu, and A.V. Ellis. Microfabrication of PDMS microchannels using SU-8/PMMA moldings and their sealing to polystyrene substrates. *Smart Mater. Struct.*, 16:367, 2007.
[235] Y. Song, C.S.S.R. Kumar, and J. Hormes. Fabrication of an SU-8 based microfluidic reactor on a PEEK substrate sealed by a flexible semi-solid transfer (FST) process. *J. Micromech. Microeng.*, 14:932, 2004.
[236] G. Kotzar, M. Freas, P. Abel, A. Fleischman, S. Roy, C. Zorman, J.M. Moran, and J. Melzak. Evaluation of MEMS materials of construction for implantable medical devices. *Biomaterials*, 23:2737–2750, 2002.
[237] E. Leclerc, Y. Sakai, and T. Fujii. Cell culture in 3-dimensional microfluidic structure of PDMS (polydimethylsiloxane). *Biomed. Microdevices*, 5:109–114, 2003.

[238] J. Tian and M. Bartek. Simultaneous through-silicon via and large cavity formation using deep reactive ion etching and aluminum etch-stop layer. In *Proc. of IEEE ECTC*, pages 1787–1792, 2008.
[239] L. Riegger, O. Strohmeier, B. Faltin, R. Zengerle, and P. Koltay. Adhesive bonding of microfluidic chips: influence of process parameters. *J. Micromech. Microeng.*, 20:087003, 2010.
[240] V. Jokinen and S. Franssila. Capillarity in microfluidic channels with hydrophilic and hydrophobic walls. *Microfluid. Nanofluid.*, 5:443–448, 2008.
[241] D. Quéré. Wetting and roughness. *Annu. Rev. Mater. Res.*, 38:71–99, 2008.
[242] D. Juncker, H. Schmid, U. Drechsler, H. Wolf, M. Wolf, B. Michel, N. de Rooij, and E. Delamarche. Autonomous microfluidic capillary system. *Anal. Chem.*, 74:6139–6144, 2002.
[243] R. Niekrawietz. *TopSpot: highly parallel nanoliter dispensing operating conditions and design rules*. PhD thesis, IMTEK - University of Freiburg, 2009.
[244] O. Gutmann. *Production of custom microarrays using a highly parallel pressure driven nanoliter dispenser*. PhD thesis, IMTEK - University of Freiburg, 2006.
[245] Automated Cancer Screening Based on Real-time PCR (AUTOCAST). http://www.genoid.net/autocast/ (2014).
[246] HealthCARE by Biosensor Measurements And Networking (CARE-MAN). http://www.careman.eu (2013).
[247] O. Gutmann, C. P. Steinert, G. Dernick, B. de Heij, C. Fattinger, U. Certa, R. Zengerle, and M. Daub. Fast selective surface modification of microfluidic printheads for improvement of droplet ejection. In *Proc. of μTAS*, 2005.
[248] M. A. Hopcroft, W. D. Nix, and T. W. Kenny. What is the young's modulus of silicon? *J. Micromech. Microeng.*, 19:229–238, 2010.
[249] MicroChemicals. High-resolution photoresist processing, 01. http://www.microchemicals.eu/technical_information/high_resolution_photoresist_processing.pdf (2012).
[250] X. Mao, J. Yang, A. Ji, and F. Yang. Two new methods to improve the lithography precision for SU-8 photoresist on glass substrate. In *Proc. of IEEE MEMS*, pages 337–340, 2012.
[251] HSG-IMIT. Process flow sheets for TopSpot printheads.

ACKNOWLEDGMENTS

I wish to thank Prof. Dr. Roland Zengerle for the opportunity to work on this exciting topic and for his encouragement to combine scientific research and engineering. The excellent conditions and the interdisciplinary and dynamic environment in the Laboratory for MEMS Applications helped me staying focused and are among the major contributors to this thesis.

I like to thank Prof. Dr. rer. nat. Heinz Kück for the kind acceptance to co-referee my thesis.

I wish to thank Dr. Peter Koltay, head of the non-contact microdosage group at the Laboratory for MEMS Applications and COO of Biofluidix, for supervising my thesis and for the many fruitful discussions and suggestions throughout my work. I deeply appreciate the opportunity to work so industry-oriented and in close cooperation with the highly motivated Biofluidix team.

This work has been supported by MicroMountains Applications AG.

When I look back, I realise how many other people have contributed to this thesis. I like to express appreciation to:

Ludwig Gutzweiler and Michael Bleile for their support and enthusiasm to work with me on this topic;

Gerhard Birkle, Horst Holzwarth and Guido Müller for their support in all technical issues;

Claas Müller from the Laboratory for Process Technology for being helpful with SEM, PDMS and plasma related issues;

Peter Nommensen and Stefan Bekesi from HSG-IMIT for providing all relevant information regarding the fabrication of TopSpot printheads;

the members of the group for non-contact microdosage systems and Biofluidix: Andreas Ernst, Wolfgang Streule, Lutz Riegger, Chris Steinert, Azmi Yusof, Dong Liang, Klaus Mutschler, Stefan Bammesberger, André Gross, Nils Lass, Andreas Madjarov, Jonas Schöndube and Laurent Tanguy for the fruitful discussions in our weekly meetings and the nice atmosphere in the lab;

the entire cleanroom team, Dr. Michael Wandt for his support in creating process sheets and helpful discussions on costs, and Armin Baur, Michael Reichel, Tsvetelina Hugger, Nico Lehmann and Martin Bauer for their everyday help in the cleanroom;

Melanie Baumann and Ulrike Grundmann for managing all administrative issues;

Nils Paust, Tobias Hutzenlaub and Artur Tropmann for the nice time we spent together in and outside the lab;

and of course all other members of the lab, in particular Daniel Mark, Sascha Lutz, Matthias Heck, Michael Laufer, Maximilian Focke, Bernd Faltin, Thomas van Oordt, Günter Roth, Sven Kerzenmacher, Nicolai Wangler, Dominique Kosse, Jürgen Burger and Frank Schwemmer.

I like to express my appreciation to my parents Maria and Todor for enabling my education and supporting me in every possible way, and to my brother Atanas for the relaxed moments in our home. My special “Thank you!” goes to my wife Zora and my daughter Anelia, for their never ending patience during the final writing up of my thesis.